



Universitat Politècnica de Catalunya



Institut de bioenginyeria
de Catalunya

Institut de Bioenginyeria de Catalunya

Doctoral Program

Biomedical Engineering

Doctoral thesis

Invasive and non-invasive assessment of upper airway
obstruction and respiratory effort with nasal airflow and
esophageal pressure analysis during sleep

Dipl.-Ing. Christian Morgenstern de Muller

Biomedical Signals and Systems (SISBIO) group, Universitat Politècnica de Catalunya (UPC)

Biomedical Signal Processing and Interpretation (BIOSPIN) group, Institut de Bioenginyeria de
Catalunya (IBEC)

Barcelona, January 24th 2010

Thesis advisor: Dr. Raimon Jané Campos

Dedicado a mi familia, mi padre Rudolf, mi madre María, mi hermana Patricia y mi hermano Albert, por todo su amor, su respeto y paciencia conmigo. Por ser lo más importante de mi vida. Gracias por ser una familia tan maravillosa.

Das grosse Lalula

*Kroklokwaſzi? Se[̄]eme[̄]i!
Seiokrontro -- praſriplo:
Bifzi, baſzi; hulale[̄]i:
quasti baſti bo...
Lalu lalu lalu lalu la!*

*Hontraruru miromente
zasku zes rü rü?
Entepente, leiolente
klekwapuſzi lü?
Lalu lalu lalu lala la!*

*Simarat kos malzlpempu
silzuzankunkrei (;)!
Marjomar dos: Quempu Lempu
Siri Suri Sei []!
Lalu lalu lalu lalu la!*

Christian Morgenstern, 1905

Die unmögliche Tatsache

*Palmström, etwas schon an Jahren,
wird an einer Straßenbeuge
und von einem Kraftfahrzeuge
überfahren.*

*Wie war (spricht er, sich erhebend
und entschlossen weiterlebend)
möglich, wie dies Unglück, ja -:
daß es überhaupt geschah?*

*Ist die Staatskunst anzuklagen
in Bezug auf Kraftfahrwagen?
Gab die Polizeivorschrift
hier dem Fahrer freie Trift?*

*Oder war vielmehr verboten
hier Lebendige zu Toten
umzuwandeln - kurz und schlicht:
Durfte hier der Kutscher nicht -?*

*Eingehüllt in feuchte Tücher,
prüft er die Gesetzesbücher
und ist alsobald im klaren:
Wagen durften dort nicht fahren!*

*Und er kommt zu dem Ergebnis:
Nur ein Traum war das Erlebnis.
Weil, so schließt er messerscharf,
nicht sein kann, was nicht sein darf.*

Christian Morgenstern, 1910

Acknowledgements

First of all I would like to give my deepest thank to Dipl.-Ing. Matthias Schwaibold of MCC GmbH & Co. KG, Karlsruhe. He was the one who initiated this whole adventure by offering to start this cooperation. Matthias, you have been a great advisor and a great friend. Thank you for your precious advice and your patience, always finding time in your busy schedule for my questions and always remaining in such a great mood. It is always a great and rewarding experience working with and for you.

I would also like to thank all the other guys at MCC-Med GmbH & Co. KG, Karlsruhe, Germany Mr. Dirk Sommermeyer, Ms. Anne Oltmann, Ms. Miskina Saka and Mr. Bernd Schöller, and all the fantastic team at MCC that does a great work day after day in research and development in order to improve the diagnosis and treatment of people suffering of SDB.

A big thank you goes also to Prof. Dr. Winfried Randerath, Dr.-med. Wolfgang Galetke, Mr. Norbert Anduleit, Mr. Marcel Treml and Ms. Kerstin Richter of the Zentrum für Schlaf- und Beatmungsmedizin, Krankenhaus Bethanien, Solingen, Germany for their assistance and support during the development of this study. Without their hard and dedicated work and their ability to convince patients to sleep with a Pes catheter, this study would not have been possible.

Another big thank you goes to Prof. Dr. Armin Bolz, my former advisor at the Institute of Biomedical Engineering of the University of Karlsruhe (TH). I am very thankful for all of his encouragement and support during all these years And that that, even though I have been living abroad for all these years, we are still keeping in touch and cooperating.

Last but not least, I would like to thank my advisor Prof. Dr. Raimon Jané of the

Universitat Politècnica de Catalunya (UPC) for his advice, support and guidance during the development of this thesis. His support and advice especially in the search for the fundings of this project and the publication of the results has been critical for the success of the whole thesis. Also his diplomacy and capacity to make everything and everybody work together and pull in one direction at the right time have been of critical importance. Thank you for your effort and your comprehension.

A big thank you goes also to all of my friends and colleagues at the UPC, the IBEC and CIBER-BBN, who have always been there with and for me during the good and the hazardous time. It's been great with all of you guys! I would also like to thank all of my friends all around the world, Germany, Spain, the U.S. and wherever else you may now be, for always giving me your friendship, support and encouragement.

Finally, I would like to give my biggest thanks to my family for their unlimited patience, love and support. I know through all of this time I have been a hard piece of work, so thank you for supporting me and never giving up on me!

This work was supported in part by the Grant 2008FIC00238 of *the Generalitat de Catalunya*, Spain, by the Spanish *Ministerio de Ciencia e Innovación* under grant TEC2007-68076-C02-01, by the Institut de Bionenginyeria de Catalunya (IBEC) and the CIBER de Bioingeniería, Biomateriales y Nanomedicina (CIBER-BBN).

Abstract of the doctoral thesis

“Invasive and non-invasive assessment of upper airway obstruction and respiratory effort with nasal airflow and esophageal pressure analysis during sleep”

Doctoral student: **Christian Morgenstern de Muller**

Advisor: **Dr. Raimon Jané Campos**

The assessment of respiratory effort during sleep is of major importance for the correct identification of respiratory events in sleep-disordered breathing (SDB), the correct diagnosis of SDB-related pathologies and the consequent choice of treatment. Currently, respiratory effort is usually assessed in night polysomnography (NPSG) with imprecise techniques and manually evaluated by human experts, resulting in a laborious task with significant limitations and missclassifications.

The main objective of this thesis is to present new methods for the automatic, invasive and non-invasive assessment of respiratory effort and changes in upper airway (UA) obstruction. Specifically, the application of these methods should, in between others, allow the automatic invasive and non-invasive differentiation of obstructive and central respiratory events during sleep.

For this purpose, a completely new NPSG database consisting of 28 patients with systematic esophageal pressure (Pes) measurement was acquired. Pes is currently considered the gold-standard to assess respiratory effort and identify respiratory events in SDB. However, the invasiveness and complexity of Pes measurement prevents its use in clinical routine, underlining the importance and difficulty to acquire this new

database. All the processing methods developed in this thesis have consequently been validated with the gold-standard Pes-signal in order to ensure their clinical validity.

In a first step, an (invasive) automatic system for the classification of inspiratory flow limitation (IFL) in the inspiratory cycles is presented. IFL has been defined as a lack of increase in airflow despite increasing respiratory effort, which normally results in a characteristic inspiratory airflow pattern (flattening). A total of 38,782 breaths were extracted and automatically analyzed. An exponential model is proposed to reproduce the relationship between Pes and airflow of an inspiration and achieve an objective assessment of changes in upper airway obstruction. The characterization performance of the model is appraised with three evaluation parameters: mean-squared-error when estimating resistance at peak-pressure, coefficient of determination and assessment of IFL episodes. The model's results are compared to the two best-performing models in the literature. The results indicated that the exponential model characterizes IFL and assesses levels of upper airway obstruction with the highest accuracy and objectivity.

The obtained gold-standard IFL annotations were then employed to train, test and validate a new automatic, non-invasive IFL classification system by means of the nasal airflow signal. Discriminant Analysis, Support Vector Machines and Adaboost algorithms were employed to objectively classify breaths non-invasively with features extracted from the time and frequency domains of the breaths' flow patterns. The new non-invasive automatic classification system also succeeded identifying IFL episodes, achieving a sensitivity of 0.87 and a specificity of 0.85.

The differentiation between obstructive and central respiratory events is one of the most recurrent tasks in the diagnosis of sleep disordered breathing, but only Pes measurement allows the gold-standard differentiation of these events. Recently new techniques have been proposed to allow the non-invasive differentiation of hypopneas.

However, their adoption has been slow due to their limited clinical validation, as the creation of manual, gold-standard validation sets by human experts is a cumbersome procedure. In this study, a new system is proposed for an objective automatic, gold-standard differentiation between obstructive and central hypopneas with the esophageal pressure signal. An overall of 769 hypopneas of 28 patients were manually scored by human experts to create a gold-standard validation set. Then, features were extracted from each hypopnea to train and test classifiers (Discriminant Analysis, Support Vector Machines and adaboost classifiers) to differentiate between central and obstructive hypopneas with the gold-standard esophageal pressure signal. The automatic differentiation system achieved promising results, with a sensitivity, a specificity and an accuracy of 0.90. Hence, this system seems promising for an automatic, gold-standard differentiation between obstructive and central hypopneas.

Finally, a non-invasive system is proposed for the automatic differentiation of central and obstructive hypopneas. The nasal airflow signal is proposed for the differentiation of hypopneas. Features extracted from the inspiratory cycles of the hypopnea, such as the flattening patterns, are used to train and test the classifiers. This automatic, non-invasive system is a combination of the systems presented before and it was also validated with the gold-standard scorings obtained with the Pes-signal by human experts. The outcome of the automatic, non-invasive system is compared to the results obtained by human scorers that applied a new non-invasive algorithm for the manual differentiation of hypopneas. The automatic non-invasive system's results are promising and show the feasibility of the methodology employed. Once validated, this algorithm has been proposed to be used in therapy devices developed by one of the partner institutions cooperating in this project.

Glossary

AI	Apnea Index
AHI	Apnea/Hypopnea Index
CNS	Central nervous system
CSA	Central sleep apnea
CSAHS	Central Sleep Apnea/Hypopnea Syndrome
CSH	Central sleep hypopnea
DA	Discriminant Analysis
HI	Hypopnea Index
IFL	Inspiratory Flow Limitation
MA filter	Moving Average filter
NREM	non Rapid-Eye-Movement
NPSG	Night PolySomnoGraphy
OSA	Obstructive sleep apnea
OSAHS	Obstructive Sleep Apnea/Hypopnea Syndrome
OSH	Obstructive sleep hypopnea
Pes	Esophageal Pressure
PSG	PolySomnoGraphy
R&K	Rechtschaffen & Kales [80]
REM	Rapid-Eye-Movement
RERA	Respiratory Effort Related Arousal
RIP	Resistive Inductance Plethismography
SD	Standard Deviation
SDB	Sleep Disordered breathing
SpO₂	Arterial oxygen saturation
SVM	Support Vector Machine

UA	Upper Airway
UAR	Upper Airway Resistance
UARS	Upper Airway Resistance Syndrome

Index

Chapter I: Introduction	1
Sleep Disordered Breathing (SDB) and state of the art in non-invasive diagnostics in night polysomnography.....	1
Objectives of this thesis	4
Organization of this thesis.....	7
Chapter II: Sleep Disordered Breathing (SDB).....	9
Introduction	9
The human Upper Airway	10
Anatomy of the Upper Airway	10
Physiology of the Upper Airway.....	16
Models of the Upper Airway	18
Model of the Upper Airway as a Starling resistor	18
A mathematical, multi-dimensional model of the Upper Airway	20
Syndromes of SDB	22
The obstructive sleep apnea/hypopnea syndrome (OSAHS).....	22
The Upper Airway Resistance Syndrome (UARS)	25
The central apnea/hypopnea Syndrome (CSAHS).....	28
Conclusions	29
Chapter III: Concepts of sleep monitoring and nocturnal polysomnography (NPSG).....	31
Introduction	31
Classical nocturnal polysomnography (NPSG)	31
NPSG recording techniques to assess respiratory effort	35
Respiratory monitoring in NPSG: nasal cannula vs. plethysmography	36
Esophageal pressure measurement.....	39
Conclusions	48

Chapter IV: New patient study and NPSG database with esophageal pressure measurement .	51
Introduction	51
Recording protocol and measurement devices	53
Patient's demographic data	59
Manual, invasive classification of hypopneas	64
Manual, non-invasive classification of hypopneas.....	66
Conclusions	66
Chapter V: Pre-processing and automatic identification of inspiratory cycles.....	69
Introduction	69
Filtering and alignment	71
Signal drifting and baseline estimation	73
Identification of inspirations	74
Conclusions	77
Chapter VI: Automatic identification of inspiratory flow limitation with esophageal pressure .	79
Introduction	79
The P/\dot{V} -relationship	80
Introduction	80
Implementation.....	83
Classical criteria	84
Clark's criteria.....	85
Models of the P/\dot{V} -relationship	85
Introduction	85
Hudgel's hyperbolic model.....	85
Mansour's 3 rd degree polynomial model	88
Comparison of the hyperbolic vs. the polynomial model	90
Exponential model	94

Subjects	95
Evaluation criteria for the mathematical models	96
Results	99
Discussion	101
Conclusions	104
Chapter VII: Techniques used in pattern classification	107
Introduction	107
Discriminant Analysis (DA)	108
Support Vector Machines (SVMs)	111
Adaboost	113
Stepwise forward feature selection	116
Receiver Operator Characteristic (ROC).....	118
K-Means Clustering	119
Linear Least Squares Approximation.....	121
Cross-correlation	123
Conclusions	123
Chapter VIII: Non-invasive, automatic identification of inspiratory flow limitation during sleep	125
Introduction	125
Analysis of snoring.....	125
Cyclical Alternating Patterns (CAPs).....	127
A non-invasive IFL classifier with the airflow signal.....	128
Non-invasive identification of IFL.....	129
Results	133
Discussion.....	135
Conclusions	136
Chapter IX: Automatic differentiation of central and obstructive hypopneas with esophageal pressure during sleep.....	137

Introduction	137
Methodology	138
Subjects	138
Feature extraction	141
Training and testing of the classifiers.....	145
Results	148
Discussion	150
Conclusions	151
Chapter X: Non-invasive, automatic differentiation of central and obstructive hypopneas....	153
Introduction	153
Methodology	155
Subjects	155
The Solingen algorithm	157
A new automatic, non-invasive differentiation algorithm	159
Training and testing of the classifiers.....	162
Results	163
Discussion	164
Outlook: A continuous measurement of IFL by analyzing flattening patterns	167
Conclusions	172
Chapter XI: Conclusions.....	173
Contributions of this thesis	173
Database.....	173
IFL detection.....	174
Differentiation of hypopneas	174
Outlook.....	175

Appendix A 177

Bibliography 184

Publications derived from this thesis 199

Chapter I: Introduction

Sleep Disordered Breathing (SDB) and state of the art in non-invasive diagnostics in night polysomnography

Sleep Disordered Breathing (SDB) describes a group of disorders characterized by abnormalities of respiratory pattern (pauses in breathing) or the quantity of ventilation during sleep [1, 2]. SDB comprises syndromes such as the obstructive sleep apnea/hypopnea syndrome (OSAHS), Cheyne-Stokes respiration, the upper airway resistance syndrome (UARS) [3] and others [1, 2].

According to recent studies [2, 4, 5] the prevalence of OSAHS is between 5 - 17% of the general population in dependence of the syndrome's severity. While apneas represent a complete ($> 90\%$) cessation of flow, hypopneas are defined by a clear decrease ($> 50\%$) from baseline in the amplitude of a valid measure of breathing during sleep or is associated with either an oxygen desaturation of $> 3\%$ or an arousal, and both events have to last for at least for 10 seconds [6, 7], see fig. 1.1. The clinical consequences of SDB syndromes usually are sleep fragmentation and excessive daytime sleepiness [3], hypertension [8, 9] and related cardiovascular diseases [2]. The clinical consequences of obstructive sleep hypopnea syndrome (OSHS) are almost identical to obstructive sleep apnea syndrome (OSAS) [8].

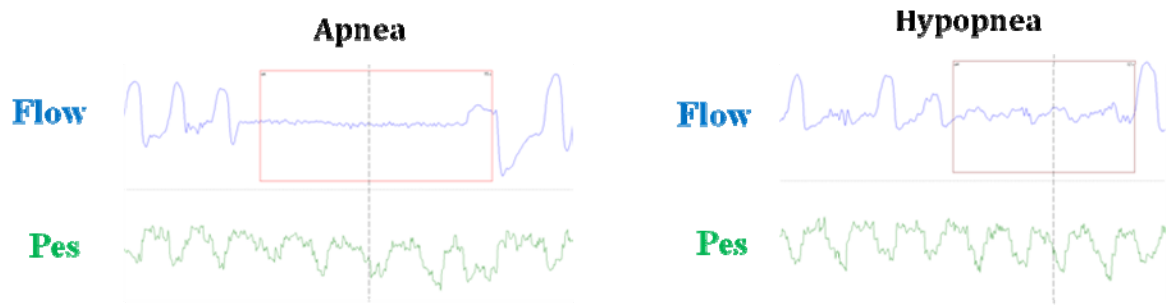


Figure 1.1: Examples of an obstructive apnea and an obstructive hypopnea. The represented flow signal was recorded with a nasal cannula device, while respiratory effort is represented by the esophageal pressure (Pes) signal.

Thus, one of the most important aspects of the diagnosis of SDB in regards of the appropriate choice of treatment, is the correct identification of respiratory events. Particularly, the correct differentiation between central and obstructive apneas/hypopneas is one of the most recurrent tasks due to the commented prevalence of the corresponding OSAHS and central sleep apnea/hypopnea syndromes (CSAHS). The difference between central and obstructive events relies in the differences in respiratory effort at the onset of the event. While a sequential increase in respiratory effort is observed during obstructive events, central events show no increase, sometimes even a decrease, in respiratory effort [6, 7], see fig. 1.2. Currently, esophageal pressure (**Pes**) measurement is considered the gold-standard technique for measurement of respiratory effort and the identification of obstructive and central events [6, 7]. Still, the complexity and invasiveness of esophageal pressure manometry and its impact on sleep [10] limits its usage in clinical routine.

So, researchers have been recently trying to develop non-invasive techniques for the differentiation between central and obstructive apneas/hypopneas [11-13]. Most systems try to find a reliable non-invasive indicator for respiratory effort and UA resistance that could represent a valid, non-invasive alternative to esophageal pressure measurement.

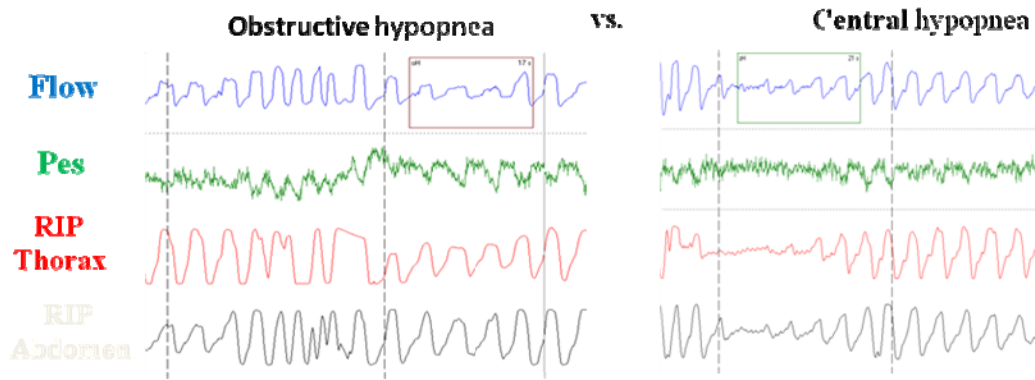


Figure 1.2: Examples of an obstructive and a central hypopnea. Observe the incremental evolution of the Pes swings during the obstructive event, while there is almost no variation of pressure swings during the central hypopnea.

For example, events caused by increased UA resistance, such as inspiratory flow limitation (IFL), seem to cause a characteristic inspiratory flow pattern in the airflow signal that is considered to contain information on these changes in UA [14 - 16]. IFL has been defined as a lack of increase in airflow despite increasing respiratory effort. Thus, techniques such as flow shape clustering [15-18], neural-network classification [19] and other signal processing methods [20, 21] have been used to identify IFL and increased UA resistance. Also other techniques, such as Pulse-Transit-Time (PTT) [11, 22], forced-oscillation-technique (FOT) to determine respiratory resistive impedance [23, 24], intercostal EMG signal filtering [25 - 27], critical pressure measurement with therapy devices [28 - 31], the phase angle modification of thoracic and abdominal muscle movement measured by Resistive Inductance Plethysmography (RIP) belts [32, 33], Cyclical Alternating Patterns (CAPs) [34, 35] or analysis of the snoring [36 – 39, 41, 43, 131] and respiratory sound signals [40, 42, 44 - 46], are promising and interesting approaches.

However, the clinical adoption of these techniques has been slow, mostly due to their limited clinical validation. The bottleneck when creating a gold-standard validation set

is usually found in the manual identification of the mentioned events by a human expert, as it is a cumbersome procedure that may suffer of interscorer differences and subjective interpretation. Hence, the development of an objective and efficient method for automatic invasive assessment of central and obstructive events is desirable, while the development of a simple and robust automatic, non-invasive method is also still necessary.

Objectives of this thesis

This thesis has the main objective of finding non-invasive alternatives to esophageal pressure measurement in order to reliably assess increased upper airway resistance (UAR) and respiratory effort. The study will focus on obtaining the necessary information through signal processing techniques out of non-invasive signals recorded in standard clinical routine NPSGs. We will try to find viable and robust techniques to automatically identify and estimate respiratory effort and upper airway (UA) resistance, as these are the most important parameters to successfully differentiate the most important SDB events [6, 7] and correctly diagnose SDB related pathologies. Finally, the developed techniques should allow us to differentiate between central and obstructive respiratory events by invasive (Pes signal) and non-invasive means.

The work developed in this thesis can be divided into three main stages:

- In the first stage an extensive literature review was performed in order to review the state of the art in invasive and non-invasive methods to assess UA resistance and respiratory effort. Conventional and freely available NPSG databases were not valid for our purposes as they do not include the gold-standard esophageal pressure signal in its recordings. Given these limitations a new NPSG patient database was designed and developed in collaboration

with the group of Prof. Dr. WJ Randerath at Klinikum Bethanien hospital in Solingen, Germany hospital. We wanted to obtain a whole new set of NPSG recordings with a systematic recording of the gold-standard Pes measurement for each patient. The NPSG protocol was designed from scratch in cooperation with the mentioned clinic, in order to create a new signal database that includes all the necessary signals and information which will be needed to develop the techniques proposed in stage 2. A latter validation study will be necessary in order to assess the efficacy of the developed techniques, see stage 3. The authors thus had the unique opportunity to influence decisions in the pre-study design and have a word on the selection of parameters such as which signals were recorded, the signal characteristics, the number of patients to be recorded and select previously some characteristics of the patients in order to include or exclude certain pathological cases, in between others. All NPSG recordings were afterwards manually revised and analyzed by human experts of the clinic to manually classify and differentiate respiratory events and sleep stages.

- In the second stage we analyzed the NPSG recordings of the database we had obtained in stage 1. We exhaustively analyzed the Pes signal to evaluate respiratory effort and tried to find complementary information primarily in the airflow signal to objectively identify respiratory events. The airflow signal was chosen in between all signals of the NPSG recordings, as it reliably reflects events occurring in the respiratory system and contains direct information on changes in UA resistance and respiratory drive and could therefore be promising to achieve our purposes. In order to achieve the invasive identification of respiratory events, techniques like the assessment of inspiratory flow limitation (IFL) were developed by means of analyzing the

Pes signal. For the non-invasive automatic identification of respiratory events, we implemented a system that used the spectral analysis of the airflow signal for the detection of IFL episodes. Finally, these insights were used in order to implement the invasive and non-invasive differentiation of obstructive and central respiratory events during sleep. Manually scored markers by a human expert with the flow and Pes signal represent the gold-standard scorings, allowing the validation of these newly developed techniques, see stage 3. As human scoring is subjective and presents interscorer differences, most of the applied techniques are methods belonging to the family of supervised machine learning that try to emulate human behavior. One of the specific purposes of this thesis is to use the techniques developed to assess UA resistance and respiratory effort for the differentiation between central and obstructive respiratory events during sleep with and without the gold-standard Pes signal. Our system focused on the differentiation of hypopneas, because Pes swings during a hypopnea are more subtle than during other events, therefore being considered one of the most challenging tasks [2, 3].

- In the third stage the algorithms developed in the second stage were validated with the manual scorings obtained in stage 1. The manual scorings performed with the Pes-signal represent the gold-standard [6, 7] for respiratory event scorings and differentiation. These scorings should allow us validating any computational algorithm for clinical purposes.

Organization of this thesis

Chapter I: Introduction. A brief introduction is given on SDB and the state of the art in apnea/hypopnea classification. The thesis objectives are briefly outlined and the structure of the thesis is described.

Chapter II: Sleep disordered breathing. In order to give an overview of the respiratory system, the anatomy and physiology of the UA is described. Then mathematical models that explain the physiology of the UA are commented. Finally the most important syndromes in SDB are listed.

Chapter III: Concepts of sleep monitoring and night polysomnography (NPSG). The general concepts of NPSG are described and the criteria for sleep stage scorings to create a hypnogram are detailed. The sensors for flow and Pes measurement are commented, as well as other commonly recorded signals, such as SpO₂, RIP belts, etc.

Chapter IV: New patient study and NPSG database with esophageal pressure measurement. The recording protocol of the new patient database and the demographic data of the patients are presented. The criteria for the manual scoring of respiratory events are described.

Chapter V: Pre-processing and automatic detection of inspiratory cycles. A scheme of the signal pre-processing system that is common to all of the proposed techniques is outlined. Filtering, signal alignment and inspiratory cycle detection are described in detail.

Chapter VI: Automatic identification of inspiratory flow limitation with esophageal pressure. The pressure/flow (P/V) relationship is introduced as a help for an objective classification of IFL. Classical and Clark's criteria are introduced for IFL

classification. Finally a new exponential model is proposed to classify IFL and its performance is compared with several criteria to the other models described in the literature. The models' evaluation criteria are also described and the comparison results presented.

Chapter VII: Techniques used in pattern classification. A brief introduction is given into techniques used in pattern classification such as discriminant analysis (DA), Support Vector Machines (SVMs) and boosting algorithms like Adaboost. The methods presented in the following chapters for respiratory event classification will be mainly based upon these techniques.

Chapter VIII: Non-invasive, automatic identification of inspiratory flow limitation during sleep. For the automatic, non-invasive detection of IFL, the spectral information contained in the inspiratory flow pattern was analyzed. Features were extracted and supervised machine learning classifiers were trained and tested to identify IFL.

Chapter IX: Automatic differentiation of central and obstructive hypopneas with esophageal pressure during sleep. For the automatic, invasive differentiation of central and obstructive hypopneas, a visual localization index is proposed to analyze and make a relative comparison between the respiratory effort during a hypopnea and the two minutes prior to the event. Features are extracted and again supervised machine learning techniques were used to differentiate the events.

Chapter X: Non-invasive, automatic differentiation of central and obstructive hypopneas. The information contained in the IFL patterns is used (also see chapter IX) for the automatic, non-invasive differentiation of central and obstructive hypopneas. For this purpose the systems presented in chapters VI and IX are combined. Features were

again extracted from the signal and classifiers were trained and tested to non-invasively differentiate these events.

Chapter XI: Conclusions. The outcome and contributions of this thesis is summarized in this chapter and briefly presented. The outlook of the further development of the techniques presented here is given.

Chapter II: Sleep Disordered Breathing (SDB)

Introduction

Sleep is one of the most important physical and mental regenerative functions of the human body. But life quality and expectancy of 5 - 30% of the present population is being affected by sleep disorders in dependence of age, sex, constitutional features and social characteristics [47].

Sleep Disordered Breathing (SDB) describes a group of disorders characterized by abnormalities of respiratory pattern (pauses in breathing) or the quantity of ventilation during sleep [1, 2]. SDB comprises syndromes such as the obstructive sleep apnea/hypopnea syndrome (OSAHS), Cheyne-Stokes respiration, the upper airway resistance syndrome (UARS) [3] and others [1, 2]. Even mild degrees of sleep-disordered breathing (SDB) may cause symptoms such as daytime sleepiness with concomitant fatigue [3, 49, 50], and cardiovascular diseases associated to obesity like atrial fibrillation, congestive heart failure and systemic hypertension [2, 9, 51, 55, 132].

During sleep, SDB is triggered by a physiologic decrease of the muscle tone of the pharyngeal dilator muscles supporting the upper airway (UA) [15]. The hypotonic UA usually partially or complete collapses due to the negative intrathoracic pressure developed during inspiration and that it cannot further be supported by the failing UA muscles [56]. So, the cross-sectional area of the UA is reduced, UA resistance increases and the tidal volume may fall or persist [57, 58], leading to different degrees of collapse of the UA and consequently a whole spectrum of different respiratory events such as inspiratory flow limitation (IFL), hypopneas or apneas (in increasing order of UA collapse, respectively)

[15, 56]. An obstructive respiratory event has a direct incidence on the cardiovascular system, provoking a decrease in oxygen saturation and an increase in respiratory effort [2, 3, 9, 16]. Usually such an event leads to a micro-arousal or a related respiratory effort related arousal (RERA) which, in case of repetitive events, will finally cause sleep fragmentation [3, 14].

In the following chapter we will describe in detail the anatomic and physiological characteristics of the human UA and the mathematical models that have been proposed to predict its behavior during sleep. Also the most important SDB syndromes, such as OSAHS and UARS, will be described in detail.

The human Upper Airway

Anatomy of the Upper Airway

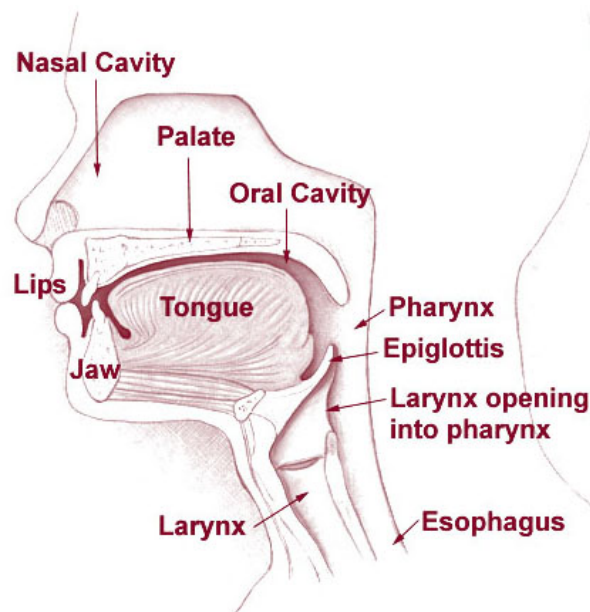


Figure 2.1: Saggital view of the anatomical structures of the upper airway. (courtesy of Seer Training Modules, NCI, USA)

The larynx and the pharynx are two specialized structures associated with the digestive and respiratory tracts, located in the neck. The **larynx**, see figs. 2.1 and 2.2, is a semi-rigid structure at the upper part of the lower airway and it is only in very seldom cases related to

OSA or SDB [64]. The **pharynx**, see figs. 2.1 and 2.2, is considered the main structure of the human upper airway. It is the part of the neck and throat situated immediately posterior to the mouth and nasal cavity, and cranial to the esophagus, larynx, and trachea. The pharynx is part of the digestive system and respiratory system and conducts air from the nose and the oral cavity to the larynx. In order to allow swallowing, the pharynx has to be collapsible. But it is the collapsibility of the pharynx that is also inherently related to the causes of various SDB syndromes like OSAHS. As stated by Drake et al. [59] (pp. 937) “The pharynx is a half cylinder of muscle and fascia attached above to the base of the skull, and below to the margins of the esophagus. On each side, the walls of the half cylinder are attached to the lateral margins of the nasal cavities, the oral cavity, and the larynx. The two nasal cavities, the oral cavity, and the larynx therefore open into the anterior aspect of the pharynx, and the esophagus opens inferiorly.”

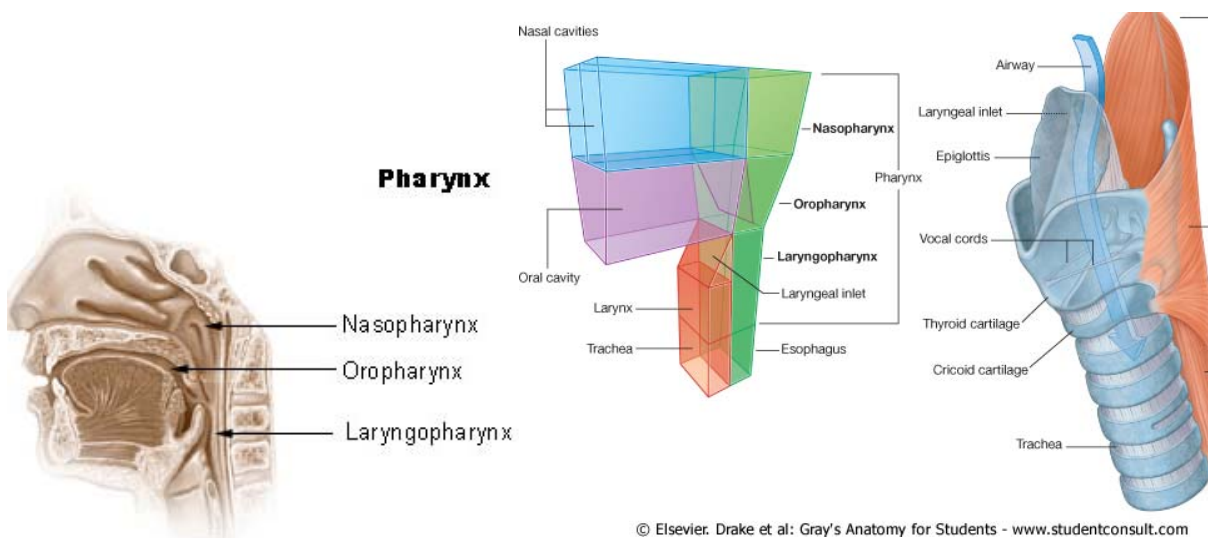


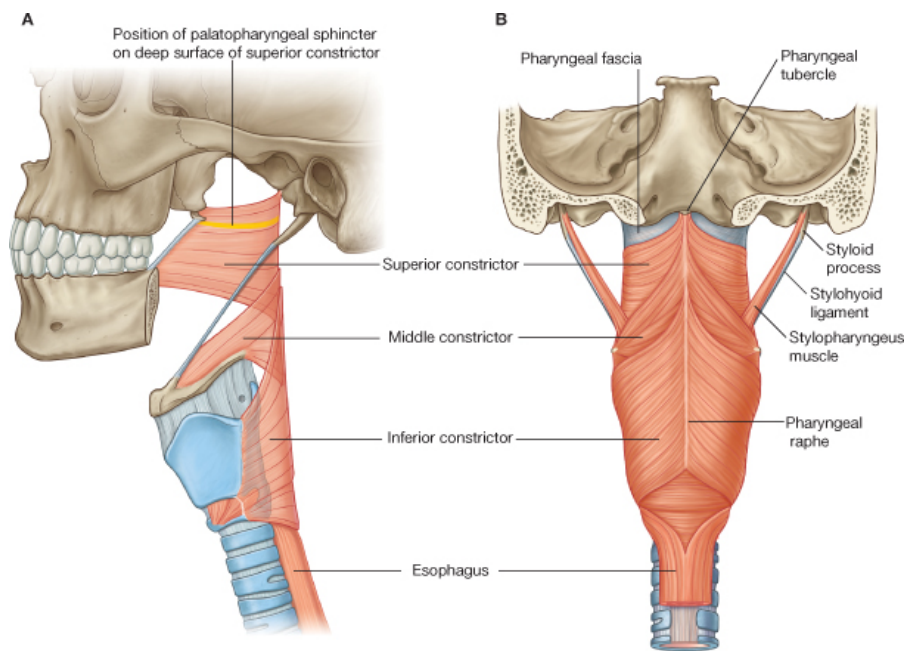
Figure 2.2: Sagittal view of the anatomical structures of the upper airway (left), conceptual view (center), anatomical view (right) [59]

More than 30 pairs of muscles control the functions of the pharynx and that together control the pharyngeal collapsibility. As stated by Drake et al. [59] (pp. 939 ff.) “The major muscle groups of the neck include:

- muscles of the pharynx (constrict and elevate the pharynx);
- muscles of the larynx (adjust the dimensions of the air pathway);
- strap muscles (position the larynx and hyoid bone in the neck);
- muscles of the outer cervical collar (move the head and upper limb);
- postural muscles in the muscular compartment of the neck (position the neck and head).

Constrictor muscles

The structure of the pharyngeal wall is mainly composed by the three constrictor muscles for each side of the wall (superior, middle and inferior), see fig. 2.3. Posteriorly, the muscles from each side are joined together by the pharyngeal raphe. Anteriorly, these muscles attach to bones and ligaments related to the lateral margins of the nasal and oral cavities and the larynx. The constrictor muscles overlap each other in a fashion resembling the walls of three flower pots stacked one on the other. The inferior constrictors overlap the lower margins of the middle constrictors and, in the same way, the middle constrictors overlap the superior constrictors. Collectively, the muscles constrict or narrow the pharyngeal cavity. When the constrictor muscles contract sequentially from top to bottom, as in swallowing, they move a bolus of food through the pharynx and into the esophagus.



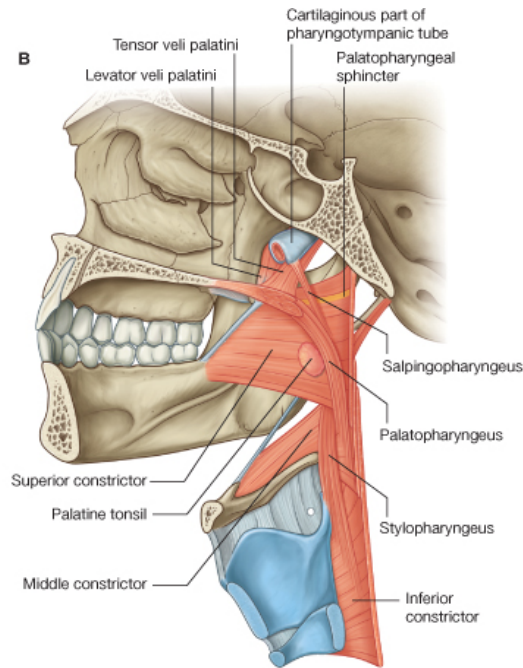
© Elsevier. Drake et al: Gray's Anatomy for Students - www.studentconsult.com

Figure 2.3: Saggital and posterior view of the constrictor muscles of the pharynx that constitute the pharyngeal wall [59]

Longitudinal muscles

The three longitudinal muscles of the pharyngeal wall, see fig. 2.4, are named according to their origins: stylopharyngeus from the styloid process of the temporal bone, salpingopharyngeus from the cartilaginous part of the pharyngotympanic tube (salpinx is Greek for tube), and palatopharyngeus from the soft palate. From their sites of origin, these muscles descend and attach into the pharyngeal wall. The longitudinal muscles elevate the pharyngeal wall, or during swallowing, pull the pharyngeal wall up and over a bolus of food being moved through the pharynx and into the esophagus.”

Many more muscles are directly or indirectly related to pharyngeal patency. If these muscles are impaired, like post-mortem or under anesthesia, the UA is prone to collapse [69].



© Elsevier. Drake et al: Gray's Anatomy for Students - www.studentconsult.com

Figure 2.4: Sagittal view of the longitudinal muscles structures of the pharynx [59]

The pharynx consists of three parts:

Oropharynx

The oropharynx lies posterior to the oral cavity, inferior to the level of the soft palate and superior to the upper margin of the epiglottis. As stated by Drake et al. [59] (pp. 945) “The anterior wall of the oropharynx inferior to the oropharyngeal isthmus consists of the base of the tongue and the epiglottic vallecula, the lateral wall is made up of the tonsil, tonsillar fossa, and tonsillar (faucial) pillars and the superior wall consists of the inferior surface of the soft palate and the uvula. The palatoglossal folds (arches), one on each side, that cover the palatoglossal muscles, mark the boundary between the oral cavity and the oropharynx. When holding liquid or solids in the oral cavity, the oropharyngeal isthmus is closed by depression of the soft palate, elevation of the back of the tongue, and movement toward the midline of the palatoglossal

and palatopharyngeal folds. This allows a person to breathe while chewing or manipulating material in the oral cavity. On swallowing, the oropharyngeal isthmus is opened, the palate is elevated, the laryngeal cavity is closed, and the food or liquid is directed into the esophagus. Due to the collapsibility of the pharynx, a person cannot breathe and swallow simultaneously, as the airway is closed at the pharyngeal isthmus and the larynx. “

Nasopharynx

The nasopharynx lies posterior to the apertures of the nasal cavity and superior to the soft palate. Postero-superiorly it extends from the level of the hard and soft palates to the sloping base of the skull (the posterior part of the body of the sphenoid bone and the basal part of the occipital bone). As stated by Drake et al. [59] (pp. 943 ff.) “The ceiling and lateral walls of the nasopharynx form a domed vault at the top of the pharyngeal cavity that is always open. The cavity of the nasopharynx is continuous below with the cavity of the oropharynx at the pharyngeal isthmus. The position of the pharyngeal isthmus is marked on the pharyngeal wall by a mucosal fold caused by the underlying palatopharyngeal sphincter, which is part of the superior constrictor muscle. The ground consists of the superior surface of the soft palate.

Elevation of the soft palate and constriction of the palatopharyngeal sphincter close the pharyngeal isthmus during swallowing and separate the nasopharynx from the oropharynx. There is a large collection of lymphoid tissue (the **pharyngeal tonsil**) in the mucosa covering the roof of the nasopharynx. Enlargement of this tonsil, known then as adenoids, can occlude the nasopharynx so that breathing is only possible through the oral cavity.”

Laryngopharynx

The laryngopharynx extends from the the superior margin of the epiglottis (C4 vertebral level) to the top of the esophagus (level C6). it includes the pharyngo-esophageal junction (postcricoid area), the piriform sinus, and the posterior pharyngeal wall. As stated by Drake et al. [59] (pp. 945) “The laryngeal inlet opens into the anterior wall of the laryngopharynx. Inferior to the laryngeal inlet, the anterior wall consists of the posterior aspect of the larynx. The cavity of the laryngopharynx is related anteriorly to a pair of mucosal pouches (**valleculae**), one on each side of the midline, between the base of the tongue and epiglottis. There is another pair of mucosal recesses (**piriform fossae**) between the central part of the larynx and the more lateral lamina of the thyroid cartilage. The piriform fossae form channels that direct solids and liquids from the oral cavity around the raised laryngeal inlet and into the esophagus”. Like the oropharynx located superiorly, the laryngopharynx serves as a passageway for food and air. It lies inferior to the upright epiglottis and extends to the larynx, where the respiratory and digestive pathways diverge. At that point, the laryngopharynx is continuous with the esophagus posteriorly. Air enters the larynx anteriorly while the esophagus conducts the bolus to the stomach.

Physiology of the Upper Airway

Even though the nose has been described to be responsible of 2/3 of the total airway resistance during sleep [70] and it even may increase in dependence of body position, it is the UA that is the critical cause for SDB [69].

The pharynx conducts air from the nose and oral cavity to the larynx, see fig. 2.5, and during breathing the pharynx remains patent. However, as it is also necessary for swallowing, the pharynx has the ability to collapse. Thus, the noncartilaginous segment of the UA (which extends from the nares to the vocal cords) is a hollow tube that, exceptuating the nares and the small intrapulmonary airways (the two ends of the respiratory airway), is the only collapsible region of the respiratory tract [60]. Thus, the pharynx has several shared functions that compete with and may impair each other. In fact, swallowing is associated with a short central apnea with laryngeal closure [69]. Furthermore, and in comparison to animals, the human's ability to perform complex speech and to walk in upright position inherently predisposes the UA to collapse. Studies have identified that the mechanism responsible for pharyngeal collapse depends on both anatomical [67] and active neuromuscular control factors [62], like abnormalities of the central nervous system, ventilatory drive, local UA muscle tone, sensation and reflexes.

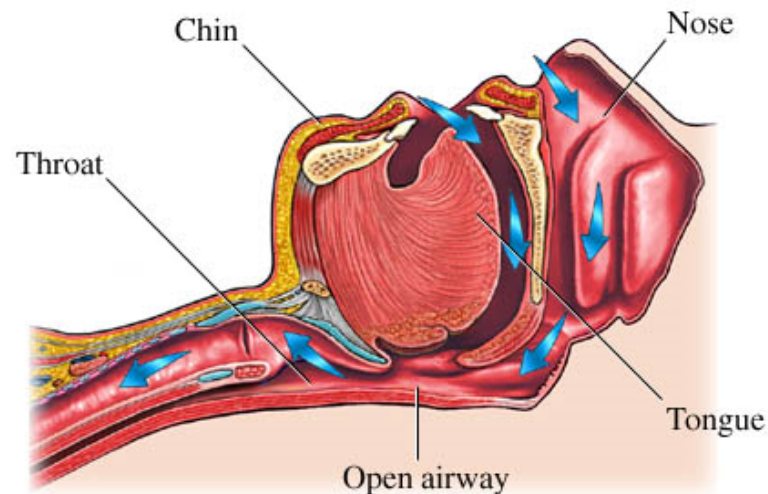


Figure 2.5: The flow of air through the normal upper airway during sleep [figure by Nucleus Communications, Inc.]

As commented before, more than 30 pairs of muscles are directly or indirectly related to pharyngeal patency. If these muscles are impaired, like during sleep, post-mortem or under anesthesia, the UA is prone to collapse [69]. During wakefulness the tendency of the UA

to collapse is countered by neuromotor mechanisms that provoke reflex muscle mechanisms in response to subatmospheric pressure and hypercapnia [69] but these mechanisms are decreased or absent after sleep onset.

The capability of the UA to resist collapse is individual and depends on such factors as the force developed by the dilating muscles of the UA. Factors that influence in pharyngeal tone include chemoreceptor afferents, UA pressure, flow receptors, changes in lung volume, sleep state and stage [69] or sleep deprivation, and pathologies, like muscular dystrophy, that weaken these muscles. Also the stiffness of pharyngeal soft tissues could result in UA collapse. Other factors such as alcohol ingestion, narcotic medicaments or fat deposits can reduce muscle tone during sleep and predispose the UA to collapse. In cases when the predisposition of UA collapsibility is high enough, some individuals may suffer of pathological events as OSA.

Models of the Upper Airway

Model of the Upper Airway as a Starling resistor

Schwartz et al. [65] and Gold et al. [66] modeled the pharyngeal airway at the velopharynx as a Starling Resistor, see fig. 2.6, and used continuous Positive Airway Pressure (cPAP) devices to determine the critical pressure below which the pharyngeal airway completely collapsed. The Starling resistor theory predicts that in a collapsible tube, inspiratory flow can increase with increasing driving pressure only up to a critical pressure value for the transmural pressure (the pressure difference between the inside and the outside of the UA), see fig. 2.6. If, during an inspiration, higher driving pressure is applied, the UA partially collapses, resulting in a stall or decrease in flow despite higher respiratory effort, also known as IFL. So, the Starling resistor model postulates that IFL occurs when the airway is highly compliant, like the hypotonic UA after sleep onset, even leading to soft tissue flutter

if the UA further collapses due to increased driving pressure. Isono et al. [60] have shown evidence that support the postulations by Schwartz et al. [65] that the velopharynx behaves like a Starling resistor for a certain range in airway pressure where it becomes very compliant. Others applied the Starling resistor theory to experimental settings to explain partial UA collapse [31] and snoring [69]. Gold et al. [66] used the critical pressure criteria to differentiate between snorers and populations with hypoapneas or obstructive sleep apneas, and in another later study, also differentiate between OSAHS and UARS patients [68].

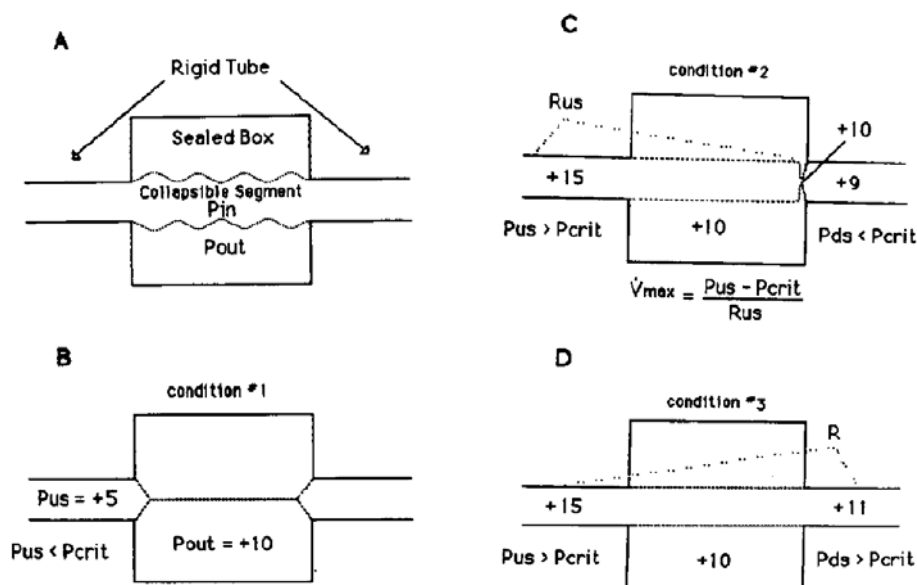


Figure 2.6: Modelling of the pharyngeal airway as a Starling Resistor. A: System overview, B: Collapsible segment remains collapsed and occluded, C: Collapsible segment flutters D: Collapsible segment is widely open [66].

Equation 1 represents the model as described by Gold et al. [66], which allows the representation of the airway resistance as the inverse of the slope of the linear regression graph, see also fig. 2.7.

$$\dot{V} = \frac{(P_{US} - P_{DS})}{R} \quad (2.1)$$

with \dot{V} being the airflow, P_{US} the pressure at the upper side of the airway, P_{DS} the pressure at the lower side of the airway, P_N the nasal pressure and R is the resistance of the airway.

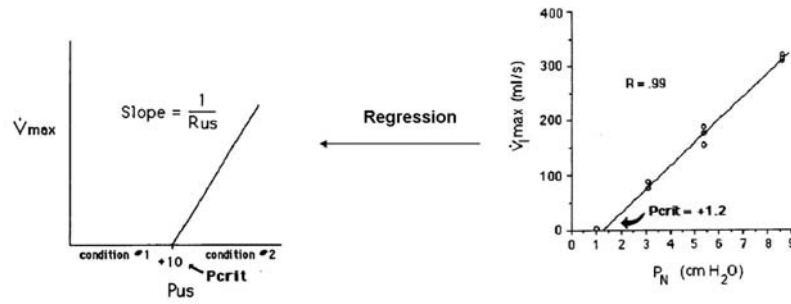


Figure 2.7: Determination by regression of the pharyngeal critical pressure [66]

A mathematical, multi-dimensional model of the Upper Airway

Starling's model presents an important limitation, as it describes the UA only as a single [70] or two [71] collapsible segments, characterizing flow by time-dependent but spatially invariant variables (lumped parameter model). This is why Aittokallio et al. [56] proposed a new, physiologically more compatible, model that also considered the longitudinal dimension of the collapsible UA, to predict the various flow traces that commonly occur in real patient populations, see fig 2.8.

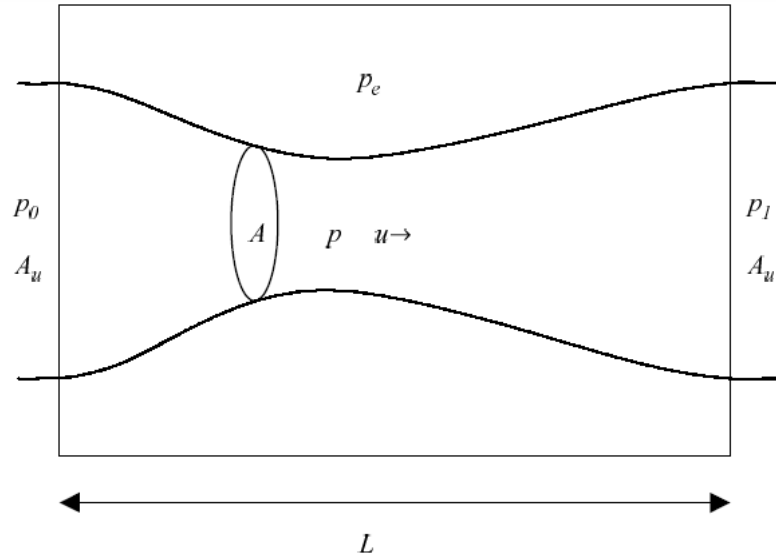


Figure 2.8: Decrease of the cross-sectional area A of the collapsible segment of the UA of length L enclosed in a chamber with external pressure (p_e). A_u is the constant uniform, cross-sectional area of the unstretched tube, while the flow is characterized by the temporally- and spatially variable cross-sectional area A , velocity u and pressure p . [56]

Aittokallio et al. [56] used a set of partial differential equations with time and space variance and some supplementary boundary conditions. Instead of analyzing the vibration of the UA (snoring sounds) his model analyzed the changes in flow shape that can be used to non-invasively assess IFL [16]. In a later study, Aittokallio et al. [15] were able to predict individual treatment responses with an adaptation of this model.

Please see Appendix A for a more detailed explanation on the origins and derivation of Aittokallio et al.'s mathematical model.

Syndromes of SDB

The obstructive sleep apnea/hypopnea syndrome (OSAHS)

Obstructive sleep apneas and hypopneas are caused by the predisposition of an individual to UA collapse. The negative pressure gradient created in the UA by the inspiratory drive may lead the UA to partially or completely collapse if the transmural forces developed by pharyngeal dilator muscles are insufficient [61, 62], see fig. 2.9 a and b, respectively. The velopharynx (the segment of the nasopharynx ventrally limited by the soft palate) appears to be the region of the pharynx most commonly associated with occlusion during OSA [63], see fig. 2.9, and therefore of utmost pathophysiological importance [60].

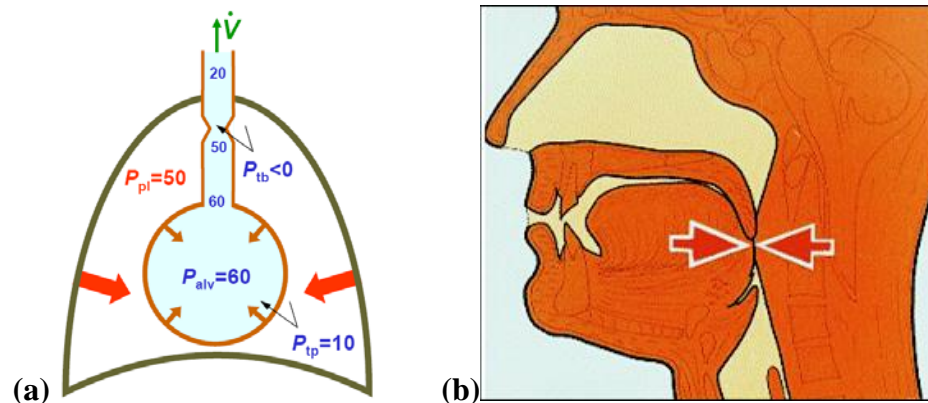


Figure 2.9: (a) when the pressure inside the UA exceeds, due to increased respiratory drive, the intramural pressure, inspiratory flow limitation (IFL) occurs (courtesy of D. Navajas, Biofísica, Universitat de Barcelona). (b) During an OSA event the velopharynx collapses, limiting the circulation of flow from the nostrils to the larynx [133].

While apneas represent a complete ($> 90\%$) cessation of flow, hypopneas are defined by a clear decrease ($> 30 - 50\%$) in airflow, lasting both a minimum of 10 seconds [6, 7]. Thus, while during a hypopnea or inspiratory flow limitation episode the UA collapses partially, see fig. 2.9a, during an apnea the upper airway collapses completely (which corresponds to

infinite UAR [72]), see fig. 2.9b. This leads to oxygen de-saturation, as the oxygen concentration in blood falls drastically and, as a consequence, the brain reacts with a micro-arousals which reactivates the tone of the pharyngeal dilator muscles, re-opening the UA. However, these micro-arousals cause sleep-fragmentation, which affects the quality of sleep. Severe OSAH syndromes are characterized by more than 70 arousals in an hour, leading to severe sleep fragmentation, see fig. 2.10. Even mild degrees of OSAHS may be associated with significant morbidity, including excessive daytime somnolence [3, 49, 50], long-term cardiovascular complications [9, 51, 55] and significant societal costs [49-54]. Even though hypopneas are caused only by a partial collapse of the UA and may appear as a more subtle event, subsequent hypopneas also lead to RERAs and consequently the clinical consequences of OSHS are almost identical to OSAS [8].

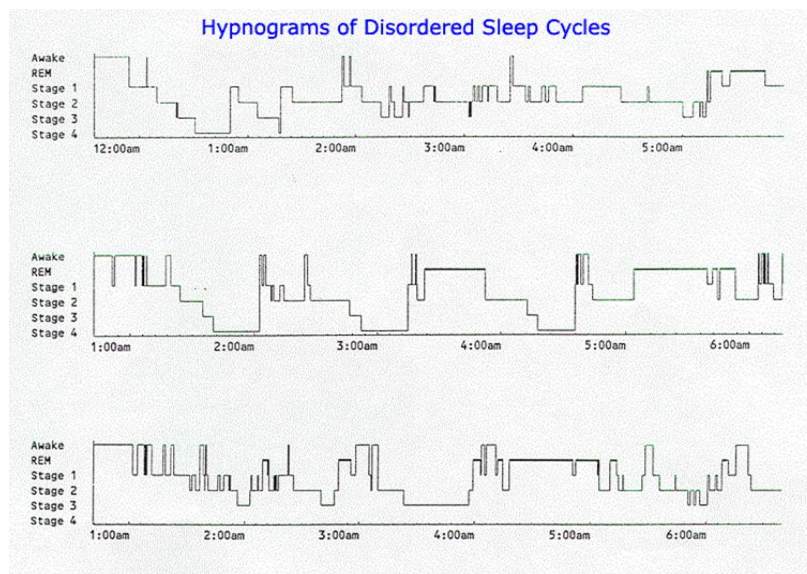


Figure 2.10: Sample hypnograms of patients with fragmented sleep. Notice that sleep stages are constantly interrupted by arousals, caused by OSAs, with a recurrent back-fall from sleep to the wake stage.

Studies have shown a high prevalence of the obstructive sleep apnea syndrome (OSAHS) in approx. a 5- 17% of the general population in dependence of the syndrome's severity [2, 5]. OSAHS usually affects approx. 5% of the population, concretely 2-4% of middle aged

males and 1-2% of middle-aged females [2, 5, 47, 48]. There are a number of risk factors for obstructive sleep apnea, see Table 2.1. As stated by Bao et al. [72] “In the middle-aged adult population, the most important risk factor is obesity, and even moderate increases in weight increase the risk of OSA. Obesity increases the rate of progression of disease, and weight gain further accelerates disease progression. In the elderly, however, OSA is not as closely associated with obesity. In children, the major risk factor for OSA is adenoidal-tonsillar hypertrophy. OSA is common in patients with craniofacial disorders; however, even in individuals without a specific disorder, alterations in craniofacial structure confer risk for OSA.” The typical patient affected by OSAHS has been reported to be mostly an obese (BMI > 27), male snorer over 40 years old [72].

Medscape® www.medscape.com		
Feature	UARS	OSAHS
Age	All ages	Children Male > 40 y old Female after menopause
Male:female ratio	1:1	2:1
Sleep onset	Insomnia	Fast
Snoring	Common	Almost always
Apnea	No	Common
Daytime symptoms	Tiredness Fatigue	Sleepiness (less common in children)
Body habitus	Slim or normal	Obese
Somatic functional complaints	Fibromyalgia Chronic pain Headaches	Rare
Orthostatic symptoms	Cold hands/feet Fainting Dizziness	Rare
Blood pressure	Low or normal	High
Neck circumference	Normal	Large
Source: Curr Opin Pul Med © 2004 Lippincott Williams & Wilkins		

Table 2.1: Clinical Differential Features in Upper Airway Resistance Syndrome (UARS) and Obstructive Sleep Apnea-Hypopnea Syndrome (OSAHS) [72]

Continuous positive airway pressure (cPAP) devices have been proven to be a valid therapy for OSAHS and represent presently the treatment of choice for this syndrome [2]. A nasal mask is usually attached to the patient's nose and the cPAP device creates a positive pressure in the UA of the patient, helping to avoid UA collapse during an OSA, see fig.

2.11. Alternative therapies like uvulopalatopharyngoplasty (UPPP) or intraoral devices that reposition the mandible forward during sleep, have not shown a comparable outcome to cPAP devices and are therefore only taken into consideration when cPAP therapy can not be applied [2]. As stated by Guilleminault et al. [77] (pp. 189) “The reasons why dental appliances may not completely relieve a patient are multiple, from problems involving soft tissues attached to the maxilla and advancing the mandible, to a narrow airway at the base of the tongue and difficulty shifting the hyoid bone forward even with nasal continuous positive airway pressure (CPAP).”

Therapy

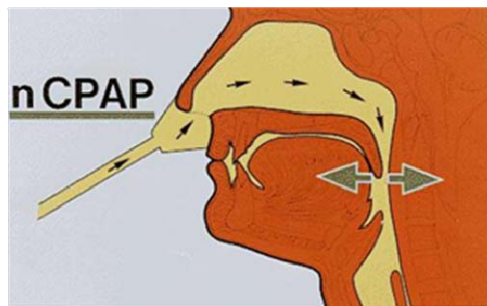


Figure 2.11: A typical cPAP mask attached to a patient's nose that creates a positive pressure flow that keeps the airway open [133]

The Upper Airway Resistance Syndrome (UARS)

Being OSAHS the most common and best diagnosed pathology in present day sleep labs, there still is a wide array of other obstructive, respiratory-effort related pathologies which are comparable to OSAHS in severity, but are much more difficult to diagnose and affect other type of populations [3, 32, 72]. One of these syndromes is the upper airway resistance syndrome (UARS) [3], although there is still significant controversy between experts if UARS is a distinct syndrome to OSAHS [73].

Repetitive Increased Upper Airway Resistance (IUAR) is defined as increasingly negative respiratory drive (respiratory effort) concomitant with decreased oronasal airflow in the

absence of frank apnea or oxygen desaturation. IUAR periods last one to three breaths and result in an EEG arousals with a duration of 2 - 14s [74]. IUAR is usually caused by a partial collapse of the UA that is followed by IFL. IFL has been commonly defined as a lack of increase in airflow despite increasing respiratory effort (respiratory drive). IFL is one of the more subtle respiratory events, being much more subtle than a hypopnea or an apnea. The hypotonic UA after sleep onset is highly compliant and can partially collapse due to high inspiratory drive, which can even lead to soft tissue flutter (snoring) if the UA further collapses due to increased driving pressure, see fig. 2.9. In order to diagnose UAR events and differentiate other pathologies, like e.g. differentiating between central and obstructive apneas, it is compulsory to use Pes measurement, as it is the gold-standard to assess respiratory effort [6, 7]. The absence of Pes measurement makes it difficult for sleep experts to diagnose and treat the listed pathologies and syndromes. However Pes measurement is not used in clinical routine due to its complexity and invasiveness.

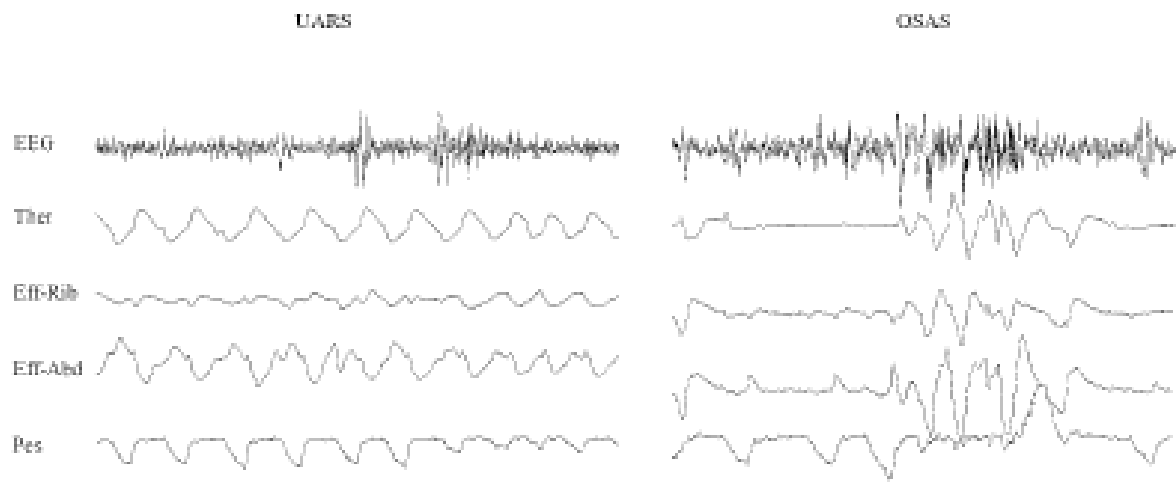


Figure 2.12: A RERA event in an UARS and in an OSAS patient. Note the absence of apnea in the UARS patient. [75]

IUAR events can be divided into two components:

1. **Increased Effort:** Pes manometry demonstrates a pattern of progressive negative Pes terminated by a change in pressure to a less negative pressure level associated with an arousal or microarousal.
2. **Arousal:** Brief arousals (3s to 10s shift to alpha or fast theta in EEG frequency)

As stated by Loube et al. [75] “The Respiratory Effort Related Arousal (RERA) is an event characterized by increasing respiratory effort for more than 10s leading to an arousal or microarousal from sleep that did not fulfill the criteria for hypopnea or apnea”, see fig. 2.12. There are several polysomnographic scoring criteria that allow the differentiation between OSAH and UAR events, see Table 2.2.

Medscape® www.medscape.com		
	UARS	OSAHS
Sleep onset latency	Long	Short
AHI	< 5	≥ 5
Minimum O ₂ saturation	> 92%	Often < 92% (rare in children)
Respiratory effort-related arousals	Predominant	Minimal
Cyclic alternating patterns	Frequent	Less common
Power spectral EEG analysis	Higher α power Higher δ in rapid eye movement	Less α or δ
AHI, apnea-hypopnea index as events per hour.		
Source: Curr Opin Pul Med © 2004 Lippincott Williams & Wilkins		

Table 2.2: Polysomnography and Power Spectral Analysis in Upper Airway Resistance Syndrome (UARS) and Obstructive Sleep Apnea-Hypopnea Syndrome (OSAHS) [72]

Increased Upper Airway Resistance (IUAR) is a recognized cause for sleep disruption and fragmentation [74]. This implies that a lot of patients with symptoms indicative of sleep disorders remain untreated and develop chronic illnesses such as EDS, Chronic Fatigue Syndrome (CFS), chronic insomnia, sleepwalking, etc. [9, 76, 35].

The central apnea/hypopnea Syndrome (CSAHS)

In the same way as OSA, central sleep apnea (CSA) is defined as a complete cessation of flow for more than 10s [6]. The cessation of flow in this case is not caused by the collapse of the UA, but because of lack of neural input from the central nervous system to the diaphragm. CSAHS is much less common than OSAHS, affecting just a 10-15% of the SDB-affected population [2], but it is usually associated with heavy snoring [78]. It usually affects subjects that, being awake, have a high sensitivity to CO₂ and low arterial Pco₂ (typically around 35.0 mm Hg), therefore being closer to the CO₂-dependent sleep apnea threshold [2]. Thus, one of the most important risk factors for CSA is hypocapnia [2]. However, during wakefulness and quiet breathing, because of non-specific stimuli that anticipate the changes in blood gases, chemosensitivity is of low importance. But the dependence on chemosensitivity increases during sleep, peaking at stages 3–4 of NREM sleep [77].

As stated by Guilleminault et al. [77], “normally, the upper airway sensors (pharyngeal and laryngeal) inform the brainstem that increased resistance has occurred and, reflexly, enhancement of contraction of upper airway dilators then occurs. Despite reduced diaphragmatic effort (owing to diminished stimulation of phrenic motor neurons associated with decrease in CO₂ sensitivity at sleep onset), this allows breathing even if shallow. If pharyngeal and laryngeal receptors are only partially or completely non-functional adjustment to sleep onset phenomena will be impaired. Since 1992, studies have demonstrated blunting or destruction of pharygo-laryngeal sensors related to the development of a local neuropathy, probably of variable severity based on duration of the problem”.

Clinically, the most common form of central apnea is found in Cheyne-Stokes’ respiration, especially in patients with stroke and with congestive heart failure [2]. CSA is treated with

a bright spectrum of different therapies that are completely different to the therapies of OSA, like drug intervention (acetazolamide has been used to treat repetitive CSA [77]), rocking bed, diaphragm pacing, nocturnal mechanical ventilation and weight reduction [79]. As the treatments of OSA and CSA are vastly different from each other, it is imperative for choosing the correct treatment, to reliably diagnose the respective syndrome. The gold-standard technique to differentiate between obstructive events is, again, Pes measurement, as it allows a reliable assessment of respiratory effort [6, 7].

Conclusions

There are several pathologies that affect respiration during sleep and belong to the family of SDB. Obstructive events such as obstructive sleep apneas/hypopneas or IFL are related to higher UA collapsibility during inspiration, while central sleep apneas/hypopneas are more related to a dysfunctional central nervous system.

Despite their different etiology, all of these pathologies have a considerable morbidity in present day's population and may result in severe clinical consequences for the affected patients. The correct diagnosis of these syndromes is essential to allow the best choice of therapy. However present day techniques are limited or too invasive for a correct differentiation between some of these events.

Chapter III: Concepts of sleep monitoring and nocturnal polysomnography (NPSG)

Introduction

The diagnosis of OSAHS and related pathologies are performed in clinical sleep laboratories where the patient usually has to stay for several nights. For decades, the classical tool for diagnosis of most of sleep-related pathologies has been full nocturnal polysomnography (NPSG).

Sleep medicine is still a young field in medical sciences but its diagnostic and therapeutic weight is becoming more and more important as we begin to understand all the consequences of sleep pathologies.

Classical nocturnal polysomnography (NPSG)

In healthy subjects, sleep presents a cyclical and continuous pattern of sleep stages [80]. Starting from the awake state, the sleep cycle usually starts with stages Non-REM (NREM) 1 and 2, which combined are considered the light sleep stage. From light sleep the transition goes to deep sleep, stages NREM 3 and 4. The cycle usually ends with a Rapid-Eye-Movement (REM) stage of variable duration. This whole sleep cycle is repeated 5 to 6 times during the total sleep time (TST), while the length of the REM stages increases over the night. A hypnogram of a healthy patient represents the transition through the different sleep stages over the whole night, see fig. 3.1.

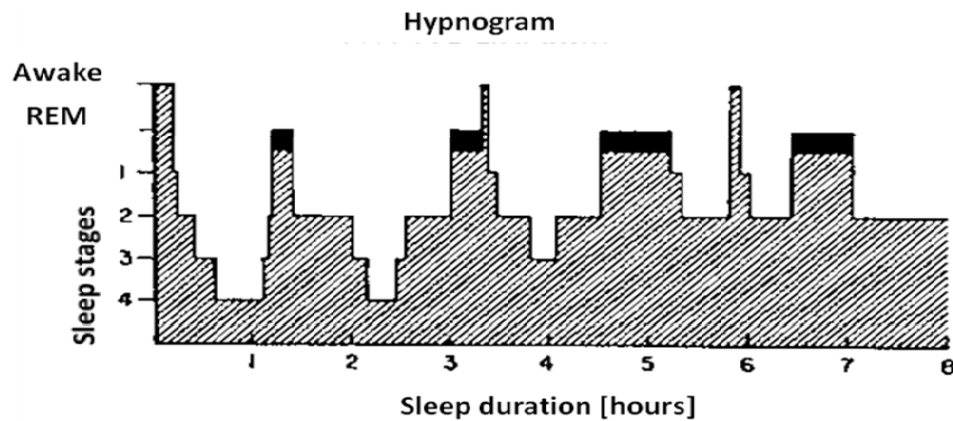


Figure 3.1: A typical hypnogram of a healthy subject [133]

Like commented in chapter II, sleep disturbances like OSAH provoke micro-arousals that interrupt the normal sleep cycle. In case of a high recurrence of OSAH during the whole night the result is a high disturbance of the transitions between sleep stages, called sleep fragmentation, see fig. 2.10 and a decrease in number and duration of REM stages. REM stages are considered to be crucial for mental and physical regeneration [6]. Thus, sleep fragmentation results in excessive daytime sleepiness and fatigue [2, 80].

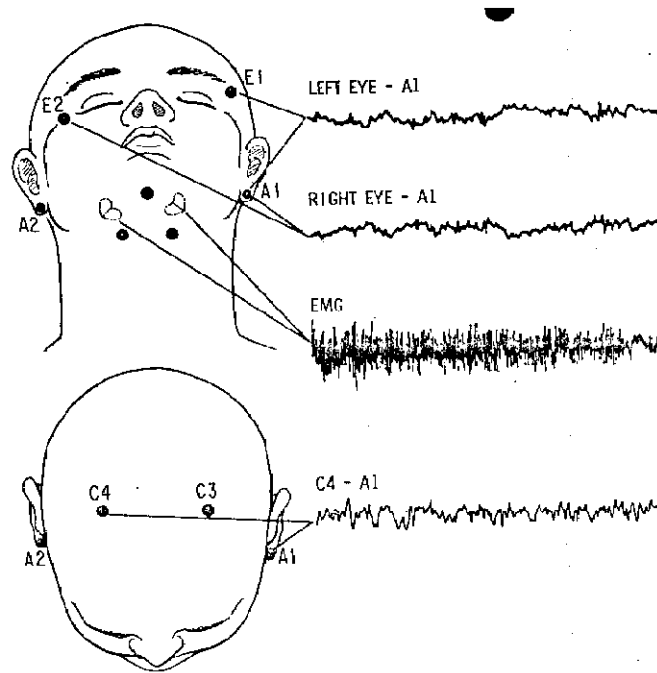


Figure 3.2: The five typical derivations needed to create hypnogram according to R&K [80], figure [133].

According to Rechtschaffen & Kales [8], five derivations are needed to determine the sleep stages and create a hypnogram, see fig. 3.2: 2 EEG channels at derivations C4A1/C3A2, 2 EOG channels (left/right) and 1 sub-mental EMG channel.

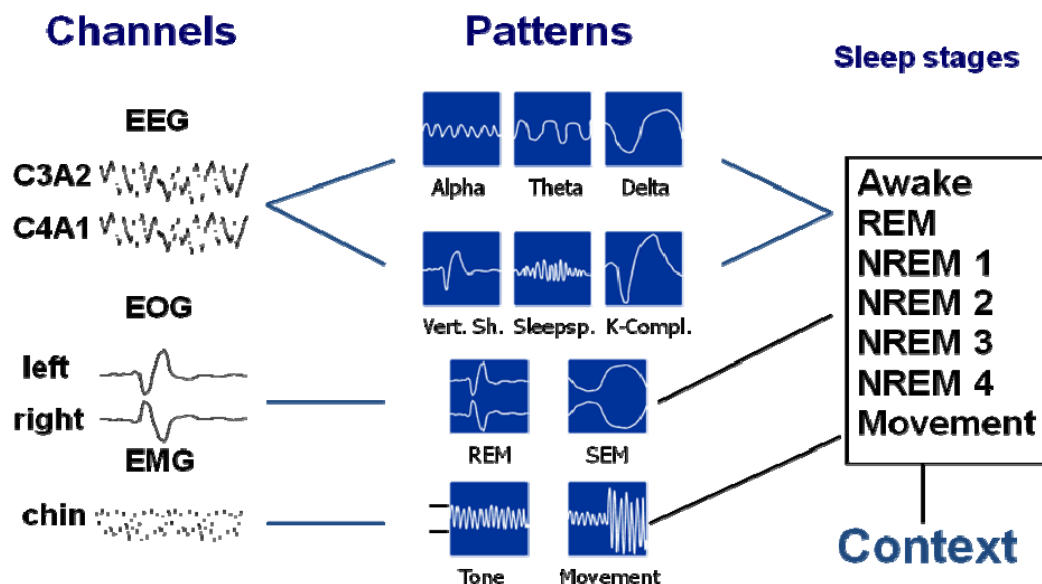


Figure 3.3: The typical signal patterns that appear in the 5 derivations of R&K (courtesy of M, Schwaibold [133])

According to R&K [80], a whole set of distinctive signal patterns can be recognized in these derivations, see fig. 3.3. The manual of R&K [80] set up a table of rules, see fig. 3.4, that indicated how the incidence of these signal patterns could be used to classify the sleep stages and create a hypnogram.

	Alpha	Theta	Delta	Vert. Sh. W.	Sleepspind.	K-Complex	REM	SEM	High Tone	Movement
Awake	✓	✗	✗	✗	✗	✗	✓		✓	✓
REM			✗		✗	✗	✓	✗	✗	✗
NREM 1		✓		✓	✗	✗	✗	✓		✗
NREM 2		✓			✓	✓	✗			✗
NREM 3	✗		✓				✗	✗		✗
NREM 4	✗		✓				✗	✗		✗
Movement										✓

Figure 3.4: The rules of R&K to classify sleep stages (courtesy of M. Schwaibold [133])

However, in present day NPSGs, the recording of more signals than the 5 R&K derivatives has become usual [6, 7], such as oronasal flow (acquired with a nasal cannula or a pneumotachograph), ECG signal, leg-EMG, blood pressure and SpO₂ (plethysmography), snoring sounds (audio signal recorded with a tracheal microphone), respiratory movements at thorax and abdomen (recorded with resistive inductance plethysmography (RIP)-belts), etc., see fig 3.5, in order to support the diagnosis of a whole spectrum of other sleep pathologies.

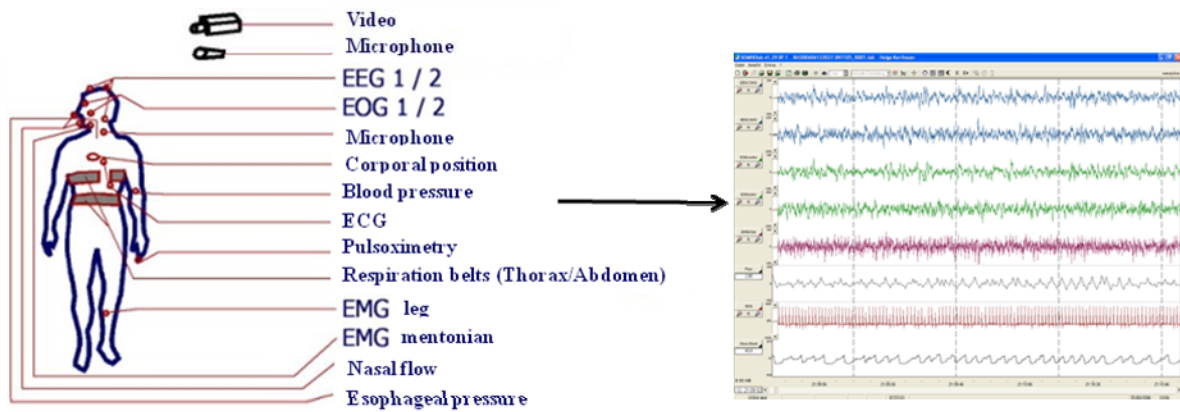


Figure 3.5: Typical set of signals recorded during full NPSG at a sleep lab in present day [133]

However, esophageal pressure (Pes) measurement, despite being the gold-standard to assess respiratory effort [6], is not commonly used in clinical routine due to being a very complex and invasive technique that causes patient discomfort and disrupts sleep [10]. This implies that not always a gold-standard diagnosis can be performed, especially in cases of more rare pathologies like UARS or CSAHS. So, a lot of patients with symptoms indicative of sleep disorders remain untreated or are not treated correctly, and can develop chronic illnesses such as EDS, Chronic Fatigue Syndrome (CFS), chronic insomnia, sleepwalking, etc. [9, 76, 35]. Therefore the developments of non-invasive techniques that assess respiratory effort are necessary, and extensive research has been performed in this direction in the last decade.

NPSG recording techniques to assess respiratory effort

On one side, and as has been commented before, esophageal pressure measurement represents the current gold-standard to assess respiratory effort and should therefore be mandatory in any study to validate new automatic classification techniques. On the other side, it appears that the airflow signal is one of the most promising non-invasive signals to assess SDB related events [14 - 16] and estimate changes in UA resistance.

Therefore, in the following, the current insights on recording sensors and techniques of the airflow signal and the esophageal pressure signal will be commented in detail.

Respiratory monitoring in NPSG: nasal cannula vs. plethysmography

SDB has finally been recognized as a common disease, thus the focus has been shifted from using the EEG to characterize sleep to a greater emphasis on respiratory monitoring. However the tools to detect respiration have only recently begun to evolve [90]. In the past, thermistors were the most commonly used devices to measure airflow, because of their ease of use and patient comfort. Thermistors allow measuring the temperature changes caused by inspiratory and expiratory airflow at the nostrils. However, thermistors have strong limitations as they represent only a qualitative indicator of airflow, see fig. 3.6, and do not allow to register events other than apneas (complete cessation of flow). So they fail in the detection of subtle respiratory events related to a partial obstruction of the UA, such as hypopneas or IFL [90, 91]. Thus, currently only two different devices, nasal cannulas and pneumotachography, are recommended for use in clinical routine of NPSG [6, 7]. In the last decade, an important discussion has flourished about which of these two devices is the optimal for use in clinical routine.

PEAK INSPIRATORY FLOW (SIMULTANEOUS COLLECTION)

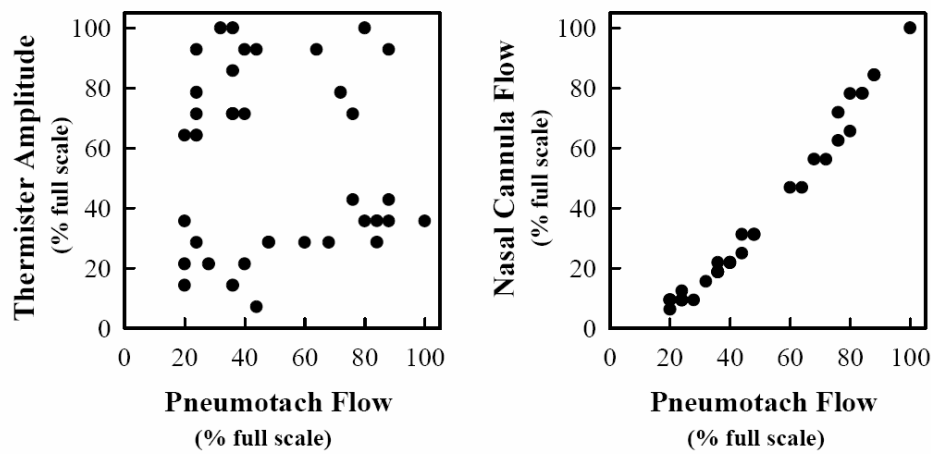


Figure 3.6: An example of the relationship between true flow amplitude, as measured by a pneumotachograph, and a thermistor (left) and a nasal cannula device (right). Note the lack of relationship between the thermistor and the pneumotachograph flow recordings. [90]

Pneumotachography represents the gold-standard to quantitatively measure airflow [6, 7] but it has the disadvantage to be relatively intrusive and depend on complex devices that are therefore not commonly used in clinical routine.

Flow measurement with a nasal cannula/pressure transducer delivers a “semiquantitative” flow shape signal [6, 14, 92] as the flow signal can not be calibrated [16, 14, 17, 18, 19]. However, Hosselet et al. [16] stated in their study that (pp. 1461) “a nasal cannula/pressure transducer system provides a noninvasive indicator of flow limitation (defined by the actual driving pressure flow characteristics) and that this can be useful to identify periods of elevated upper airway resistance in both normal subjects and patients with sleep disordered breathing”. In order to justify the use of the nasal cannula signal as “nasal flow”, Hosselet et al. [16] (pp. 1462) “demonstrated that the relationship between this signal and a simultaneous pneumotachographic flow signal is essentially linear over the relevant range”, see figure 3.7, as had also been previously shown by Montserrat et al. [92, 93].

Hence, a result obtained with a nasal cannula device should also be reproducible with a quantitative measurement technique like a pneumotachograph [16, 92, 93]. Hosselet et al.'s [16] methodology and results have in fact been quoted and reproduced by other studies using nasal cannula [14, 94] as well as quantitative pneumotachograph flow [16, 71, 94].

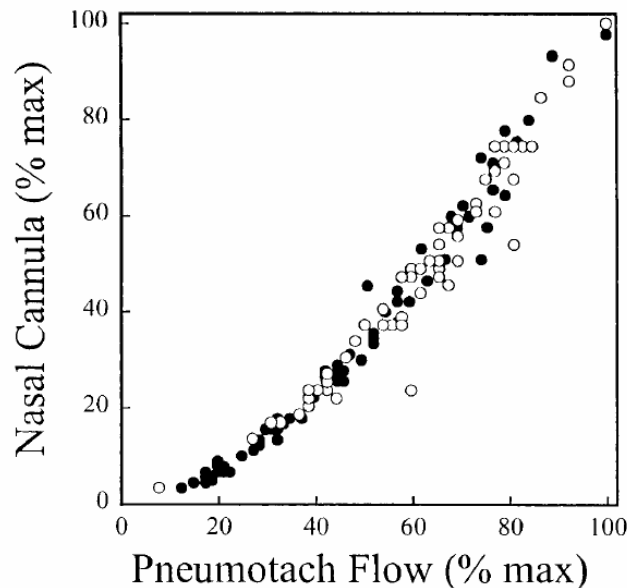


Figure 3.7: “Comparison of signal from a nasal cannula/pressure transducer system used for monitoring respiration and simultaneously obtained pneumotachograph flow from a mask. Awake flow data were collected from two subjects (*open and closed symbols*) over a range of breathing patterns and expressed as percent of maximal signal in each subject and in each signal. Flows ranged from 2 to 50 L/min. Overall, the relationship is curvilinear in nature (quadratic as shown by Montserrat et al.), but is also nearly linear in the range of normal breathing.” [16, pp. 1462]

In another study, Ayappa et al. [14] concluded that (pp. 763) “the nasal cannula/pressure transducer provides a non-invasive reproducible detector of all events in sleep disordered breathing” and that (pp. 771) “the nasal cannula is the tool of choice for monitoring respiratory airflow during sleep in both clinical and research sleep studies“. These SDB events include events such as apneas, hypoapneas, respiratory effort related arousals (RERAs) and inspiratory flow limitation (IFL) [14].

Furthermore, current NPSG guidelines [6, 7] explicitly recommend nasal cannula/pressure transducer system as flow measurement devices for clinical and

research applications for the detection of the mentioned SDB events. Norman et al. [19] and Aittokallio et al. [17, 18] did also work with and applied different classification and clustering techniques to an uncalibrated flow signal recorded with a nasal cannula/pressure transducer system. Their classification techniques were based on the identification and analysis of airflow patterns, obtaining valid and reproducible results. Nasal cannula devices are validated and commercially available devices that should deliver a reliable flow signal, as mentioned in several studies [14, 16 - 19]. Given all this evidence by the current literature, the nasal cannula/pressure transducer system should be appropriate for the purposes described in this study and should not represent any obstacle for a proper reproduction of the methodology and the results obtained here in any clinical or scientific research environment, even if quantitative recording devices, such as a pneumotacograph, are used for its reproduction [14, 16, 92, 93].

As our non-invasive classifier has the objective to be adopted in clinical routine, the flow sensor had also to be commonly used in clinical routine. Obtaining a conventional pneumotachograph flow requires a tight-fitting face mask, which may be excessively intrusive for routine sleep monitoring [16]. The nasal cannula device is a widespread and commonly used sensor and has some characteristics, like being simple, inexpensive and non-obstructive, that makes it ideal for clinical routine. For more information on flow pattern analysis, please refer to chapters VI and VII.

Esophageal pressure measurement

Esophageal pressure (**Pes**) measurement is currently the gold-standard to acquire information on respiratory effort, which is reflected by the pressure changes in the pleura [6]. Although the absolute values are only approximative, the esophagus, because of being a passive structure and due to its close location to the pleura, see fig. 3.12,

reliably transmits the relative changes in pleural pressure during inspiration and expiration.

Esophageal pressure measurement is normally performed with a catheter that is introduced through the nostrils and, after anaesthezing the nasopharynx and asking the patient to swallow, the catheter is placed in the lower third of the abdomen [82, 136], see fig. 3.8.

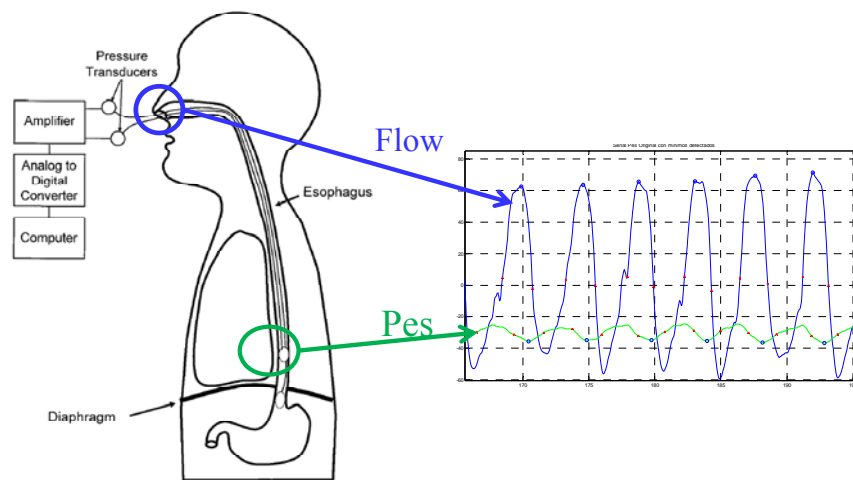


Figure 3.8: Layout of esophageal pressure measurement with a balloon catheter [82]

Catheter placement

As stated by Benditt et al. [82], also see fig. 3.9., “The lung and chest wall are 3-dimensional mechanical structures that can change in volume under the influence of pressures applied naturally by the respiratory muscles or artificially by applying positive pressure to the airway (i.e., positive-pressure ventilation) or negative pressure external to the chest wall (i.e., negative-pressure ventilation, such as the “iron lung”). The lung and chest wall move together, conjoined by the pleural space, which is in fact only a potential space. The pressure in the pleural space is denoted P_{pl} , and at rest in the upright human it is generally slightly negative, because the lung is a passive structure that is elastic and has a tendency to recoil to a smaller volume than the respiratory

system combination (lung and chest wall together). The lung is prevented from collapsing because of the tendency of the chest wall to recoil outwards and the negative value of P_{pl} . At the end of a relaxed exhalation (to functional residual capacity) and with the mouth open, the alveolar pressure (P_{alv}), the pressure at the airway opening (P_{AO} or P_m), and the atmospheric pressure (P_{atm}) are equal. Thus, at functional residual capacity with the mouth open, the distending pressure of the lung (P_L) is equal to the pressure inside the lung P_{alv} (which in this case is equal to P_{atm}) minus the pressure in the pleural space P_{pl} (Fig. 3.9). The importance of this is that the distending pressure across the lung (transpulmonary pressure) determines the volume of the lung. Changes in distending pressure result in changes in lung volume and therefore ventilation. Thus, to understand ventilation—a primary objective in respiratory medicine—we must understand and be able to measure P_{pl} and P_{alv} . This will in turn allow us to calculate the all-important distending pressure of the lung, chest wall, and respiratory system.

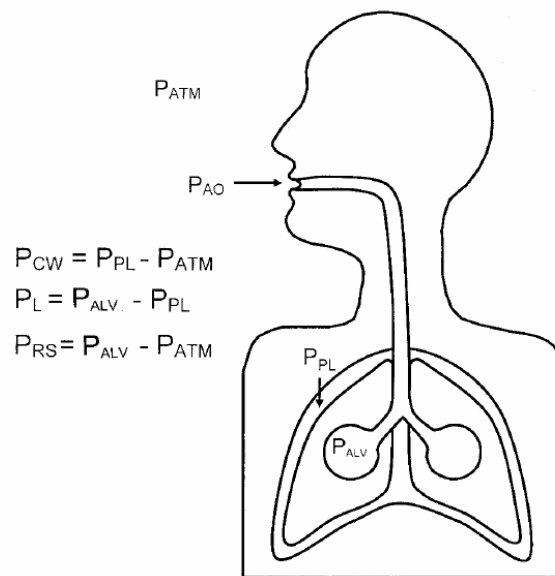


Figure 3.9: Elastic properties of the lung, with P_{AO} as the pressure at the airway opening, P_{CW} as the transchest wall pressure, P_{RS} as the trans-respiratory system pressure, P_{atm} as the atmospheric pressure, P_{pl} as the pressure in the pleural space, P_{alv} as the alveolar pressure (pressure inside the lung) and P_L as the distending pressure of the lung (transpulmonary pressure) [82]

As noted above, P_{alv} is measured by assessing P_{AO} during a static maneuver when, with an open glottis and uninterrupted airway, $P_{alv} = P_{AO} = P_{atm}$. We can easily measure P_{atm} , and by convention, P_{atm} is said to equal a pressure of zero. P_{pl} is measurable directly only by placing a catheter in the pleural space, which is not usually possible in clinical practice. Fortunately, the pressure in the lower one third of the esophagus (P_{es}) closely approximates the pressure in the adjacent pleura when the subject is in the upright posture.”...”Because the body of the esophagus is essentially a passive structure (except during a swallow), able to transmit pressure from the adjacent pleural space (P_{pl}) to the measurement catheter in the esophagus, P_{es} is a reasonably close surrogate for P_{pl} in a human being in the upright posture. This does not necessarily hold true in the supine posture, in which the mediastinum may compress the esophagus, and compression of the posterior and inferior portions of the lung can create large regional differences in pleural pressure. In addition to the measurement of P_{es} , it is also possible to measure the gastric pressure (P_{ga}) by placing another catheter more distally, in the stomach. P_{ga} closely approximates the pressure in the abdominal cavity. With accurate measurements of P_{pl} and abdominal cavity pressure, a wide variety of useful measurements of the mechanical respiratory system can be determined.”...” The balloon catheter (or catheters) is passed through the nares (nose) into the posterior pharynx. At this point the subject is instructed to swallow (if spontaneously breathing) and the catheter is passed into the esophagus and then into the stomach. The catheter is attached to the transducer/recorder system, and 2.0 mL of air is injected into the balloon. Then 1.5 mL of air is withdrawn, to leave 0.5 mL of air in the system to partially inflate the balloon and the catheter. The presence of a positive pressure deflection during inspiration indicates that the balloon is located in the stomach, if the diaphragm is functioning. The catheter is then slowly withdrawn into the esophagus, where the pressure reads negative

during inspiration. The catheter is then withdrawn another 10 cm after the initial negative deflection, to ensure that the entire catheter is within the esophagus. The catheter will be posterior to the heart, and cardiac pulsations appear on the waveform. The catheter tip will be approximately 35–45 cm from the nares. It is helpful to mark the catheter at 10-cm intervals prior to placement, and some commercially made devices are pre-measured and marked.“

As there is no official guide or consensus for the positioning of the catheter, each study used a different technique to assure the right positioning:

- As stated by Stoos et al. [26], “A standard, closed-end, esophageal latex balloon system with a total length of 86 cm and a 9.5 cm distal balloon was placed transnasally after local anaesthesia in the distal oesophagus (**subject height · 0.288 cm from the nares**), inflated with 1 cc of air, and connected to the pressure transducer of the Viasys PSG recording system. A 4-point calibration (atmospheric pressure, 10, 20, and 30 cmH₂O) using a water-filled manometer was performed at the beginning and end of the study.”
- As stated by Loube et al. [75], “measurement of Pes” was performed “with a 2.7-mm-diameter electronic pressure catheter with the tip positioned in the midesophagus by radiograph. Once correctly positioned, the catheter was secured at the nose with adhesive tape. The catheter tip transducer was referenced to atmospheric pressure and calibrated with a water manometer to 250 cm and 150 cm H₂O.”
- As stated by Horiuchi et al. [85] “Pes was recorded simultaneously using a microtip type pressure transducer (MPC500: Millar, Houston Tex) that was inserted 35 cm from the nostrils. Signals from the transducer were amplified by

a signal conditioner and converted by a four channel A/D converter (Power Lab/4s: ADI Instrument Pty. Ltd., Castle Hill, Australia)”).

Catheter specifications

Prior esophageal manometry systems used either water-perfused or solid-state pressure transducer but even more considerable clinical skills were necessary to obtain accurate results [87, 89]. The hydraulic or pneumatic pressure differences were then converted with an external transducer into an electrical signal. Recently developed single-use, disposable esophageal manometry catheters seem to be promising alternatives to solid-state manometry systems in measuring intra-esophageal pressure [88, 89].

Also a flexible microtransducer catheter has become available for medical monitoring. This new generation of catheter tip pressure transducers may provide a simpler and more reliable tool for assessing transpulmonary pressure changes in infants [87]. The use of a pediatric feeding catheter instead of the esophageal balloon has made the procedure more tolerable in both adults and children [72]. However, nowadays most catheters are uni- or bi-directional pressure-tip catheters with a piezoresistive pressure sensor that translates the mechanical forces into electrical values directly in the catheter’s tip. The pressure sensor normally consists of a microchip with a pressure-sensitive membrane on its surface. A Wheatstone bridge converts the slight deformations of the membrane into an electrical signal. Finally, the electrical signal normally has to be amplified with an external signal amplifier before being digitally processed.

Other commercially available catheters used in the literature are

- Standard, closed-end, esophageal latex balloon system, Ackrad Laboratories, distr. by Advantage Medical Inc. USA – 2004 with a total length of 86 cm and a distal balloon length of 9.5 cm [26, 27]

- Electronic pressure catheter, Gaeltec, Hackensack, NJ, USA – 1999 with a diameter of 2.7 mm [75]
- Microtip pressure transducer MPC500 by Millar, Houston Tex and a four channel A/D converter by Power Lab/4s: ADI Instrument Pty. Ltd., Castle Hill, Australia [85].

Problems with Pes measurement

Problems with esophageal pressure measurement comprise

a) False measurements due to changes in body position

- In the supine posture the mediastinum may compress the esophagus. The compression of the posterior and inferior portions of the lung can create large regional differences in pleural pressure [85]
- In supine position the $\Delta P_{es} / \Delta P_m$ ratio tends to increase when the balloon is being moved towards the cardia, suggesting that in supine position there is a horizontal gradient in changes of pleural surface pressure, with the greater values towards the lung base. [86]

However with repositioning the balloon at a different level this measuring error can be corrected [86]. Thus, the correct positioning of the balloon requires a lot of experience and clinical practice.

As stated by Benditt et al. [82], in order “to assure that the esophageal catheter is in the correct position, a dynamic “occlusion test” is performed to assure that P_{es} is changing in concert with P_{AO} . In this test the subject makes inspiratory and expiratory efforts against a closed airway. Equivalence of P_{AO} and P_{es} over a range of pressures during respiratory effort is believed to ensure the accuracy of the P_{es} measurement.”

b) Influence on sleep

Esophageal manometry has been associated with small but statistically significant ($p < 0.05$) decrements [10] in

- total recording time
- total sleep time
- sleep efficiency
- percent Stage 2 sleep and percent rapid-eye-movement (REM) sleep
- increases in latency to REM sleep
- latency to persistent sleep
- percent Stage 3/4 sleep.

However the differences are of such a small magnitude so that their clinical significance is questioned. Pes measurement did not have any influence in the number of awakenings per hour of sleep, latency to sleep onset and percent Stage 1 sleep.

It was concluded that the effects of monitoring Pes on sleep architecture are minimal, and that the decision of whether or not to use the technique can be based to a large extent on whether quantitative information about respiratory effort will be useful. [38]

c) Patient discomfort

Inspiratory effort is determined by estimating pleural pressure by monitoring esophageal pressure (Pes), which is invasive and uncomfortable, and may adversely affect sleep, and is thus not routinely used by most sleep centers [6, 10, 21]. These problems are major hurdles in clinical practice and the main reason why esophageal pressure measurement is not included in present clinical routine. Thus, to find a non-invasive alternative to esophageal pressure

measurement which is as reliable reflecting respiratory effort, is of great importance and one of the major problems in present SDB diagnostics.

Characteristics of the esophageal pressure signal

The esophageal pressure signal (Pes) represents the pressure changes in the pleura during inspiration (and expiration). The harder the breathing effort is, the deeper will be the pleural pressure values reflected in the Pes signal. Three abnormal forms of Pes tracing can be described [72]

- A “**Pes crescendo**” is a progressively increased negative peak inspiratory pressure in each breath that terminates with an α -wave EEG arousal or a burst of δ -wave. Unlike a hypopnea, this event is not associated with a drop in oxygen saturation of 3%.
- Another characteristic event is the “**Continuous Sustained Effort**”: the Pes tracing shows a relatively stable negative peak inspiratory pressure that is more negative to that seen in the baseline and nonobstructed breaths and lasts longer than four breaths.
- The “**Pes reversal**” represents an abrupt drop in respiratory effort indicated by a less negative peak inspiratory pressure after a sequence of increased respiratory efforts independent of the EEG patterns, see fig. 3.10.

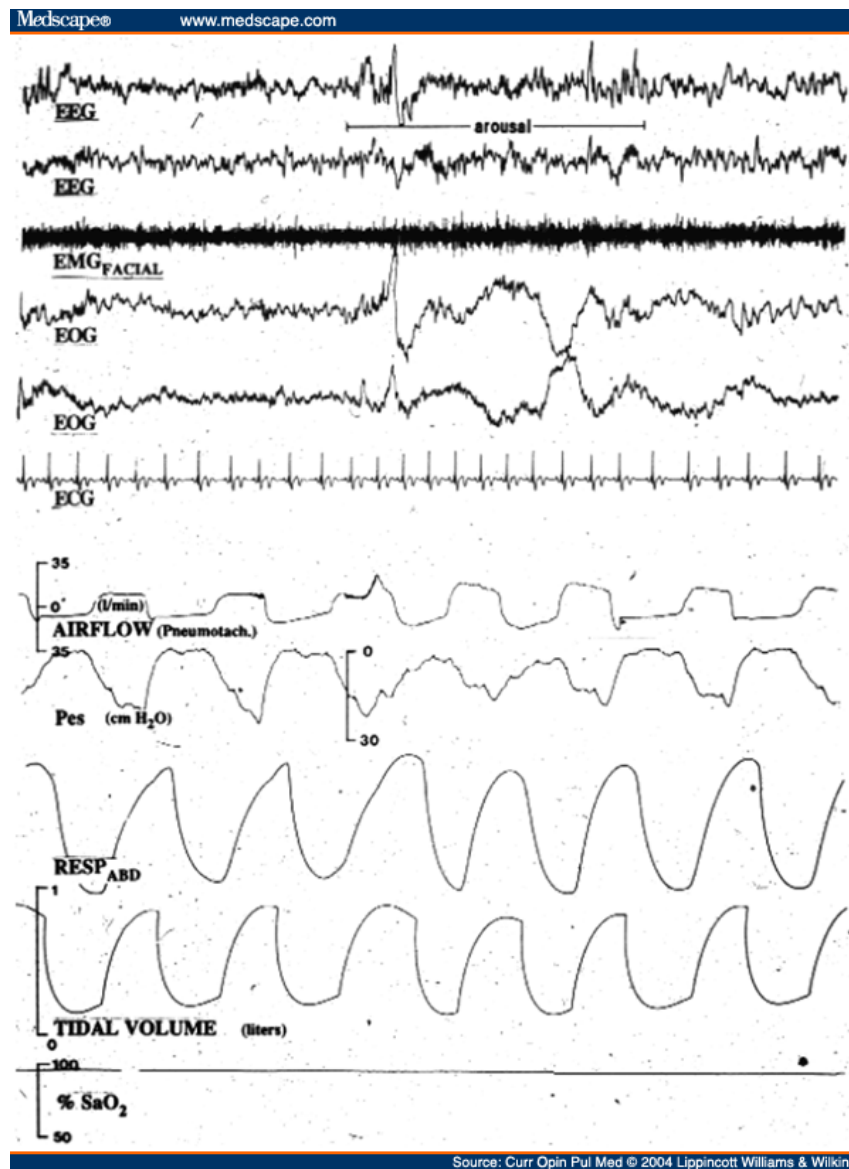


Figure 3.10: A flow limitation is seen in the flow signal (pneumotachograph), associated with abnormal peak end inspiratory Pes on the first 2 breaths on the left side of figure. An EEG arousal occurs at the end of the flow limitation event with an abrupt decrease in respiratory effort (Pes signal), a *Pes reversal* (it starts with the third breath from left) that is associated with the EEG arousal. [72]

Conclusions

For the last decades, NPSG has been the standard method to diagnose sleep-related pathologies and assess a subject's hypnogram. Esophageal pressure measurement represents the gold-standard to measure respiratory effort but, due to its invasiveness and patient discomfort, it is not used in clinical routine. Several promising techniques

have been explored to find a non-invasive alternative to Pes-measurement for reliably diagnosing SDB-related pathologies, such as snoring analysis, analysis of the presence of CAPs, PTT, etc. However, it appears that for respiratory related events, the flow signal is the most promising signal to acquire UA-resistance and respiratory related information. Nasal cannula devices have proven to reliably reflect changes in UA-resistance and permit the diagnosis of most SDB events and, unlike pneumotachography, these devices are non-obtrusive, comfortable and commonly used in clinical routine.

Chapter IV: New patient study and NPSG database with esophageal pressure measurement

Introduction

The basis of this thesis was the development of a completely new NPSG patient database with the systematic recording of esophageal pressure measurement. For this purpose a cooperation between our institution and the groups of Dipl.-Ing. Matthias Schwaibold at MCC Gmbh & Co. KG, Karlsruhe, Germany, Prof. Dr. Armin Bolz of the Institute of Biomedical Engineering of the University of Karlsruhe (TH), Karlsruhe, Germany and Prof. Dr. Winfried Randerath of the Wissenschaftliches Institut of the Klinikum Bethanien in Solingen, Germany was set up, see fig. 4.1. The group of Prof. Randerath possesses an extraordinary scientific, experimental and clinical experience in NPSG studies [95 - 103], making them an excellent and reliable partner. An external stay at the IBT of the University of Karlsruhe (TH), Karlsruhe with regular visits to Solingen was performed September through October 2006 to kick off the cooperation. During this stage the clinical and recording protocols were defined during several meetings with the mentioned groups. During these visits, the author also introduced the medical staff into the new recording equipment, conducted technical briefings and clarified all points related to instrument calibration and study objectives. An extensive bibliographic review on esophageal pressure manometry was also performed and handed out to the medical personnel for optimal guidance.

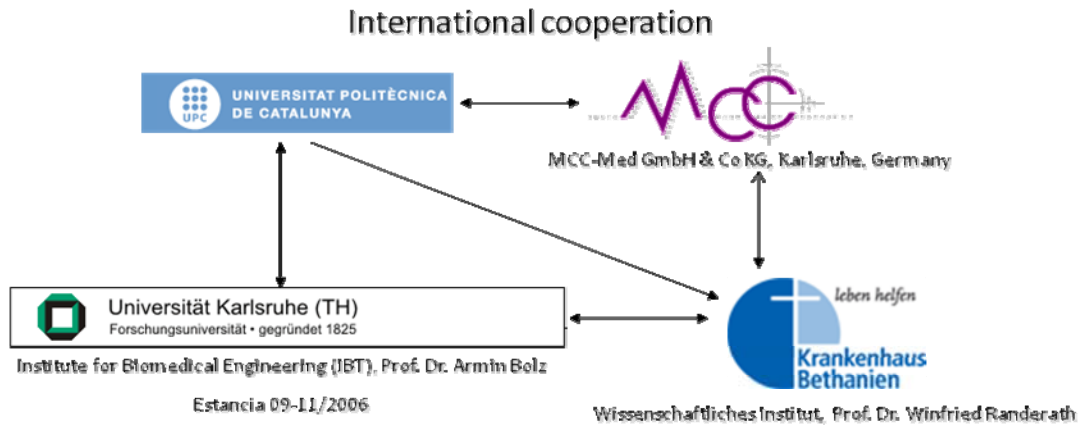


Figure 4.1: An international cooperation between the mentioned institutions in Germany and the UPC was set up for this thesis.

The sleep lab at Klinikum Bethanien was equipped with the newest PSG recording equipment (Somnocheck 2, Weinmann GmbH, Hamburg) and the esophageal pressure catheter. The clinical PSG study focused on creating a record database versatile and broad enough to allow a reliable posterior non-invasive detection and identification of IFL and the objective differentiation of hypopneas. The study design was partly based upon the accumulated experience, data formats and formal parameters of other more extensive european multi-centric studies [103, 104].

Once a full-night recording had been recorded, human experts proceeded to manually and automatically [105] score relevant respiratory events and sleep stages [80] according to defined standard criteria [6, 7]. For special study purposes, the Solingen group also attempted a non-invasive differentiation of hypopneas only with the air flow signal by using a new algorithm exclusively developed by them. This study will later be used to compare the performance of our automatic, non-invasive algorithm, see chapter X.

Furthermore, a human expert at MCC proceeded to manually differentiate central and obstructive hypopneas by means of the Pes signal (gold-standard scorings). These

scorings were then used for the validation of the developed automatic scoring and differentiation algorithms.

Recording protocol and measurement devices

Thirty-one lung-healthy subjects without asthma nor COPD, had full nocturnal polysomnography (NPSG) with an 18-channel recorder (Somnolab PSG system V2.01, Weinmann GmbH, Hamburg, Germany) at the sleep laboratories of *Klinikum Bethanien* hospital in Solingen, Germany, according to a protocol completely new designed for this purpose and approved by the hospital's Ethics Committee. The signals that were recorded can be seen in Tables 3 to 5. Exceptionally for this study, all patient records included esophageal pressure measurement, as it is normally not routinely included in clinical PSG routine. The NPSG recording equipment consisted of three separate components (headbox, bodybox and transferbox) for the connection of the described NPSG signals. This segmentation into components facilitates the disconnection of the different sensors just with one cable, increasing the mobility for the patient in case he/she needs to leave bed. The signals of the head- and bodyboxes were collected in the transferbox, which allowing the correct synchronization of the signals. The Pes signal was obtained by connecting to an auxiliary port of the transferbox, being synchronized like the other signals.

Three patients of this cohort had full NPSG while receiving therapy with a cPAP device (Weinmann GmbH, Hamburg, Germany). The rest had typical, full NPSG only for diagnosis purposes.

A nasal cannula device (Weinmann GmbH, Hamburg, Germany) that was connected to a pressure transducer system (Weinmann GmbH, Hamburg, Germany) was used to obtain the respiratory signal. Nasal cannula device/pressure transducer systems have

been indicated for identification of IFL and RERAs [6, 7] and have been routinely used in studies [16, 14, 17, 19, 18] for IFL analysis, as it reliably reproduces flattening and permits an objective and accurate detection of IFL events [16, 14]. The flow channel was recorded with a sampling frequency of 32Hz [7] and an 8-bit resolution. A nasal/cannula pressure transducer system delivers a semi-quantitative flow shape signal [92], as the airflow signal can not be calibrated. However, Hosselet et al. [16] and Montserrat et al. [92, 93] have shown that the relationship between this signal and a simultaneous pneumotachographic flow signal is essentially linear over the relevant range. Montserrat et al. [92, 93] concluded that the overall signal obtained from a nasal cannula/pressure transducer system is comparable in both shape and amplitude to that of a conventional pneumotachograph if a quadratic root conversion is performed. This mathematical conversion was directly integrated and performed by our registration device for each individual recorded flow sample. This should allow the methodology and results reported in this study to be reproducible with nasal cannula devices as well as pneumotachographs [16, 92, 93].

Esophageal pressure was systematically measured with an unidirectional pressure-tip catheter (UniTip catheter by UNISENSOR AG, Attikon, Switzerland) with a piezoresistive pressure sensor with an accuracy of ± 0.6 mmHg, a sensitivity of 5 $\mu\text{V/V/mmHg}$ and a typical resolution of $[-100...+300 \text{ mmHg}]$, and a separate pressure amplifier (ISOPRE-P amplifier, Standard instruments GmbH, Karlsruhe, Germany) with a resolution of $[-99 \text{ mmHg}...+200\text{mmHg}]$. The manufacturers of the sensor/catheter for esophageal pressure measurement and for the pressure amplifier confirmed on our request that their devices have been developed and validated under CE guidelines, obtaining the CE mark as medical devices, and having sold over 10.000 sensors so far. Other relevant scientific studies were found that had used the same

pressure sensor [107 - 109]. The Pes signal was recorded with a sampling frequency of 16Hz and a 12 bit resolution. Each time before the pressure catheter was to be employed on a patient, a sensor impedance measurement, a biosignal test and a manual calibration test were performed in order to assure that the pressure sensor correctly functioned and was correctly calibrated. The calibration test consisted in introducing the catheter in a sealed cylinder, manually incrementing the pressure inside the cylinder with a pressure manometer from 0 mmHg to 100mmHg and manually setting the calibration markers in the pressure amplifier. After the NPSG recording, the sensor was placed for 2 hours in 0.5% Teralin. Every 12 months the sensor was sent to the manufacturer for a routine maintenance check. No incidences have been reported. After the nasopharynx was sprayed with Xylocaine, the catheter was placed trans-nasally and positioned in the lower third of the esophagus [82], see fig. 4.2. Then, the catheter was taped to the nose of the patient. Patients were actively monitored during the night and medical personnel intervened in case of any sensor displacement or malfunction.

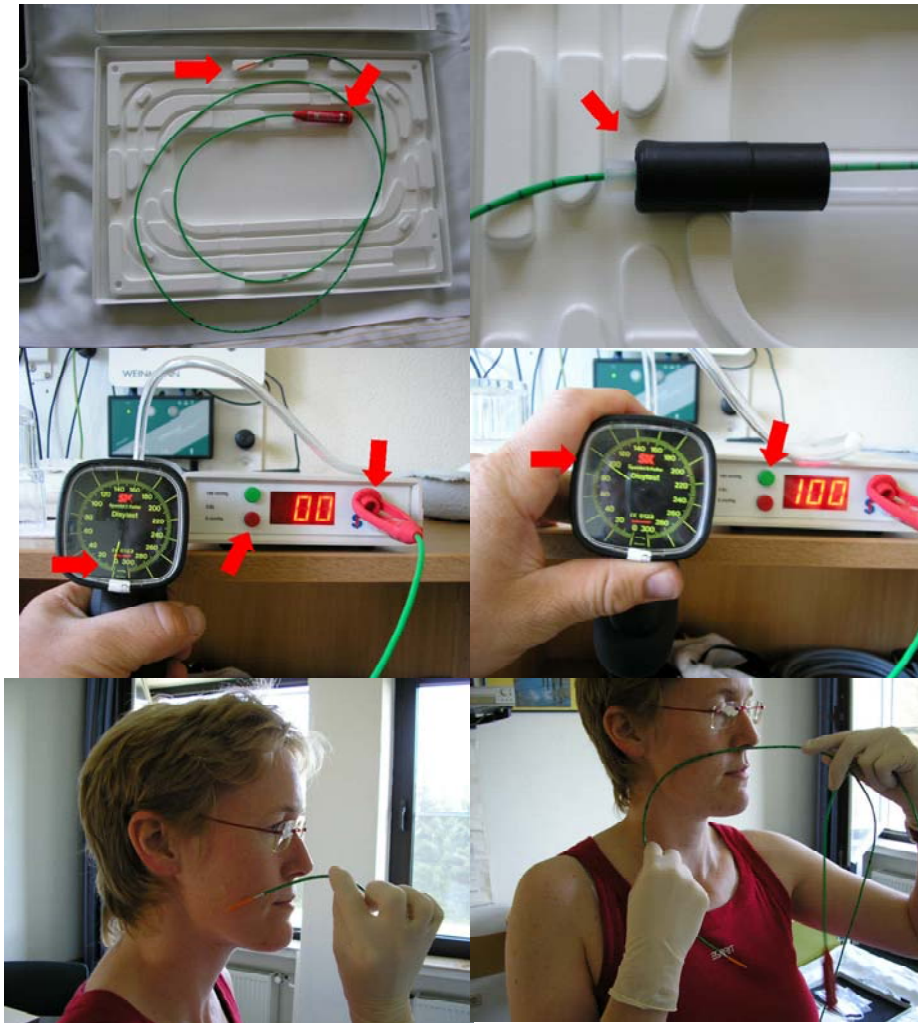


Figure 4.2: Sketch of how the Pes-recording protocol was implemented (figures courtesy of
Klinikum Bethanien, Solingen, Germany)

Other physiological signals recorded with an 8-bit resolution were arterial oxygen saturation (SpO_2), body position, pulse and plethysmography (ProTech, Services Inc, Mukilteo, WA, USA). Furthermore, 2 electroencephalogram channels (C3-A2/C4-A1), 2 electrooculogram (right/left), 1 submental electromyogram (EMG), 1 leg-EMG and an electrocardiographic (ECG) channel were recorded each with a sample frequency of 256Hz and a 12-bit resolution. An overview of the recorded signals can be seen in Tables 4.1 – 4.3.

Sleep stages were scored manually and automatically with the ARTISANA algorithm [105] following standard criteria [80]. Apneas and other respiratory events were scored applying standard criteria [6].

Signal name	Sensor/Channels	SOMNOlab
EEG	C3/C4	Standard (S)
EOG	O1/O2	S
EMG	Chin and leg	Chin: S, 1 leg: S
Chest	RIP belt + piezo sensor	Piezo: S
Abdomen	RIP belt + piezo sensor	RIP: Head-Box(HB)
Nasal Airflow	Nasal cannula (diagnosis) or pneumotacograph (therapy)	Cannula: S, Therapy: TB
Esophageal Pressure		TB
SO2		S
Audio signal (breathing sounds)	Tracheal microphone	Sibel or A/D
ECG (heart rate automatically calculated by SOMNOlab and represented as separate signal)		S
Pulse Wave (pulse rate automatically calculated by SOMNOlab and represented as separate signal)	Photoplethysmography	TB
Body Position		S

Table 4.1: Standard PSG signals to be recorded in the PSG clinical study

Transfer Box (TB) – Auxiliary channels

Diagnosis cohort	Therapy cohort
Pulse wave (raw data!)	Flow 32 Hz (calculated through PAP motor revolutions)
Pes signal	ODS or Pes (if measurement is possible) 32 Hz
	Pulse wave 50 Hz

Table 4.2: Auxiliary signals to be recorded in the PSG clinical study**Head Box (HB)**

ECG
RIP1
RIP2
EMG leg or intercostal

Table 4.3: Additional signals to be recorded in the PSG clinical study

As the subject acquirement for our database has been an ongoing process since 2005, a different number of subjects was available during the development of the methodology that will be exposed in the coming chapters. The addition of the patients to our database was sequential, so that the ID values in the first column of Table 4.4 also reflect the chronology of the patient's addition. For the purposes described in this thesis, only the diagnostic patients, see column "Type" in Table 4.4., were used.

Patient's demographic data

In the following tables, the demographic data of the recorded patients is described in detail.

ID	Sex	Date	Type	Age	BMI	EDS	AHI	AHI REM	AHI NREM	AI	HI	Snoring	Snoring	ASDA arousals
			-	(years)	(kg/m ²)	Y(1) / N(0)	Nr./h TST	Nr / hREM	Nr / hNREM	Nr /hTST	Nr /hTST	TST	% of TST	Nr /hTST
1	M	27/11/2006	Diag nosti cs	72	26,8	1	11,53	15,5	9,79	0,35	11,18	61,4	14,6	3,7
2	M	21/12/2006	Diag nosti cs	52	26	1	2,27	7,6	0,68	0,87	1,4	170,8	31,6	0,3
4	M	30/11/2006	Diag nosti cs	56	24,7	0	91,24	78,5	92,06	90,14	1,11	191,8	44,6	52,0
5	M	30/08/2005	Diag nosti cs	78	31,4	1	33,2	22,5	34,52	14,23	18,97	305,1	59,4	15,9
6	M	07/09/2005	Diag nosti cs	38	24	0	27,64	0,9	34,2	19,72	7,92	204,2	47,7	21,1

7	M	17/10/2005	Diag nosti cs	44	29,42	1	5,85	27,7	2,53	0,49	5,37	184,9	36,4	3,2
8	M	16/12/2005	Diag nosti cs	46	28,7	0	16,07	23,7	15,03	2,68	13,39	74,2	22,1	7,5
9	M	29/05/2006	Ther apy	46	29	1	k.A.	k.A.	k.A.	1,39/A wz	2,43/A WZ	80,8	15,6	3,4
10	M	22/06/2006	Ther apy	56	32	1	3,03	0,8	3,83	0,2	2,82	75,6	18,4	2,2
11	F	12/06/2006	Ther apy	40	39,19	1	4,28	0,0	4,28	0,5	3,78	0,0	0,0	0,0
12	M	19/05/2008	Diag nosti cs	38	30,10	Score 13	6,74	4,7	7,01	0	6,74	78,0	23,7	4,9
13	M	16/06/2008	Diag nosti cs	71	24,9	Score 9	15,59	7,6	16,99	6,05	9,54	100,7	39,0	9,7
14	M	30/06/2008	Diag nosti cs	50	30,35	Score 1	18,3	10,6	20,7	0,3	18,0	182,7	48,3	11,3
15	M	21/07/2008	Diag	64	30,72	Score	34,0	48,8	32,9	6,6	27,3	196,2	83,5	7,7

			nosti cs			7								
16	M	25/08/2008	Diag nosti cs	55	27,2	Score 2	27,46	9,1	29,38	21,25	6,21	126,1	29,8	20,6
18	M	28/08/2008	Diag nosti cs	57	26,7	Score 7	5,36	3,6	5,71	0,00	5,36	4,0	1,1	1,6
19	M	08/09/2008	Diag nosti cs	73	24,6	Score 6	9,36	21,2	5,22	0,61	8,75	173,0	37,4	3,7
20	M	15/09/2008	Diag nosti cs	30	40,2	Score 3	13,25	65,9	3,81	6,11	7,13	221,0	48,8	4,3
21	M	22/09/2008	Diag nosti cs	68	30,1	Score 0	28,07	4,1	32,14	4,15	23,92	125,0	29,8	19,8
22	M	19/01/2009	Diag nosti cs	65	21	Score 5	21,67	35,0	20,51	4,68	16,99	76,0	16,9	11,8
23	F	26/01/2009	Diag nosti	48?	27,6	Score 11	9,53	2,2	11,20	0,20	9,32	118,0	39,9	7,7

			cs											
24	M	01/02/2009	Diag nosti cs	42	32,4	Score 2	3,07	2,1	3,06	0,41	2,66	90,0	28,9	1,7
25	F	16/02/2009	Diag nosti cs	71	41,9	Score 2	56,18	66,8	54,44	49,11	7,07	189,0	60,2	7,3
26	M	19/02/2009	Diag nosti cs	37	27,8	Score 1	11,82	6,9	12,82	1,50	10,32	74,5	20,7	8,7
27	F	02/03/2009	Diag nosti cs	55	24,5	Score 11	20,07	0,0	21,47	1,06	19,01	74,5	21,7	17,5
28	F	18/05/2009	Diag nosti cs	23	27	Score 2	2,26	0,0	2,43	0,35	1,92	344,5	11,3	10,0
29	M	07/06/2009	Diag nosti cs	33	27,5	Score 19	10,51	6,8	11,15	0,00	10,51	297,0	7,5	26,0
30	M	08/06/2009	Diag nosti cs	45	23,1	Score 10	5,97	7,2	5,70	0,16	5,81	372,0	90,5	7,0

31	M	17/08/2009	Diag nosti cs	28	31,1	Score 2	13,82	18,75	12,57	0,91	12,91	374,0	64,3	49,0
32	F	24/08/2009	Diag nosti cs				12,27	21,95	9,62	2,04	10,22	381,5	52,2	2,0
33	M	31/08/2009	Diag nosti cs				15,96	14,52	16,32	2,88	13,08	312,0	14,6	48,0

Table 4.4: Demographic data of the recorded patients. BMI: Body-Mass-Index, EDS: Excessive Day Sleepiness, AHI: Apnea/Hypopnea Index, TST: Total Sleep Time, AI: Apnea Index, HI: Hypopnea Index, ASDA: American Sleep Disorders Association

	Age	BMI	EDS	AHI	AHI REM	AHI NREM	AI	HI	Snoring	Snoring	ASDA arousals
	(years)	(kg/m ²)	Y(1) / N(0)	Nr./h TST	Nr / hREM	Nr / hNREM	Nr /hTST	Nr /hTST	TST	% of TST	Nr /hTST
Mean (28 diagnosis patients)	52,56	28,46	18,9	19,1	18,7	8,5	10,4	182,2	36,7	0	13,7
STD (28 diagnosis patients)	15,60	4,50	18,51	21, 5	19,25	19,01	6,60	108,11	21,78	0	14,32

Table 4.5: Demographic data of the global population of the 28 recorded diagnostics patients

Manual, invasive classification of hypopneas

Two human experts reviewed the NPSG recording for all patients and scored relative respiratory events such as apneas or hypopneas according to the standard criteria [6]. The final hypopnea scorings were reconciled.

But in order to differentiate between obstructive and central events, esophageal pressure (Pes) measurement is necessary, as it is currently considered the gold-standard technique for measurement of respiratory effort and the identification of obstructive and central events [6, 7]. The differentiation of hypopneas is considered the more challenging task, as pressure swings during a hypopnea are more subtle than during other events.

According to these criteria [6], a hypopnea is identified by a clear decrease ($>50\%$) from baseline in the amplitude of a valid measure of breathing during sleep and lasts for at least 10 seconds. The baseline is defined as the mean amplitude of stable breathing and oxygenation in the two minutes preceding onset of the event. For the scoring of a central apnea/hypopnea, a clear reduction in esophageal pressure swings from baseline (as defined before) is required. According to this guideline [6], there is no relative or absolute reduction in esophageal pressure inside the event's interval that can be used to distinguish a central from an obstructive, event, which increases the difficulty of the automatic differentiation.

A human expert reviewed the full-night recordings of our patients and manually scored hypopneas with the mentioned criteria, primarily using Pes signal. The scored hypopneas can be seen in Table 4.6. The discrepancies between the Solingen hypopnea scoring and the MCC Pes scoring are caused mainly that the human expert at MCC discarded hypopneas because of artifacts at the Pes signal during the hypopnea, such as

coughing, swallowing or baseline shift, that would not allow the posterior differentiation of the hypopnea into obstructive or central. The Solingen scorer only just the classical signals [6] for the hypopnea detection, like the airflow and the SpO₂ signals, without consideration of the Pes signal's quality.

Patient	Overall number of differentiated Hypopneas (Solingen)	Overall number of differentiated hypopneas (Pes-signal)	Overall number of overlapping hypopneas (reconciliation Solingen/Pes)
1	55	24	21
5	90	32	32
6	45	38	37
7	9	4	2
8	74	19	19
13	22	17	13
14	97	37	26
15	105	6	5
16	32	11	10
18	22	12	12
19	37	22	19
20	30	14	14
21	122	109	100
22	126	21	21
23	16	1	1
24	14	2	2
25	37	36	36
26	63	44	43

27	89	75	72
28	9	10	9
29	52	18	18
30	36	36	36
31	85	85	85
32	65	64	64
33	73	73	72
Total	1405	810	769

Table 4.6: Manually scored hypopneas by human experts

Manual, non-invasive classification of hypopneas

Researches in Solingen have been working on a manual classification algorithm for human experts based upon a decision tree protocol in order to differentiate between central and obstructive hypopneas non-invasively using only the airflow signal. The algorithm consisted in a multi-step evaluation of flattening incidence and the context of events around a hyopnea (such as the incidence of other hypopneas, presence of arousals, type of crescendo, etc.) in order to allow the final hypopnea differentiation. The preliminary classification results of this manual, non-invasive algorithm are promising, see chapter XI, even though the development of this algorithm is still ongoing.

Conclusions

A new patient database with a complete new recording protocol was designed from scratch in order to have new NPSG recording with systematic esophageal pressure measurement during the whole night. Patient demographics correspond to the typical population suffering from OSAHS. Hypopneas, other respiratory events and sleep stages were manually and automatically classified according to standard criteria. Hypopneas were manually differentiated by a human expert according to standard

criteria with the Pes-signal. These scorings represent the current, gold-standard for hypopnea differentiation that will be used for validation purposes of the automatic algorithms to be developed. The NPSG patient database described in chapter IV has been in ongoing development since the year 2005, with patients being added every year. The techniques and results presented in the coming chapters (VI, VIII, IX and X) were developed at different stages of this project and with the patients available in the database at that particular moment. Therefore the number of patients used for the development may vary from one technique to another and will be respectively indicated in each chapter.

Chapter V: Pre-processing and automatic identification of inspiratory cycles

Introduction

As commented in previous chapters, the development of the methodology in this thesis will mainly be based upon the analysis of the nasal airflow and esophageal pressure (Pes) signals, see fig. 5.1. Both signals present some intrinsic physiological and technical disturbances and noise that need to be processed, before the information contained in the signals can be thoroughly analyzed.

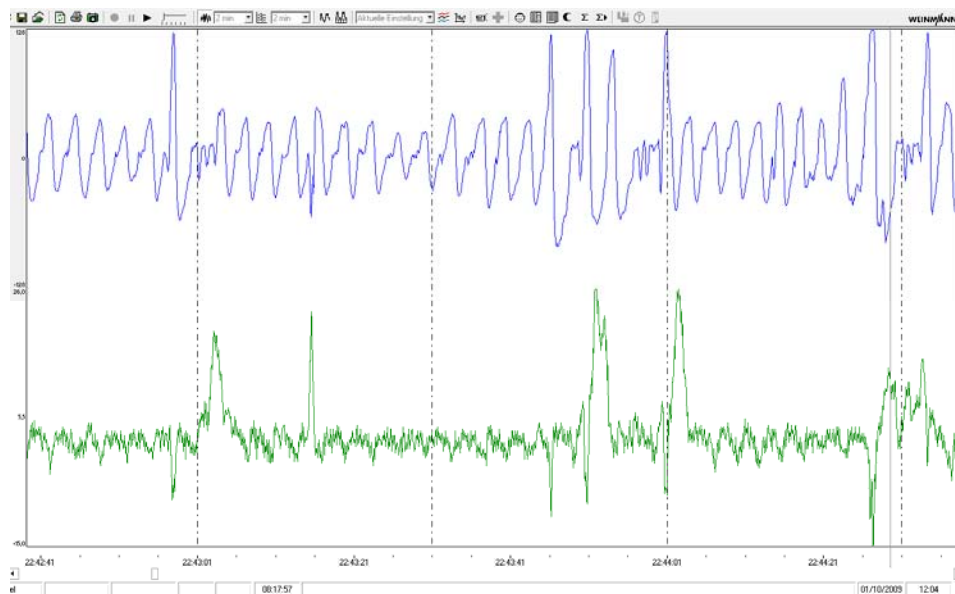


Figure 5.1: Examples of the recorded airflow (above) and Pes (below) signals. Observe the high-frequency noise and the artifacts (positive pressure peaks) on the Pes signal (screenshot of one of our NPSG recordings displayed by the Somnolab software V2.01, Weinmann GmbH & Co. KG, Hamburg, Germany)

The pre-processing stage consists of digital filtering of both signals in order to ease up the later processing and allow a better focus on each signal's informational content, see fig. 5.2. Also an automatic alignment had to be performed between both signals. The

Pes signal sometimes showed a slight delay in relationship to the flow signal probably due to both technical and physiological origins.

The detection and identification of the inspiratory cycles was also of utmost importance for the later processing and analysis. Even though methods on detection of respiratory cycles in the airflow signal have been published [17, 18, 81], few has been reported on the detection of respiratory cycles in the Pes signal. This is why a complete new automatic respiratory cycle detection system had to be developed in order to be able to analyze corresponding respiratory cycles in the airflow and Pes signals. In a first step, a baseline estimation was performed and then maxima and minima of the inspiratory/expiratory respiration cycles were detected. With this information, the beginning and ending of each inspiratory cycle were then identified in the flow and Pes signals and each inspiration was then extracted for a separate processing and analysis.

Pre-processing stages

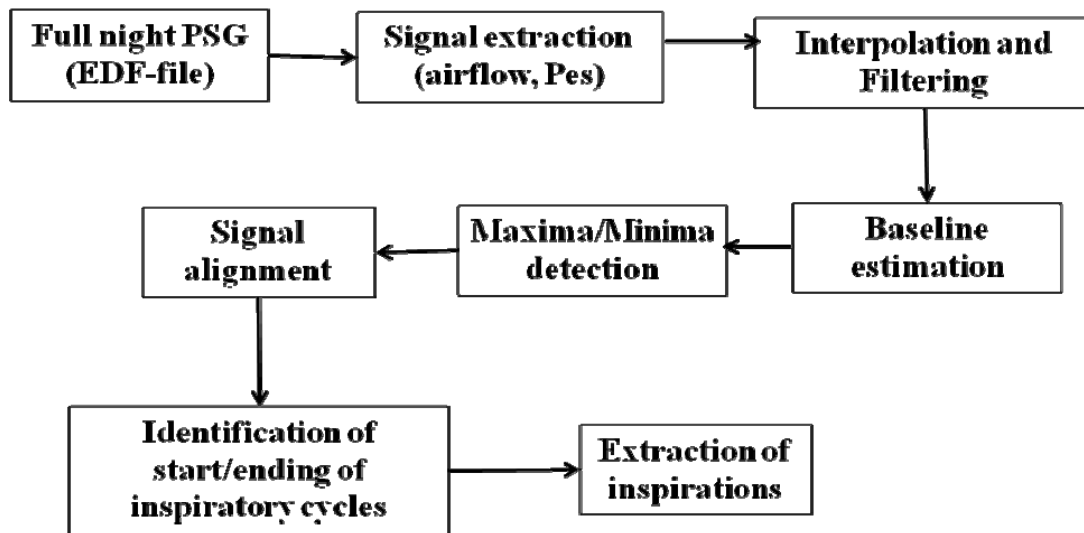


Figure 5.2: System overview of the typical pre-processing steps and identification of inspiratory periods

Most of the commented methods and pre-processing steps will later be shared by and are common to the automatic processing algorithms that will be described in the coming chapters.

Filtering and alignment

In a first step, all NPSG recordings were manually converted from the proprietary Somnolab format to the more common EDF format [103].

In regard to filtering, studies [17, 18] have shown that a low-pass filter with a cut-off frequency of 2.5 Hz is adequate to analyze the underlying flow shape of a flow signal with flattening, if snoring is not to be analyzed. The main frequency content of the esophageal pressure signal has been reported to be located below 1 Hz [106]. So, after interpolating the Pes-signal to 32Hz, moving average (MA) filters were applied to the flow and the Pes-signal (5 and 15 point MA filters with cut-off frequencies of 2.9 Hz and 1 Hz at -3 dB, respectively) in forward and reverse directions in order to achieve zero-phase. The MA filters used here act as low-pass filters in order to suppress high-frequency oscillations, see fig. 5.3. The basic flattening flow pattern, which is essential for recognition [6, 17, 19, 18], is preserved, while peak flow detection was not affected by the filtering.

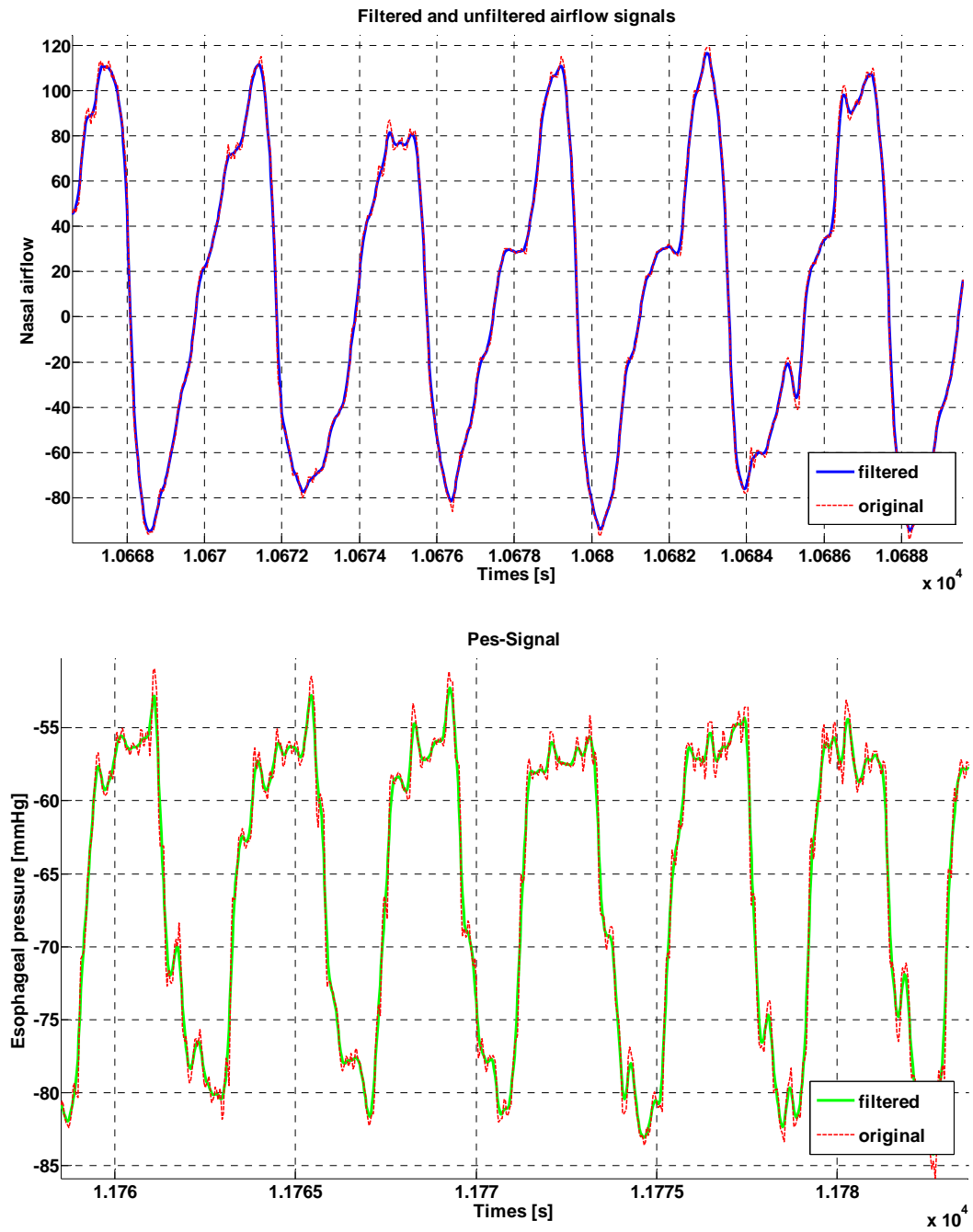


Figure 5.3: Examples of the filtered and unfiltered airflow (above) and Pes-signals (below)

Signal drifting and baseline estimation

The flow signal showed in rare cases an approximately constant baseline offset that was subtracted. The baseline of the Pes-signal often showed drifts during the night, mostly because of small catheter displacements due to body movements, see fig. 5.4, so the baseline was estimated using a sliding window that consisted of 1600 points (50s). Then, each individual Pes-inspiration was subtracted to a zero baseline.

Most of the observed Pes-baseline drifts should be related to small displacements of the catheter due to changes in body position. As reported in the literature [82], drifts related to body movement usually happen during Pes measurements and are difficult to avoid. Even though our catheter was always fixed with tape to the nose of the patient, small displacements of the catheter may result in the migration of the Pes signal's baseline. Also the compression of the thoracic cage in lying position could have an influence in the absolute values of the Pes signal. However, changes in absolute values of the esophageal pressure signal are not critical, as long as the relative pressure changes (that reflect the relative changes in respiratory effort) are correctly reproduced by the sensor. As commented before, the functionality of our sensor was exhaustively tested before each measurement, so our measured pressure signal reliably and correctly replicated respiratory effort. Furthermore during the pre-processing phase each Pes-inspiration was subtracted to a zero baseline. Thus, the absolute baseline drifts were compensated for every individual Pes-inspiration and were of no further relevance for posterior analysis, as only the relative pressure changes were analyzed. So, the relative changes in esophageal pressure were correctly replicated by the pressure sensor, implying that the absolute baseline drifts had no incidence on posterior analysis.

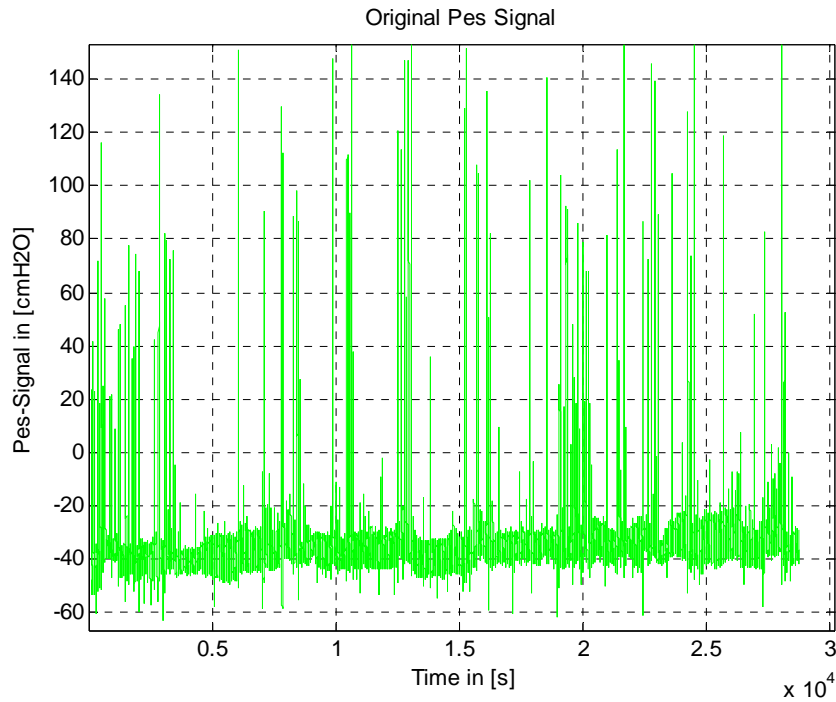


Figure 5.4: An example of a full night Pes-recording of one patient. The positive peaks observed in the images are swallowing (sometimes coughing) artifacts. Note the drifting of the baseline during the night.

Regarding the absolute values, fig. 5.4 shows a typical Pes-signal, which we believe is a correct representation of intrathoracic pressure. Unlike pharyngeal pressure, intrathoracic pressure has consistent negative values [82] that can become of even higher magnitude especially for patients that suffer of conditions that involve high respiratory effort. As our pressure sensor was placed in the lower third of the esophagus, as indicated for esophageal pressure measurement [7, 82], the measured negative pressure values should correctly reflect the physiological conditions in that area.

Identification of inspirations

In order to accurately identify the inspiration's beginning and ending, we first detected the corresponding peaks of each inspiration with the standard derivative function. We

defined thresholds for minimum peak distance (1 sec., which should approximately correspond to 50% of normal inspiratory breathing separation time, as the frequency of the inflow wave during sleep is approximately 0.5 Hz [17, 18]), for the minimum flow peak height (20% of the standard deviation of a patient's flow amplitude) and minimal area for a flow inspiration (20% of the mean area of a patient's inspirations) to avoid artifacts and small peaks of oscillations around the baseline, see fig. 5.5.

Then, start and ending of flow inspirations were identified with “zero-line” (baseline) crossing [17, 81]. In regard to sample frequency related imprecision, always the sample with the minimal distance to the baseline was chosen as the start or ending point. Finally, an exhaustive visual examination of the preprocessing results was performed for each patient to validate the inspiratory detection. Apneas were excluded from the analysis.

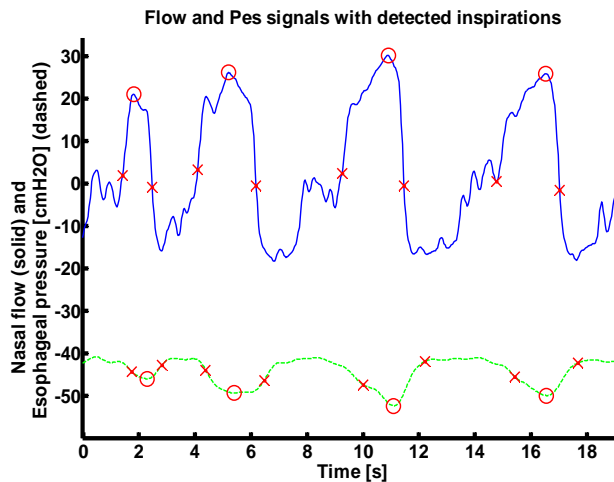


Figure 5.5: An example of pre-processed flow (solid line) and Pes signals (dashed line) with detected maxima and minima (circles) and the inspiration's start and ending points (crosses). The latter are not always symmetrical because of sample frequency related imprecision.

A variable delay with absolute mean values of 0.34 ± 0.25 sec. was identified between corresponding flow- and Pes-inspirations throughout the night. We suppose that a component of the delay could be of technical origin, while a part of the delay could also have physiological origins. The pulmonary system and the UA can have a capacitive or

inductive behavior [134, 135] possibly influencing the delay between an inspiration's corresponding Pes minimum and Flow maximum, especially if we consider that we are measuring respiratory effort from outside the pulmonary system (esophagus).. However, the detected starting point of an inspiration may, in some cases, show an intrinsic variability due to the presence of variations in the inspiration's shape around the zero-line that can not be removed without altering the inspiration's shape, consequently inciding on the delay's calculation. The pressure sensor is a piezoresistive microchip that directly translates pressure values into an electrical signal. Thus, according to the manufacturer, the catheter-related transmission delay is negligible. No digital or analog filters are integrated in the pressure sensor. In the flow pressure transducer system, the mathematical conversion of the flow samples (root-square) is performed for each individual sample before sample storage, so no relevant delay is caused by this procedure. Although the analog and digital filters integrated in the recording box had similar anti-aliasing properties for all channels, they could result in a small delay between channels. There are also other components that could add-up to cause a small delay, such as the length of the hose of the nasal cannula, etc.. These possible sources for small delays are difficult to measure individually but summed up, they should explain the small delay observed between the flow and Pes-signals. The digital filters during the pre-processing phase were applied, as indicated before, in forward and reverse directions to achieve zero-phase. However, the delay had no further impact on the posterior analysis because of the described pre-processing stages that aligned each flow inspiration with the corresponding Pes nadir. In order to align the inspirations, the closest Pes-nadir was located for each flow inspiration once the beginning and end of the flow inspirations had been determined. Then the duration of the flow inspiration was equally distributed around the corresponding Pes nadir in order to establish equivalent

start and ending points. When a corresponding flow/Pes pair could not be found (e.g. because of a swallowing artifact), the complete inspiration was discarded.

Conclusions

The pre-processing stage was optimized for the airflow and Pes signals, the two signals that will be mainly analyzed in this thesis. For this purpose, filtering, baseline detection and signal alignment were performed to subtract artifacts, avoid high-frequency noise and compensate signal delay and baseline drifting. The inspiratory cycles were automatically identified with a robust methodology that was visually validated by human experts. For the later processing stages, the inspiratory cycles will be available separately as flow/Pes inspirational pairs for easier processing and manipulation.

Chapter VI: Automatic identification of inspiratory flow limitation with esophageal pressure

Introduction

The automatic invasive and non-invasive identification of changes in upper airway (UA) obstruction is an ongoing challenge in sleep analysis. During sleep, the partial collapse of the UA, with the consequent increase in UA resistance, usually results in Inspiratory Flow Limitation (IFL) [62, 56], which is defined as a lack of increase in airflow despite increasing respiratory effort (decreasing intrathoracic pressure). The identification of IFL episodes is necessary to assess respiratory-effort related arousals (RERAs), that consist of multiple episodes of increasing respiratory effort (because of the increased UA resistance) resulting in a microarousal [16, 6]. RERAs detection is essential to diagnose multiple pathologies in Sleep Disordered Breathing (SDB), such as the upper airway resistance syndrome (UARS) that causes daytime hypersomnolence and cardiovascular diseases [2].

The bottleneck when creating a gold-standard validation set is usually found in the manual identification of IFL with the invasive Pes signal, as it is a cumbersome procedure that may suffer of interscorer differences and subjective interpretation. Thus, the development of an objective and computationally efficient method for automatic invasive assessment of IFL and related changes in UA obstruction in large datasets is also desirable.

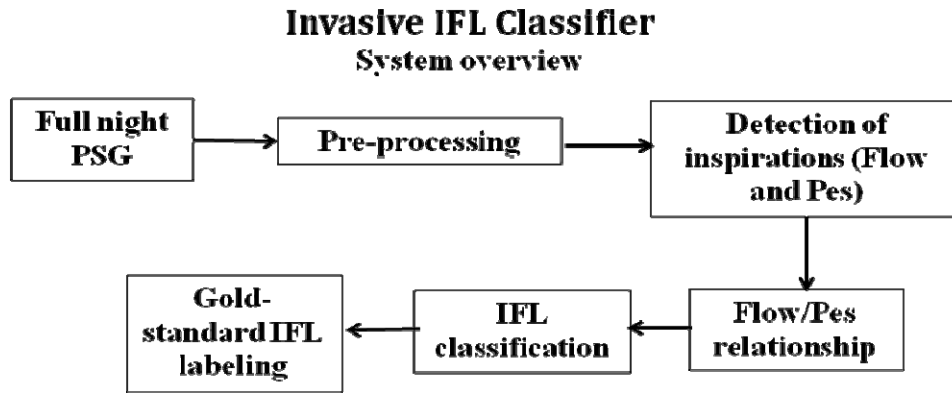


Figure 6.1: System overview of the automatic classifier of IFL with the esophageal pressure signal (invasive classifier)

In the present chapter we propose a new exponential model [Morgenstern 2008a, 2008c, 2009a, 2009b] that should permit to objectively reproduce the esophageal pressure/flow (P/\dot{V})-relationship of breaths with IFL or subtle changes in UA obstruction. An automatic invasive annotation system will be developed with this model in order to identify IFL episodes with high accuracy, robustness and computational efficiency, see fig. 6.1. The model should also allow a reliable prediction of respiratory resistance. After presenting the model, its characterization performance is compared to the current best-performing mathematical models in the literature [94, 57].

The P/\dot{V} -relationship

Introduction

As commented in chapter III, the flow signal may be one of the most useful signals to non-invasively assess respiratory-related pathologies and changes in UA obstruction, as it is commonly recorded in clinical routine [6, 7].

Condos et al. [31] found out in 1994 that an identification of a plateau on the inspiratory waveform correlated with an increased UA resistance in patients under cPAP treatment. Hosselet et al. [16] later also showed that inspiratory flow limitation (IFL) was reflected

in the inspiratory flow pattern during spontaneous breathing, reliably reflecting even the most subtle changes in UA resistance. IFL has been defined as a lack of increase in airflow despite increasing respiratory effort [6, 16]. In a first try to classify the severity of IFL with the flattening of the contour, Hosselet et al. [16] used the esophageal pressure – airflow (P/\dot{V}) relationships to differentiate between 3 different types of contours: normal, intermediate and flattened contour, see fig. 6.2.

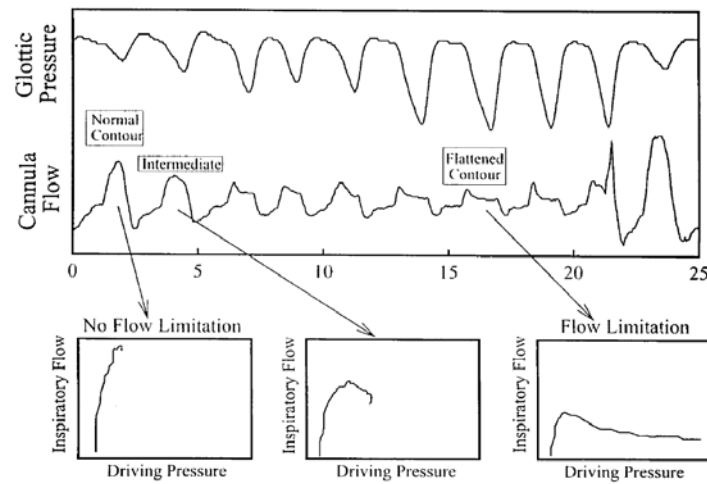


Figure 6.2: Classification of flow contours by Hosselet et al. [16]

In a similar approach, Clark et al. [81] used the P/\dot{V} -relationship of each inspiration to measure the extent of flow limitation. In this study the classification was based upon the invasive pharyngeal pressure signal. Even though esophageal pressure is usually measured in the lower third of the abdomen [82], pharyngeal pressure also reflects respiratory effort, still representing a valid “gold-standard” reference. As seen in fig. 6.3, Clark et al. [81] also divided the flow limitations into four levels of ascending severity, also see Table 6.1.

Level	Criterion 1	Logical operator	Criterion 2
1	$\dot{V}(P) = a \cdot P^b$ with $b \geq 0.8$	AND	not level 3 or 4
2	$\dot{V}(P) = a \cdot P^b$ with $b < 0.8$	AND	not level 3 or 4
3	$\frac{\partial \dot{V}}{\partial P} = 0$ for $\Delta P = 1 \text{ cmH}_2\text{O}$	OR	$\frac{\partial \dot{V}}{\partial P} \leq 0$ for $0.75 < \Delta P < 2 \text{ cmH}_2\text{O}$
4	$\frac{\partial \dot{V}}{\partial P} < 0$ for $\Delta P = 1 \text{ cmH}_2\text{O}$	OR	$\frac{\partial \dot{V}}{\partial P} \leq 0$ for $\Delta P \geq 2 \text{ cmH}_2\text{O}$

Table 6.1: Clark’s classification criteria for inspiratory flow limitation (IFL)

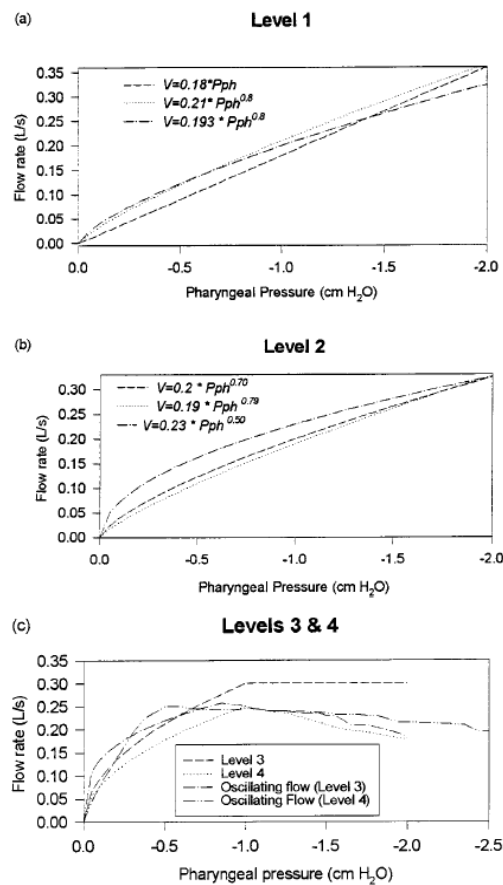


Figure 6.3: Clark et al. [81] created comparative “gold-standard” levels of flow limitation by plotting airflow vs. pressure, Level 1: non flow-limited inspiratory cycles, Level 2: mildly flow-limited inspiratory cycles, Level 3: no pressure dependence, Level 4: severe, decreasing flow rate with negative pressure dependence [81]

In order to determine the flow limitation by non-invasive methods Clark et al. [81] used an area index representing the area below the inspiration's contour in the airflow signal, as seen in fig. 6.4, to evaluate the inspiratory breath contour and consequently created a relationship between this area index to the commented gold-standard reference levels in order to classify every breath into one of the defined flow limitation levels.

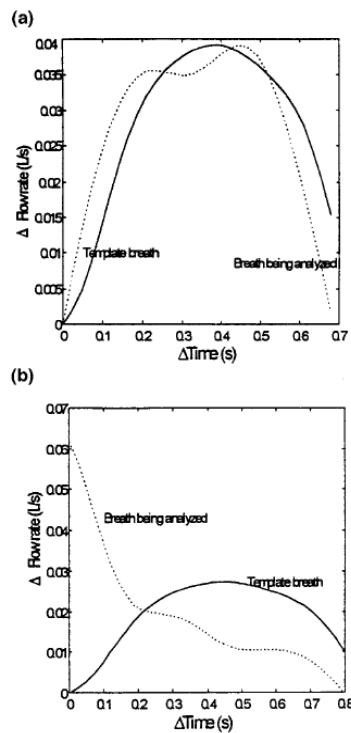


Figure 6.4: Clark et al. [81] used an area index to evaluate the flattening of the airflow pattern contour [81]

However, Clark's study was performed with asymptomatic snorers and not with symptomatic patients with syndromes associated with SDB, thus limiting the validity of the study. It is therefore important that this or similar algorithms for non-invasive flow limitation detection and discrimination are validated in a larger clinical population.

Implementation

After pre-processing the flow and Pes signals (fig. 6.5a), also see chapter V, all inspirations were available in form of flow-Pes inspiration pairs (fig. 6.5 b, c) with

which the P/\dot{V} -relationship of each breath was constructed (fig. 6.5 d). As the values beyond the pressure nadir do not contain IFL-related information (increasing P_{es}) [16, 94, 81], each inspiration was cut at the time value of the P_{es} nadir to avoid the hysteresis. The P_{es} -values before the P_{es} nadir were transformed to absolute values during the construction of the P/\dot{V} -relationship, to support the hyperbolic model [57, 71].

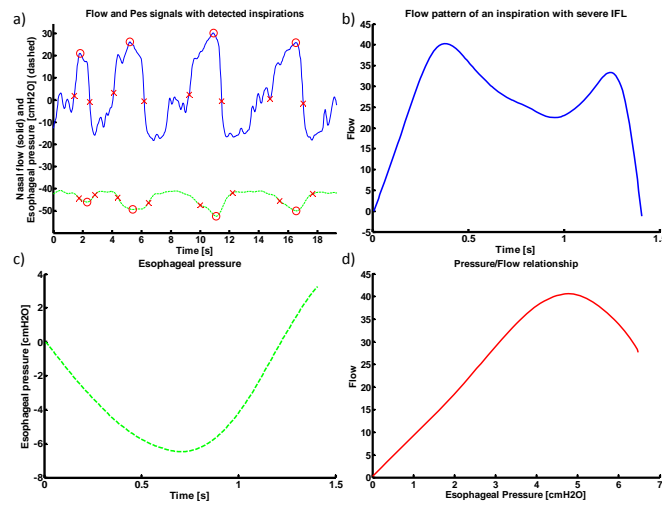


Figure 6.5: (a) An example of pre-processed flow (solid line) and P_{es} signals (dashed line) with detected maxima and minima (circles) and the inspiration's start and ending points (crosses). The latter are not always symmetrical because of sample frequency related imprecision. (b) An extracted flow inspiration with IFL. (c) its corresponding P_{es} -signal. The P/\dot{V} -relationship (d) presents an accentuated non-linear behavior indicating presence of IFL.

Classical criteria

Assessment of IFL was automatically performed by applying classical criteria on a breath's P/\dot{V} -relationship. IFL has been classically defined as a min. decrease of 1 cmH₂O (0.7356 mmHg) of intrathoracic pressure without a corresponding increase in airway flow rate [16, 14, 57, 94, 81, 71].

Clark's criteria

An additional automatic assessment of UA obstruction was performed by applying Clark's criteria [81] on a breath's P/\dot{V} -relationship. Clark's criteria were chosen because they are based upon classical classification criteria but allow differentiating four separate levels of IFL with ascending severity (Table 1). Thus, these criteria allow observing a model's characterization capability of more subtle changes in UA obstruction than the classical criteria.

Models of the P/\dot{V} -relationship

Introduction

During an IFL episode, transiently elevated UA resistance prevents the increase of inspiratory flow despite increasing respiratory effort (decreasing P_{es}), hence the P/\dot{V} -relationship of an inspiration becomes non-linear [16, 81] (fig. 6.5d). Thus, most of the IFL-related information is contained in the non-linear segment of the P/\dot{V} -relationship, as it indicates if flow stalls or falls for increasing respiratory effort. Several mathematical models have been proposed to reproduce the P/\dot{V} -relationship of an inspiration and achieve an objective automatic assessment of IFL, such as a hyperbolic equation [57, 71] or a 3rd degree polynomial equation [94], although none of these were specifically designed to reproduce the non-linear segment of a P/\dot{V} -relationship.

Hudgel's hyperbolic model

Classically the P/\dot{V} -relationship had been modeled by the Rohrer equation, see eq. 6.1. However, the Rohrer equation assumes that the caliber of the conduit through which airflow passes is constant but during flow-limitations, such as those caused by OSAHS,

UARS and others, the diameter of the airflow conduit narrows considerably. So the Rohrer equation, as shown by Tamisier et al. [71], has strong limitations modeling the pharyngeal airway during flow limitations.

$$P = K_1 \cdot \dot{V} + K_2 \cdot \dot{V}^2 \quad (6.1)$$

with \dot{V} being flow, P pressure, K1: y-intercept (constant), K2: slope (constant)

Hudgel et al. [57] proposed a new way to model the P/\dot{V} -relationship with the hyperbolic eq. 6.2 by considering the narrowing of UA's diameter during flow limitations.

$$\dot{V} = \frac{\alpha P}{\beta + P} \quad (6.2)$$

with \dot{V} being flow, P: pressure, α : asymptote for peak flow, β : pressure at 50% of peak flow

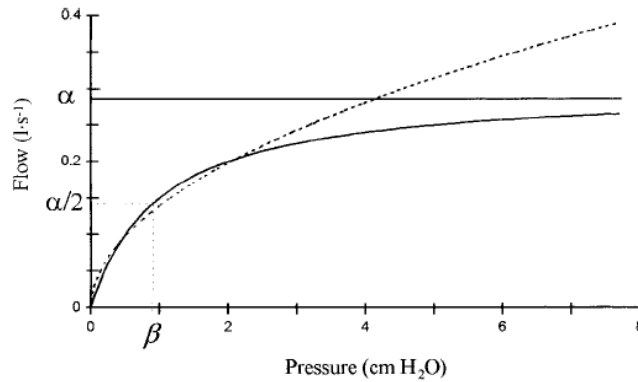


Figure 6.6: Representation of Hudgel's equation. The α and β parameters are shown in the ordinate and abscissa axes [71]

The α and β parameters represent the cut of the curve with the axes, see also fig. 6.6. The alpha parameter represents the asymptote for the peak flow while the beta

parameter represents the pressure at 50% of the peak flow. Thus, parting from the classical representation of resistance in thermodynamics $R = \frac{\Delta P}{\dot{V}}$ at peak pressure, an alternative calculation of this resistance can be made by means of these parameters, see eqs. 6.3 – 6.7.

As eq. 6.2 represents a right rectangular hyperbola, which general form is given by:

$$(\alpha + Y)(\beta + X) = \text{constant} \quad (6.3)$$

The specific pressure-flow form is

$$(\alpha - \dot{V})(\beta + P) = \alpha \cdot \beta \quad (6.4)$$

Solving this equation for P , one obtains a simple algebraic expression in terms of flow

$$P = \frac{(\beta \cdot \dot{V})}{(\alpha - \dot{V})} \quad (6.5)$$

And by rearranging these expressions, we can also obtain the resistance value

$$R_{\text{Hyperbolic}} = \frac{\Delta P}{\dot{V}} = \left(\left(\frac{\alpha}{\beta} \right) - \left(\frac{1}{\beta} \right) \cdot \dot{V} \right)^{-1} \quad (6.6)$$

Thus, equations 6.5 and 6.6 allow a representation of the pressure P and the resistance R , after the determination of the constants α and β , with the airflow \dot{V} as the only variable but that can be determined by empirical measurement.

$$R_{\text{hyperbolic}} = \frac{\Delta P}{\dot{V}} = \frac{\beta}{\alpha} + \frac{\Delta P}{\alpha} \quad (6.7)$$

As shown by Tamisier et al. [57], the hyperbolic equation proved to be, as expected, the better model in comparison with the Rohrer equation as well as for normal (non-flow limited) respiratory cycles as for flow limited respiratory cycles caused by OSAHS or UARS. In the comparison between the hyperbolic resistance, see eq. 7, and the classical reference peak value $\frac{\Delta P}{\dot{V}}$ resistance, the correlation values were of approx. 0.98, also see fig. 6.7.

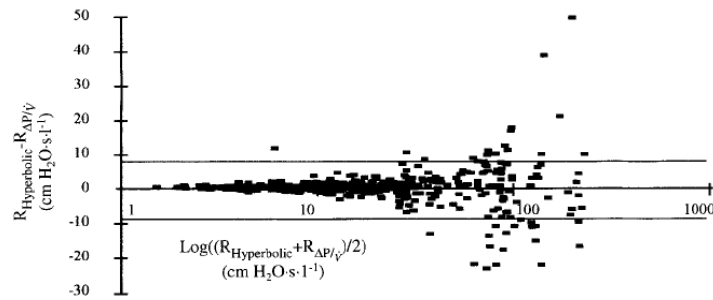


Figure 6.7: Comparison between resistance values calculated by dP/V_f low and hyperbolic model by Tamisier et al. [15]-> Difference between two measurements falls within 9.1 cmH₂O.s/L of the mean difference 95% of the time [57].

Thus the Hudgel equation seemed to be a robust method for estimation of resistance and was a true improvement in comparison to the classical Rohrer equation for pharyngeal airway narrowing.

Mansour's 3rd degree polynomial model

Mansour et al. [94] used another approach to model the P/\dot{V} -relationship with a 3rd degree polynomial model. They parted from the Bernoulli eq.

$$\frac{P_1}{\rho_1} + \frac{1}{2} V_1^2 = \frac{P_2}{\rho_2} + \frac{1}{2} V_2^2 \quad (6.8)$$

and the equation for a steady homogenous flow in a circular cylinder, assuming that the flow of air in the cylinder will expand without the loss or gain of heat.

$$F = \rho_1 A_1 V_1 = \rho_2 A_2 V_2 \quad (6.9)$$

with a density (ρ), a pressure (P), an area (A), the velocity (V), and the flow (F).

By using the heat kinematic ratio $K = \gamma/(\gamma - 1)$ and rearranging eqs. 6.8 and 6.9, they obtained the following 3rd degree polynomial equation

$$F = G + \frac{G}{2P_1} P_2 + \frac{G}{8P_1^2} P_2^2 + \frac{3G}{48P_1^3} P_2^3 + \dots \quad (6.10)$$

obtained a 3rd degree polynomial equation, also see fig. 6.8, with

$$G = \left(\frac{2\rho A_2^2 K P_1}{(1 - \Omega^2)} \right)^{\frac{1}{2}} \quad (6.11) \quad \text{and} \quad \Omega = \frac{\rho_2 A_2}{\rho_1 A_1} = \frac{A_2}{A_1} \quad (6.12)$$

They then used this polynomial equation to model the P/\dot{V} -relationship and obtained curve-fitting and IFL detection results that were superior to those of other mathematical models like the commented hyperbolic equation or a quadratic equation.

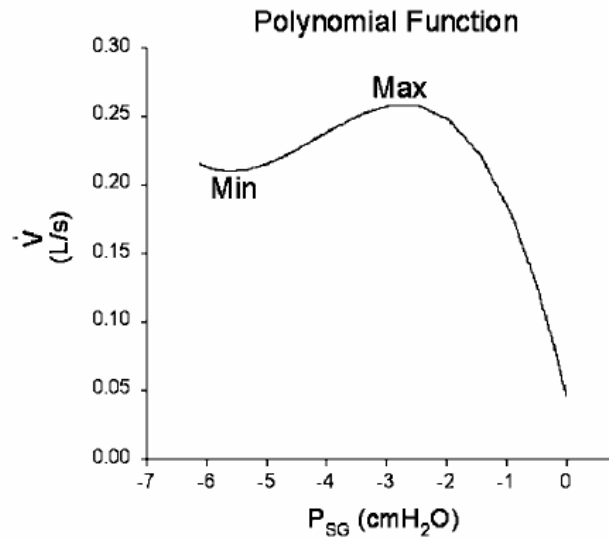


Figure 6.8: Graphical representation of the mathematical nature of polynomial function, being characterized by two deflections (max/min) [94]

Comparison of the hyperbolic vs. the polynomial model

We compared the modelling performance of the two models for a set of different inspiratory breaths and their respective P/V-diagrams, which can be seen in fig. 6.9.

The mathematical models showed some problems when reproducing certain type of P/V-diagrams as can be seen in fig. 6.10 and fig. 6.11 for the polynomial and Hudgel equations respectively.

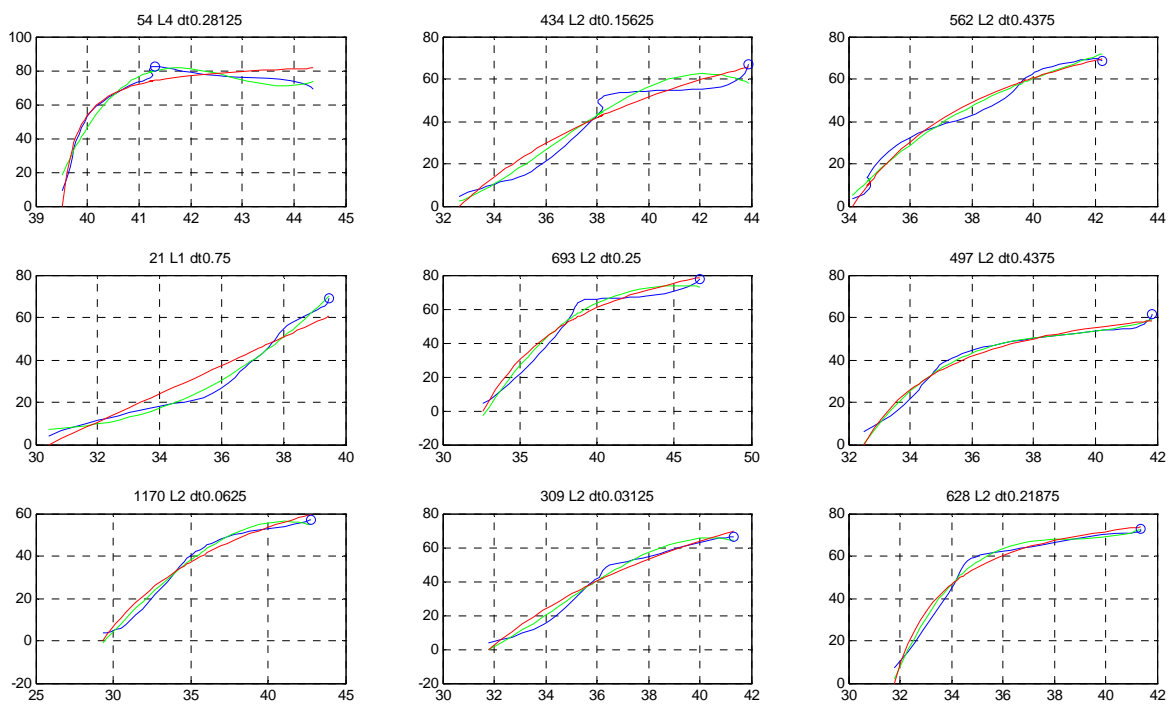


Figure 6.9: Examples of different P/V-Diagrams (each one represents one inspiratory breath). Original function (blue) modelled by the Hudgel eq. (red) and polynomial eq. (green).

Original function	Polynomial function	Hudgel's function
4	4	2
2	4	2
2	2	2
1	1	1
2	4	2
2	2	2
2	4	2
2	3	2
2	2	2

Table 6.2: Overview of the IFL Level (mis-)classifications for the predicted functions of the different models and the corresponding original function of a number of example inspirations.

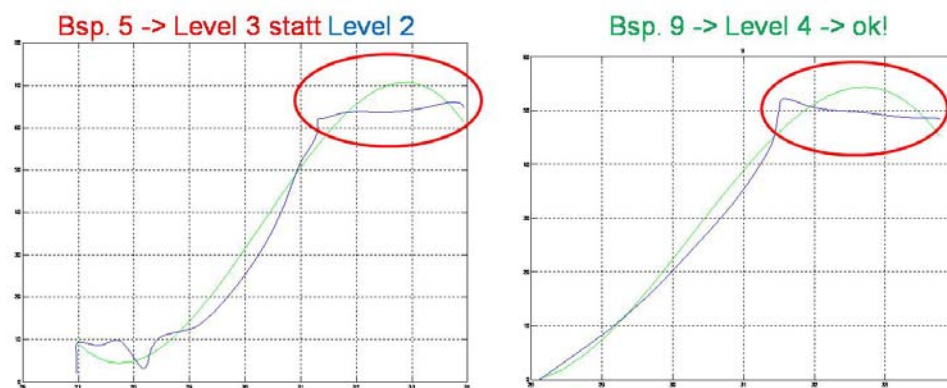


Figure 6.10: Classification problems of the polynomial equation. Observe how the predictions by the mathematical model (green line) present a steep fall in the non-linear segment in comparison to the original function (blue line), leading to a inspiratory flow level misclassification.

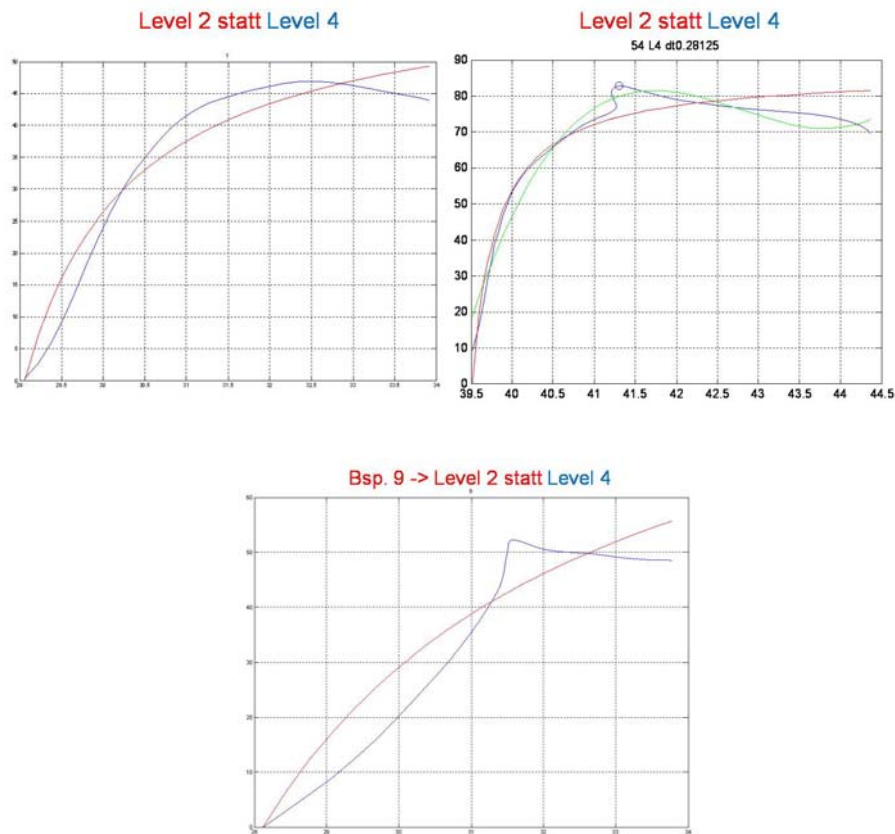


Figure 6.11: Classification problems of the Hudgel equation. Hudgel's hyperbolic model (red line) is not able to classify IFL Level 4 as its asymptotic limitation prevents it to fit the falling patterns of the original function (blue line), usually leading to an inspiratory level misclassification

Polynomial model	Hudgel's hyperbolic model
0.8391	0.5097

Table 6.3: Overall percentage (sensitivity) of correct classifications of the predicted functions by the respective models in comparison to the classification of the original function with classical criteria.

IFL Level	Polynomial model	Hudgel's hyperbolic model
1	0.8041	0.5350
2	0.9249	0.9933
3	0.5390	0
4	0.8580	0.0031

Table 6.4: Percentage (sensitivity) of correct classification of the predicted functions by the respective models in comparison to the classification of the original function by Clark et al.'s IFL level criteria.

IFL Level	Polynomial model	Hudgel's hyperbolic model
1+2	0.8434	0.6842
3+4	0.8264	0.0028

Table 6.5: Correct classifications (sensitivity) for the combination of Clark et al.'s mild IFL levels (1+2) and more severe IFL levels (3+4)

Polynomial model	Hudgel's hyperbolic model
0.9429	0.4135

Table 6.6: Mean R^2 Pearson-Coefficient calculated for the model's predictions and the original function.

IFL Level	Polynomial model	Hudgel's hyperbolic model
1	0.9890	0.7828
2	0.9139	0.6260
3	0.8519	0.3571
4	0.8831	-0.2971

Table 6.7: Mean R^2 Pearson-Coefficient calculated for the model's predictions and the original function segmented into Clark et al.'s IFL levels.

The results show that the Hudgel equation is unable to classify accurately the IFL Level 4 breaths, which are, in our opinion, the most interesting breaths overall as they present the highest severity as they present the highest UA-resistance. As the Hudgel equation is an hyperbolic equation, it will never be able to reproduce the descending end of the original P/V-diagram.

The Polynomial equation showed problems when approximating the latter part of the P/V-Diagram, sometimes resulting in misclassifications, especially in the IFL Level 3 breaths. Both equations performed well when classifying IFL Level 1+2.

Thus, a new mathematical alternative is necessary that does not show the limitations of the hyperbolic model for IFL levels 3+4 and the variance around the IFL segment as the polynomial model.

Exponential model

Clark et al. [81] proposed a model to mathematically fit the approximately linear P/\dot{V} - relationship of flow limitation levels 1 and 2 (Table 3), but they were not able to model the P/\dot{V} -relationships for levels 3 and 4 because of its non-linear behavior. Despite this limitation, Clark's model is elegant and simple, allowing a fast classification with only one coefficient value. So, we decided to build on this model and expand it to also fit non-linear P/\dot{V} -relationships by complementing it with an exponential term. The resulting equation,

$$\dot{V}(P) = a \cdot P^b \cdot e^{cP} \quad (6.13)$$

being the variable P the esophageal pressure and (a, b, c) the equation's coefficients, possess interesting characteristics that meet the previously mentioned considerations on non-linearity:

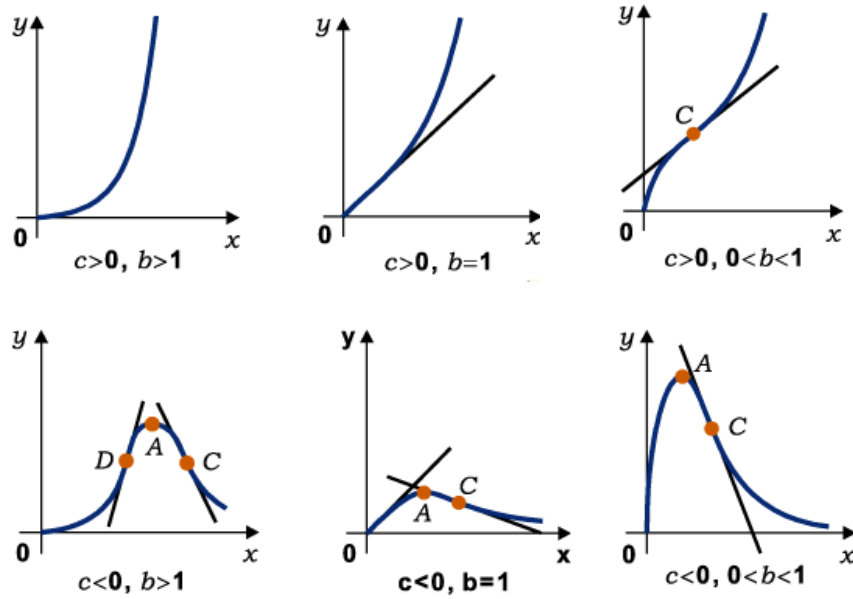


Figure 6.12: Different combinations of the coefficients b and c of eq. 2 (the x -axis represents the variable P and the y -axis the variable \dot{V}) with a positive coeff. a and positive values for x . The upper and lower row show the equation's capability to model approximately linear functions and non-linear curves, respectively (courtesy of I.N. Bronstein et al., Taschenbuch der Mathematik, Verlag Harri-Deutsch, 1999)

for different coefficient combinations, none, one or two inflection points (C , D) will appear at $P = (-b \pm \sqrt{b})/c$, while an extremum (A) will appear at $P = -b/c$ when coefficients b and c have opposite signs (fig. 6.12). Hence, we hypothesized that, because of this adaptability, eq. 6.13 could give a confident fit for linear as well as non-linear P/\dot{V} -relationships. Furthermore, other studies [60, 110] had also suggested different types of exponential equations that showed promising fitting results for IFL breaths.

Subjects

Eleven male, lung-healthy subjects without asthma nor COPD, had full nocturnal polysomnography (NPSG) with an 18-channel recorder (Somnolab PSG system V2.01, Weinmann GmbH, Hamburg, Germany) at the sleep laboratories of *Klinikum Bethanien* hospital in Solingen, Germany. Mean values \pm SD of the studied population for Apnea-

Hypoapnea Index (AHI) were 14.752 ± 12.53 events/h (range 1.8 – 46.9 events/h), body-max-index (BMI) 27.67 ± 2.72 kg/m² (range 24 – 39.19 kg/m²) and age 55.36 ± 14.03 years (range 39 – 78 years). In regards to arterial oxygen saturation (SpO₂), mean SpO₂ values were $94.43\% \pm 1.45\%$, (range 92-0% - 96.5%), minimal SpO₂ values were $85.55\% \pm 3.5\%$, (range 80% - 92%) and mean SpO₂ time under 90% was 8.38 ± 15.82 minutes, (range 00.07 – 54.54 min.).

Evaluation criteria for the mathematical models

Regression was automatically performed on the measured P/\dot{V} -relationship of each breath, see circles in fig. 6.13, in order to estimate the coefficients of the hyperbolic model [57], the polynomial model [94] and the new exponential model. Regression was performed with a standard least-square (LS) algorithm, also see chapter VII, that minimized the summed square of the residuals S :

$$\min(S) = \sum_{i=1}^n r_i^2 = \sum_{i=1}^n \left(y_i - \hat{y}_i \right)^2 \quad (14)$$

being r_i the residual of the i^{th} data-point for a total of n points, while y_i is the measured and \hat{y}_i the fitted response value. Then each model's predictions were computed, see fig. 6.10, for each breath's P/\dot{V} -relationship.

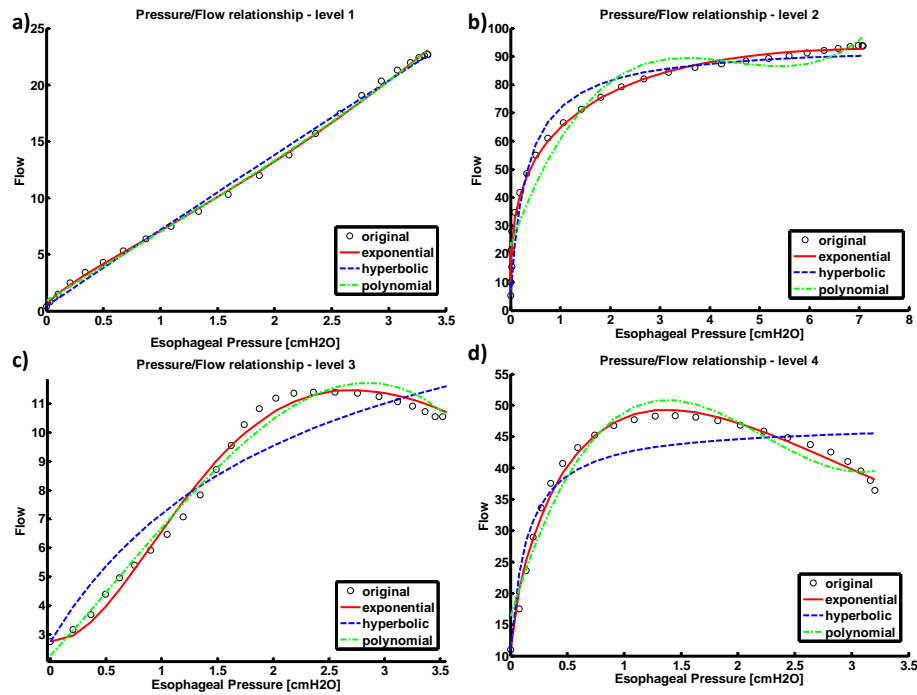


Figure 6.13: Examples of pressure/flow relationships of breaths classified as a) non-IFL (level 1) b) (level 2), c) IFL (level 3) and d) severe IFL (level 4). The functions are displayed after LS-regression on the measured values (circles).

Analyzing the coefficients of the exponential equation, individual Kolmogorov-Smirnov tests proved that none had a normal distribution ($P < 0.01$). When Clark's criteria were applied, we used the Kruskal-Wallis test to test the coefficients for significant differences ($P < 0.001$) between the 4 levels. Mann-Whitney U tests were performed to assess the between-group differences ($P < 0.05$) for classical and Clark's criteria. A Two-Step Cluster analysis (SPSS v.16.0, SPSS Inc., Chicago, IL, USA) was used to find the cluster centroids for classical criteria.

The following three evaluation parameters were employed to assess each model's characterization capabilities:

1) Mean-Squared Error when estimating respiratory resistance at peak pressure

The mean-squared error (MSE) when estimating respiratory resistance at peak-pressure [71] with $R = P / \dot{V}$, was computed as the squared difference between the estimated measured resistance and each of the models' estimated predicted resistances at peak-pressure, respectively.

2) Coefficient of determination (R^2)

In order to estimate the variability of the models' predictions in regard to the measured values, we calculated the coefficient of determination [111] which has been commonly defined as the squared coefficient of correlation or, alternatively, by the sum of squared errors (SSE) and the total sum of squares (SST):

$$R^2 = 1 - SSE / SST = 1 - \frac{\sum_{i=1}^n (y_i - \hat{y}_i)^2}{\sum_{i=1}^n (y_i - \bar{Y})^2} \quad (15)$$

being \bar{Y} the mean value of the measured values.

3) Assessment of IFL and increasing levels of UA obstruction

Assessment of IFL was automatically performed by classical criteria on the measured and on the predicted P/\dot{V} -relationship of each breath for each mathematical model. Sensitivity and specificity were then computed for each model. For Clark's criteria sensitivity and specificity were computed for increasing levels of UA obstruction [81].

Individual Kolmogorov-Smirnov tests ($P < 0.05$) proved that neither the R^2 nor the MSE were normally distributed. Mann-Whitney U tests ($P < 0.01$) were used to confirm the differences between the mathematical models.

Results

The IFL classification results for the exponential model's predictions on a total of 38,782 breaths for classical and for Clark's criteria can be found in (Tables 6.8 - 6.10).

The exponential model delivers the highest sensitivity and specificity for both criteria.

Significant differences ($P < 0.01$) were found for the R^2 coefficient between each mathematical model for classical and for Clark's criteria, with the exception of the polynomial and exponential functions for level 3 ($P < 0.05$). Significant differences ($P < 0.01$) were found for the MSE between each model for classical and for Clark's criteria, while the exponential model presented the smallest average MSEs for IFL breaths (Tables 6.8, 6.9).

When evaluating the exponential model's coefficients, the nonparametric Kruskal-Wallis test showed significant differences ($P < 0.001$) for the coefficients a , b and c between the 4 levels and between IFL and non-IFL breaths, respectively. All coefficients presented significant ($P < 0.01$) between-level differences, with the exception of coefficient b between levels 1 and 4 ($P < 0.05$). For classical classification criteria, significant differences ($P < 0.01$) were found between non-IFL and IFL breaths for all three coefficients. The coefficients' values mean and standard deviation were for coefficient a : 3.90 ± 2.49 , range (1 – 9.99), for coefficient b : 3.74 ± 2.74 range (1 – 9.99) and for coefficient c : -0.539 ± 10.79 range (-1.906 – 17.72). The Two-Step cluster analysis returned 2 clusters with a sensitivity/specificity of 1,0 and the following cluster profiles: the mean values, with a 95% confidence interval, for the cluster centroids were for parameter a 4.025 for IFL and 3.876 for non-IFL, for parameter b 3.396 for IFL and 3.806 for non-IFL and for parameter c -1.3129 for IFL and -0.3846 for non-IFL.

	No. of breaths	Evaluation parameter	Polynomial	Hyperbolic	Exponential
<i>non-IFL</i>	32,360	MSE	0.0008	0.0019	0.0017
		R ²	0.95	0.92	0.95
<i>IFL</i>	6,422	MSE	0.167	0.059	0.045
		R ²	0.90	0.71	0.89
		Se	0.84	0.04	0.86
		Sp	0.94	0.99	0.95
		Acc	0.92	0.83	0.94

Table 6.8: Characterization results for classical criteria. Coefficient of determination (R²), Mean Square Error (MSE), Sensitivity (Se), specificity (Sp) and Accuracy (Acc).

Flow limitation Level	No. of breaths	Evaluation parameter	Polynomial	Hyperbolic	Exponential
<i>1</i>	13,398	MSE	0.0003	0.0011	0.0007
		R ²	0.99	0.95	0.98
<i>2</i>	17,514	MSE	0.0007	0.0014	0.0014
		R ²	0.93	0.90	0.93
<i>3</i>	1,683	MSE	0.007	0.016	0.013
		R ²	0.90	0.81	0.90
<i>4</i>	6,187	MSE	0.17	0.06	0.05
		R ²	0.90	0.70	0.89

Table 6.9: Characterization results for Clark's criteria. Coefficient of determination (R²), Mean Square Error (MSE).

Flow limitation Level	versus Level		Polynomial	Hyperbolic	Exponential
<i>1</i>	<i>2, 3, 4</i>	Se	0.89	0.96	0.99
		Sp	0.82	0.68	0.83
<i>1, 2</i>	<i>3, 4</i>	Se	0.88	0.96	0.93
		Sp	0.72	0.03	0.72
<i>1, 2, 3</i>	<i>4</i>	Se	0.85	0.92	0.89
		Sp	0.83	0.04	0.85
<i>Overall</i>		Acc	0.84	0.78	0.88

Table 6.10: Classification results for Clark's criteria. Sensitivity (Se), specificity (Sp) and Accuracy (Acc).

Discussion

This study's focus has been on finding a methodology that automatically assesses changes in UA obstruction robustly and accurately, while still allowing an efficient computational processing. The classification and curve fitting performances of the mathematical models were tested on an overall of 38,782 breaths extracted from eleven patients, a significant increase in the total number of analyzed breaths compared to previous studies [94, 81, 71]. Thus, the methods presented here represent a promising tool for automatic invasive assessment of IFL especially for scenarios where a high number of breaths have to be analyzed. The clinical relevance is to be comprehended in combination with already developed methodology [14], in order to detect RERAs. The more accurate the identification of IFL or changes in UA obstruction, the better the RERA detection should become.

For the signal acquisition we employed esophageal pressure measurement and nasal cannula flow, as these have extensively been proven to permit a reliable reconstruction

of the P/\dot{V} -relationship and detection of IFL episodes [16, 14, 15, 19, 18]. Classical and Clark's classification criteria are defined by decreasing flow tendencies (not absolute differences), so absolute airflow values are not required for IFL detection [16, 14, 19, 81]. As our non-invasive classifier has the objective to be adopted in clinical routine, the flow sensor had also to be commonly used in clinical routine. Obtaining a conventional pneumotachograph flow requires a tight-fitting face mask, which may be excessively intrusive for routine sleep monitoring [16]. The nasal cannula device is a widespread and commonly used sensor and has some characteristics, like being simple, inexpensive and non-obstructive, that makes it ideal for clinical routine.

For the invasive assessment of relative changes in UA obstruction we sought after a model that best characterized linear as well as non-linear P/\dot{V} -relationships. The gold-standard automatic invasive classifier was implemented as described by Clark et al. [81] in order to validate the exponential model. This is an elaborate procedure, while the iterative classification algorithm for classical and Clark's criteria is computational inefficient. An automatic classification system using a model should be easier to implement, more robust if the measured data is noisy and permit a more computational efficient classification of IFL episodes. Another advantage of describing mathematically a P/\dot{V} -relationship is that it permits estimating a wide variety of other parameters (like respiratory resistance) for further breath analysis.

We chose to employ the coefficient of determination R^2 and the MSE when estimating resistance at peak-pressure as evaluation parameters, as they had been previously employed in other studies [16, 94, 71] for the same purpose. Particularly, Tamisier et al. [71] calculated resistance at peak-pressure in order to assess the hyperbolic model and measured a high correlation between real resistance values and the predictions of the

hyperbolic model. We were inclined to also employ the MSE when estimating resistance at peak-pressure in our study, as it should be a good indicator on how well the models predict resistance in the non-linear portion of the P/\dot{V} -relationship during IFL episodes.

However, during the analysis we observed that only these two parameters could fall short to evaluate a model's ability to characterize IFL, as high values did not always correlate with a correct IFL classification (Tables 6.8 - 6.10). Therefore we decided to employ the direct assessment of IFL on each model's predictions as the third and most basic evaluation parameter, permitting us to obtain an accurate insight on each model's robustness for automatic invasive IFL classification. Still, this study did not reach out to compare each model's intrinsic characterization capabilities, such as the coefficient based classification for the hyperbolic model [57] or the derivative classification method for the polynomial model [94], which should be compared in detail in a future work.

The new exponential model showed the highest average sensitivity and specificity when classical criteria were applied (Table 6.8). The hyperbolic model showed a poor performance when assessing breaths with IFL, because a hyperbola is very limited when modeling the non-linear segment of the P/\dot{V} -relationship of an IFL breath, as its asymptote prevents it from correctly fitting falling flow for decreasing pressure, see fig. 6.10 c, d. Although the difference between polynomial and exponential models is modest, it should not be neglected due to the high amount of processed breaths. When Clark's criteria were applied, the exponential model again achieved better results than the other two models (Table 6.10), implying that it delivers the most accurate reproduction of the P/\dot{V} -relationship when a higher resolution of the changes in UA

obstruction is required. All three models had problems classifying level 3 breaths, see Table 6.10, probably because they were not able to reproduce its characteristic stalling flow pattern.

Most of the observed IFL misclassifications occurred because of curve fitting problems specifically at the non-linear segment of the P/\dot{V} -relationship. For example, a R^2 value of 0.93 may indicate a good fit of the polynomial function on the overall measured P/\dot{V} -relationship shown in fig. 6.13 b) that had been previously annotated as non-IFL with classical criteria. But the polynomial model's prediction was misclassified as IFL because of the polynomial model's tendency to oscillate around the non-linear segment. This is not reflected by the R^2 coefficient because it analyzes the P/\dot{V} -relationship as a whole. For future studies, we would recommend to use, instead of the R^2 coefficient, an evaluation parameter that ponders the non-linear segment higher.

The average MSEs were relatively small for non-IFL breaths (Tables 6.8, 6.9), indicating a good fit of approximately linear P/\dot{V} -relationships for all three models. For IFL breaths, the MSEs had a two- to threefold higher magnitude for all models, indicating that the prediction of resistance at peak pressure represented the more challenging task. The exponential model achieved the best result when estimating resistance at peak-pressure, as it delivered the significant smallest average MSE, see Tables 6.8 and 6.9.

Conclusions

In conclusion, the linear P/\dot{V} -relationship was used in order to achieve a gold-standard classification of breaths for IFL. These gold-standard scorings were then used to validate different mathematical models that may help to optimize the automatic

classification process. The exponential model delivers the best characterization of changes in UA obstruction, as it achieves the highest sensitivity and specificity when assessing classical IFL episodes and the more subtle changes in UA obstruction as defined by Clark's criteria. Furthermore, the exponential model also allows predicting UA resistance at peak pressure with the lowest average MSE. We have also shown that the coefficients of the exponential model should permit developing a computational efficient automatic IFL annotation system that is solely based on the characterization of IFL by its coefficients' values. Still, alternative mathematical methods for level classification with the exponential model could also be explored, as e.g. an analysis of the exponential model's derivative function. Thus, the exponential model seems to be a promising tool for an invasive assessment of IFL and the prediction of UA resistance, in a scenario where a high number of breaths may need to be processed.

Chapter VII: Techniques used in pattern classification

Introduction

Automatic pattern identification and classification has been one of the main and most challenging tasks in computer science in recent time. Supervised machine learning techniques, like artificial neural networks (aNN) or support vector machines (SVMs), are techniques that have been commonly used for this purpose. These techniques usually try to guide the classifier's decision-taking process to emulate human behavior. Currently in most sleep laboratories SDB pattern recognition and NPSG pattern recognition for R&K sleep stage scoring are still performed manually, which is a highly inefficient and costly procedure, representing a strong burden on sleep lab human resources. Only slowly reliable automatic systems are developed and find their way into clinical routine [105]. One of the objectives of this thesis is to develop automatic systems that increase the efficiency of scoring but still are able to recreate the gold-standard results obtained by human experts. We believe that supervised machine learning methods represent a valuable tool to achieve these goals and the most important techniques of this family will be briefly introduce in this chapter to be later implemented in the coming chapters.

In supervised machine learning, a training phase is needed during which the classifier learns to solve a bi- or multi-class problem. After the training phase, the classifier's performance can be optimized and tested on validation and test sets, respectively, and the classification results are then obtained. The training, validation and test sets usually consist of a (n -times- k) feature matrix with a number k of n -dimensional elements and of

a label vector of length k , usually containing the class label $\{+1;-1\}$ for each element. The class labels have usually been obtained by manual classification of human experts. The feature matrix contains those features needed to best characterize the pattern to be recognized. The better the features characterize the sought pattern, the better the classification results usually become. When a big pool of features is available, usually selection algorithms, such as fast forward selection, are run before the training and testing, in order to narrow down the most optimal feature sets for each classifier and reduce the complexity of the classification problem.

However, the limit of any supervised machine learning approach for classification is usually found in the human decision making itself, as interhuman and interscorer differences regularly appear above the boundary of 80-85% of accuracy [123].

Discriminant Analysis (DA)

As stated in [122, 128], discriminant analysis uses training data to estimate the parameters of discriminant functions of the predictor variables which will then be applied to separate the classes in the test data. These functions, like linear DA (LDA), quadratic DA (QDA) or the related Fisher's LDA, are called the discriminant functions, and they are used in supervised machine learning to get the combination of features that separate two or more classes of events. The results can be employed just to reduce the complexity/dimensionality of a classification problem or as a classifier itself.

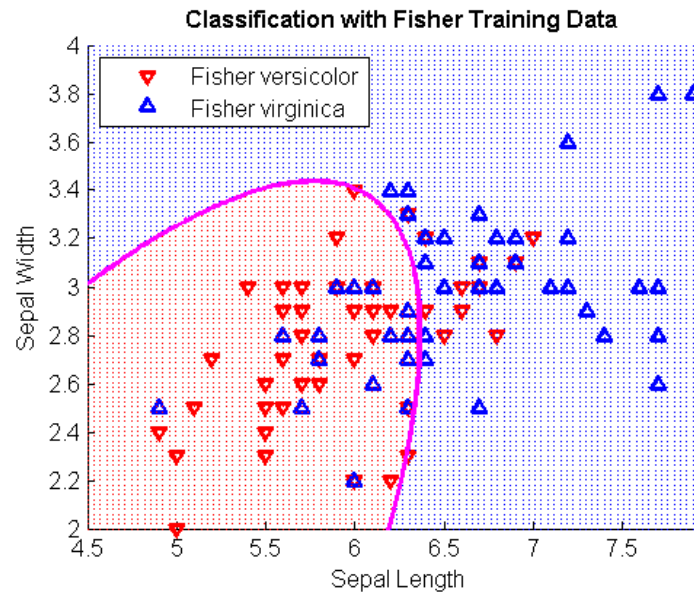


Figure 7.1: Example of a feature set of two groups separated by a quadratic function with DA

[128]

For our purposes, we used DA with the following discriminant functions as described in [128]:

- **Linear DA (LDA):** Fits a multivariate normal density to each group, with a pooled estimate of covariance. This is the default.
- **Diaglinear DA (DLDA):** Similar to 'linear', but with a diagonal covariance matrix estimate (naive Bayes classifiers).
- **Quadratic DA (QDA):** Fits multivariate normal densities with covariance estimates stratified by group.
- **Diagquadratic DA (DQDA):** Similar to 'quadratic', but with a diagonal covariance matrix estimate (naive Bayes classifiers).
- **Mahalanobis DA (MDA):** Uses Mahalanobis distances with stratified covariance estimates.

LDA attempts to express a dependent variable as a linear combination of features, thus showing some similarities to the statistical algorithm analysis of variance (ANOVA). However, for LDA the dependent variable is a categorical variable, while in ANOVA the dependent variable is numerical. [122]

As stated in [122], for the two-class LDA algorithm, we need a training set that consists of a set of features \vec{x} for each sample of an event with a known class correspondence $y \in \{+1, -1\}$. The assumption is taken that the conditional probability density functions $p(\vec{x}|y = 1)$ and $p(\vec{x}|y = 0)$ are both normally distributed. Given only one observation \vec{x} , the LDA algorithm will try to find a good predictor for the class y of any sample of the same distribution. In LDA also the simplifying assumption can be made that the class covariances are identical $\Sigma_{y=0} = \Sigma_{y=1} = \Sigma$ (homoscedastic assumption) and that the covariances have full rank. In this case the general LDA function [122] can be simplified resulting in

$$\vec{w} \cdot \vec{x} < c \quad (7.1)$$

for some threshold constant c , where

$$\vec{w} = \Sigma^{-1}(\vec{\mu}_1 - \vec{\mu}_0) \quad (7.2)$$

This means that the criterion of an input \vec{x} being in a class y is purely a function of this linear combination of the known observations. If seen in geometrical terms, see fig. 7.1, we could assume that the location of the plane is defined by the threshold c , while a feature belongs to y if a corresponding \vec{x} is located on a side of the hyperplane perpendicular to \vec{w} .

Support Vector Machines (SVMs)

Support Vector Machines (SVMs) are very powerful classifiers for pattern classification [113]. As stated by Burges et al. [112], “SVMs are widely used for learning classifiers and regression models, and are generally trained through supervised learning. Given two classes of points $\{+1;-1\}$, the main objective of an SVM is to find an optimal hyperplane that correctly classifies them and separates them as far as possible, see example in fig. 7.2. The goal of an SVM is to find the optimal separating hyperplane (OSH), which minimizes the risk of misclassifying the training data and the unseen test data. The OSH guarantees the fulfilment of the following conditions

- The largest possible fraction of points of the same class are left on the same side of the plane.
- The distance from the hyperplane of both classes is the maximum possible.

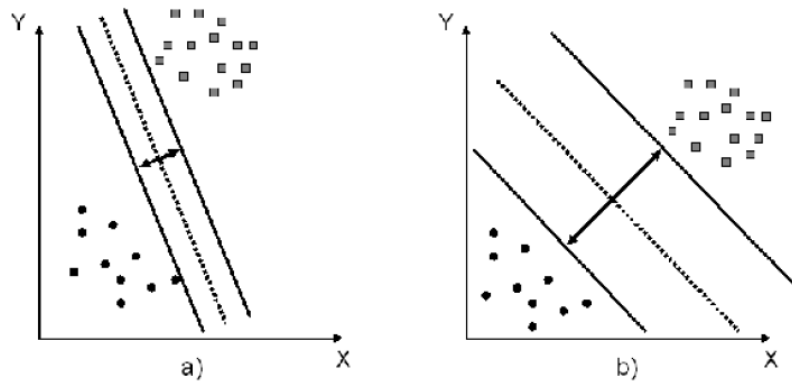


Figure 7.2: (a) A separating hyperplane with small margin with a class of points on each side (b) A separating hyperplane with larger margin. A better generalization is expected in the latter case [112]

Given a set of points $x_i \in R^n$, where $i = 1 \dots l$ and l is the number of observations or points to be shattered. Each point x_i belongs to either one of our two classes with the labels $y_i \in \{-1, 1\}$. We suppose that a linear hyperplane $x \cdot w + b = 0$, which separates

the positive from the negative examples, exists. All training examples thus satisfy the constraints

$$x_i \cdot w + b \geq +1 \text{ when } y_i = +1 \quad (7.3)$$

$$x_i \cdot w + b \leq -1 \text{ when } y_i = -1 \quad (7.4)$$

or equivalently:

$$y_i (x_i \cdot w + b) - 1 \geq 0, \forall i \quad (7.5)$$

Being this the case, the set is considered linearly separable [112]. Thus, given a linearly separable set S , the hyperplane for which the distance to the closest point of S is maximum, is called the optimal separating hyperplane (OSH). As explained in detail in [112], the solution to the linear case can be found by solving the Quadratic Programming problem with linear constraints, which results in sparse solutions. This implies that the problem can be solved by using a linear combination of a relative small percentage of the initial data points x_i , which are represented by the vector w . Given the constraints

$$y_i (x_i \cdot w + b) - 1 \geq 0 \quad (7.6)$$

with $i = 1, 2, \dots, N$, the solution becomes

$$\bar{w} = \sum_{i=1}^N \alpha_i y_i x_i \quad (7.7)$$

where N is the number of Support Vectors. The points known as Support Vectors, see fig.7.3, are the closest points to the hyperplane. As stated before, only these points are necessary to determine the final OSH.”

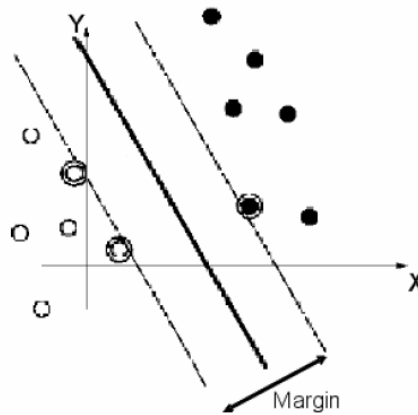


Figure 7.3: The optimal hyperplane and the circled support vectors [112]

In most cases, a linear SVM should be able to achieve the expected results. However, there are cases where the optimal separating hyperplane can not be described with a linear function. As can be seen in [112], “the data in the training problem appears in a form that allows the problem to be solved by mapping the data into a higher dimensional Euclidean space H , where it is more likely to find a hyperplane that separates both classes. Hence, it is possible to solve this problem using the transformation operator ϕ . However, the best solution is usually achieved by using a Kernel function $K(x_1, x_2)$ in the training algorithm. Instead of mapping the training data nonlinearly to a higher-dimensional feature space with the operator ϕ and constructing there the separating hyperplane with maximum margin, the kernel function can be used to compute the separating hyperplane without explicitly carrying out the map into the feature space. This allows to reduce the computational complexity.”

Adaboost

AdaBoost is one of the most popular boosting algorithms in supervised machine learning theory. The term boosting describes the process of strengthening simple,

"weak" classifiers and turning them into a "strong" classifier by combining them iteratively. A general combination classifier [114] usually takes the form

$$g(x) = \sum_{t=1}^T \alpha_t h_t(x) \quad (7.8)$$

where h_t is the hypothesis of a weak classifier which performs slightly better than random guessing and α_t is a parameter which measures the importance assigned to h_t .

Input data are the pairs of (x_t, y_t) , where $x \in X$, X being an instance space, and the label y_t belongs to a label set $Y = \{-1, +1\}$.

AdaBoost iteratively calls the weak learning algorithm in a series of rounds $t = 1 \dots T$, where at each time step t the algorithm has to

- Update the training sample distribution in order to favour the difficult examples according to the previous results of the weak classifiers. This is done with the help of a distribution of Weights $D_t(i)$ over the training set, on round t of training example i .
- Train a new weak classifier. The Weak learner's job is to find a Weak hypothesis $h_t : X \rightarrow \{-1, 1\}$ appropriate for the distribution $D_t(i)$.
- Select the new Weight parameter α_t once the the Weak hypotheses h_t has been received.

The final solution of the algorithm is the weighted sum of all Weak classifiers, as seen in equation 10. The algorithm stops if it is not able to find a Weak classifier which satisfies the condition named above of being better than random guessing. As stated in [114], the algorithm takes thus the following form:

- Given: labelled training inputs $(x_1, y_1), \dots, (x_m, y_m)$
- Initialize Weight distribution: $D_1(i) = 1/m$, all Weights are equal for the first round.
- for $t = 1 \dots T$
 - a) train Weak learner using distribution $D_t(i)$
 - b) get Weak hypothesis h_t and calculate Weighted training error ε_t :

$$\varepsilon_t = \sum_{i=1}^n D_t(i) \cdot I(y_i \neq h_t(x_i)) \quad (7.9)$$

where $I(z) = 1$ if z is true, 0 otherwise

- c) Compute Weight α_t of Weak classifier h_t :

$$\alpha_t = \frac{1}{2} \cdot \ln \left(\frac{1 - \varepsilon_t}{\varepsilon_t} \right) \quad (7.10)$$

- d) Update Weight distribution:

$$D_{t+1}(i) = \frac{D_t(i) \cdot \exp(-\alpha_t y_i h_t(x_i))}{Z_t}, \quad (7.11)$$

where Z_t is a normalization factor such as $\sum_i D_{t+1}(i) = 1$

- Output final hypothesis:

$$H(x) = \text{sign} \left(\sum_{t=1}^T \alpha_t h_t(x) \right) \quad (7.12)$$

Recent developments have suggested using Classification and Regression trees (CARTs) as the better weak classifiers. An Adaboost algorithm using CARTs with only

one split would be equivalent to the classical stump learner [114]. Also variations of the Adaboost algorithm itself have been recently proposed. Algorithms like the gentle adaboost [116] or modest adaboost [117] have each different generalization capabilities that make them interesting in different classification scenarios.

Stepwise forward feature selection

As stated in [128], sequential feature selection is a popular iterative selection method, which picks the highest correlated components out of a huge feature pool. Sequential selection normally has two variants:

- Sequential forward selection (SFS): the features are sequentially added to an empty candidate set until the addition of further features does not decrease the criterion.
- Sequential backward selection (SBS): the features are sequentially removed from a full candidate set until the removal of further features increase the criterion.

The criterion is an objective function which the algorithm usually seeks to minimize over all feasible feature subsets. Common criteria are e.g. mean squared error for regression models or the misclassification rate for classification models. Another component of the algorithm is the sequential search algorithm, which adds or removes features from a candidate subset while evaluating the criterion. Since an exhaustive comparison of the criterion value at all 2^n subsets of an n -feature data set is typically infeasible (depending on the size of n and the cost of objective calls), sequential searches move in only one direction, always growing or always shrinking the candidate set.

So, as detailed in [127], given a collection of possible predictors/templates $x_1 \dots x_N$, linear regression is performed on the initial label vector y with an approximation vector $y'_i = a \cdot x_i + b$. This results in a residual error vector v_i for every predictor x_i , where $v_i \perp y'_i$ and $i = 1 \dots N$. The predictor with the smallest error vector $|v_i| \rightarrow \min$ is selected, see fig. 74. The selected, smallest error vector v_s becomes the new response/label vector for the next iteration t . This algorithm is repeated for k rounds, which results in a set of selected predictors $x_1 \dots x_k$. Note that the same component can be selected several times in the selection process but will never appear repeated in pairs in the sequential order. The error/label vector should decrease its size with every iteration. The algorithm takes the following form in pseudo-code:

- Given the vectors $x_1 \dots x_N$, where N is the total amount of predictors available in the input set. Every single vector i contains the scalar correlation values $x_i = (x_{i1}, \dots, x_{iq})$ for all q positive and negative training samples. The label vector y represents the initial distribution of labels $(y_1 \dots y_q)$, where $y \in \{+1, -1\}$.
- for $t = 1 \dots k$ cycles do
 - a) for $n = 1 \dots N$ predictors do
 1. Given the vector x_n , approximate the label vector y with least squares and determine the scalar parameters of the linear equation $y' = a \cdot x_i + b$.
 2. Compute the error vector and its norm using the resulting approximation vector y' : $v = y - y'$, see fig. 4.
 - b) Determine the error vector with the smallest length (=smallest error) vs out of the set of all computed error vectors $v_1 \dots v_N$. The selected error vector v_s is the new label vector for the next iteration: $y_{t+1} = v_s$
- Output the selected predictors $x_1 \dots x_k$.

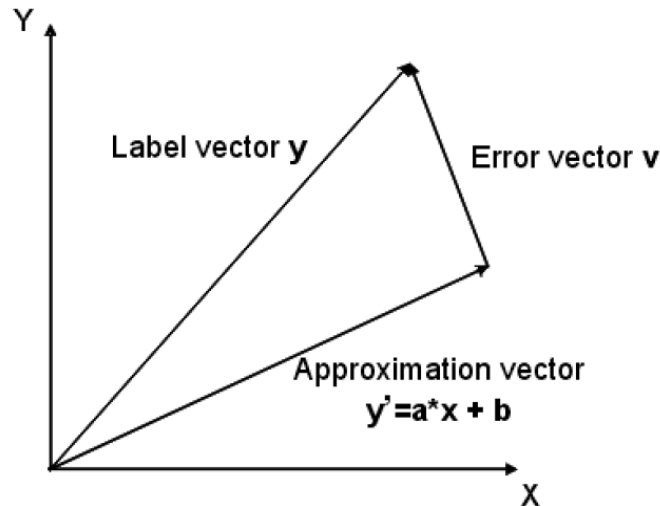


Figure 7.4: Vector distribution in forward selection: the label vector y is approximated with linear regression by $y_0 = a \cdot x + b$ resulting in the error vector v , which becomes the label vector for the next iteration [135].

Receiver Operator Characteristic (ROC)

The Receiver Operator Characteristic (ROC) displays the classification performance of a particular classifier. As seen on the plots in fig. 7.5, the percentage of correctly classified positive samples are plotted on the ordinate axis, while the percentage of false-positive samples, these are the negative samples that have been misclassified as positive, are plotted on the abscissa [124].

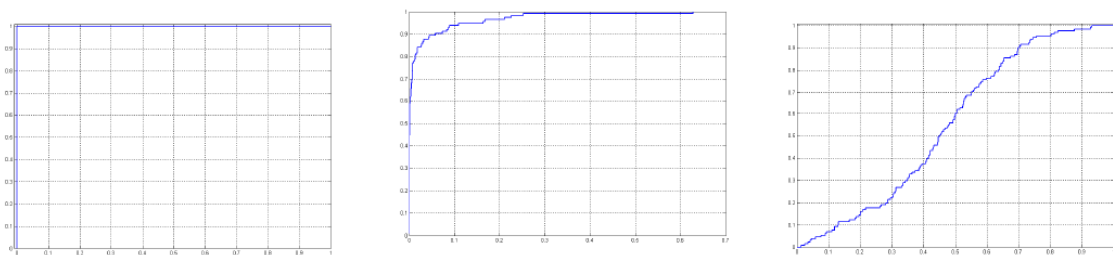


Figure 7.5: On the left the ROC of a perfect classifier, in the middle, a classifier with a good performance and on the right, a classifier with a very poor performance [135].

The ROC curve is constructed as follows: a vector containing the correlation values of a template with each of all positive and negative samples. The values of this vector are then sorted by size. The ROC curve plotting process starts with the highest correlation value of the vector.

If the first value belongs to e.g. a positive sample a step will be taken on the ordinate axis and a point will be plotted there, where the step has the value $I=p$ and p is the number of positive samples. If the next correlation value in the sorted vector belongs to e.g. a negative sample, the classifier would have done an error, as this negative sample has a higher correlation value than all other positive samples remaining. For the plot a step will have to be taken on the abscissa, parting from the previous position, and a new point will have to be plotted, where the step has the value $I=n$ and n is the number of negative samples. Thus the threshold value is given implicitly through the correlation values of the positive samples. If this process is iterated for all the vector's correlation values, we will obtain the ROC curve for that template.

The more an ROC curve approaches the upper left corner, the better is the classification performance of the system, see fig. 7.5. For example, fig. 7.5 (left) displays a perfect classification system that is able to classify the 100% of events without misclassifying a single negative sample. Fig. 7.5 (center) shows a system with a slightly lower performance, while fig. 7.5 (right) has a very low performance, as its ROC indicates that the system is misclassifying object samples. A diagonal from the bottom left to the top right of the sample would describe the process of guessing, thus the ROC of this latter classifier is not much better than guessing. Hence, a good measurement for the performance of a classifier is the area below its ROC.

K-Means Clustering

As stated in [128], K-means is a clustering technique which partitions the points of a $N \times P$ data set X into k clusters. The algorithm partitions the set iteratively by minimizing the sum of all distances of each of the clusters' data points to its corresponding cluster-center, over the sum of all clusters. Thus the value of the cluster-center, also called

cluster-centroid, changes with every iteration, defining a trajectory over all iterations, see fig. 7.6.

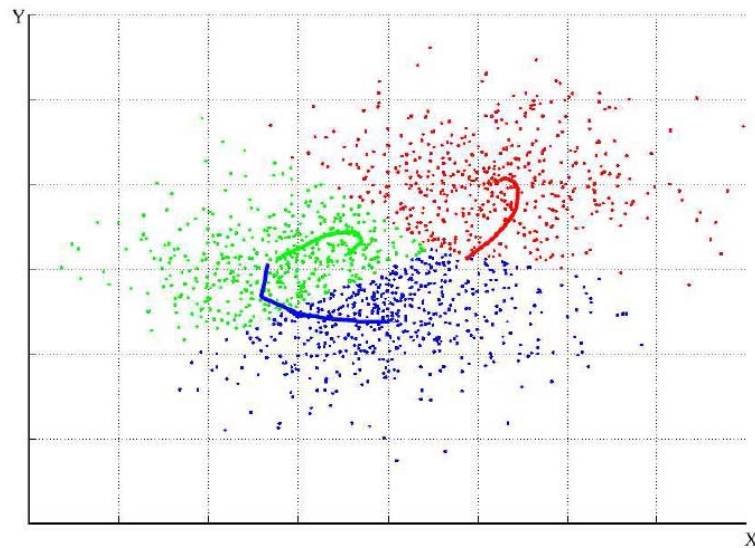


Figure 7.6: Example: Screenshot of how a 2×1500 sample data matrix is being clustered into 3 different clusters. The cluster-centroids are relocated with every iteration through the data, the trajectory is shown by the colored lines. [135]

There are different type of distance measures with which the clusters' centroid can be computed, where the most common is the squared Euclidean distance. This distance measurement implies that each cluster centroid becomes the mean of all points in that cluster.

An important parameter to set is the method used to choose the initial positions of the cluster-centers, also known as "seeds". If the algorithm fails to make a good initial distribution of the cluster centers over the data, we might get very bad separated and balanced clusters after running the algorithm. This would imply that some clusters would contain too many data points and others would contain none. This should and can be avoided by homogenously distributing the cluster centers over the initial data. There are different methods to initialize the cluster centers, e.g. picking k random observations of the initial data set X , or selecting k random points uniformly from the range of X . A more robust initialization method is to perform a preliminary clustering phase on a

small, random subsample of the initial data set X and initialize the cluster-centers parting from its results.

As already commented before, K-means minimizes, summed over all k clusters, the sum of point-to-centroid distances iteratively. The algorithm can be divided in two phases:

- The first phase is mainly used as a preprocessing phase and starting point for the next phase, as its result only an approximate solution. In this phase so called "batch" updates are implemented, where in each iteration the points are reassigned to their nearest cluster-center. Then the algorithm performs a re-computation of all the cluster-centers.
- The second phase uses so called "on-line" updates, where, as long as the sum of distances is reduced, points are individually reassigned. This phase goes through all of the points in each iteration, where after each reassignment the cluster centers are recomputed.

Linear Least Squares Approximation

As detailed in [125, 126], linear regression is the process of approximating a system's response function with a linear function that consists of the predictor data and one or more coefficients that have to be determined. The least squares method determines these unknown coefficients by minimizing the summed square of residuals. The residual r_i , where i is the current data point, is defined as the difference between the observed response value y_i and the approximated response value \hat{y}_i .

$$r_i = y_i - \hat{y}_i \quad (7.13)$$

Thus, the sum of squares error estimate S , which is the summed square of residuals, takes the form

$$S = \sum_{i=1}^n r_i^2 = \sum_{i=1}^n (y_i - \hat{y}_i)^2 \quad (7.14)$$

where n is the number of data points in the fit.

As long as the coefficients in an equation are linear, we are working with a linear model. Thus, e.g. 1st degree polynomials are linear but Gaussian-functions are not. For example, given n data points that are described by a first-degree polynomial,

$$y = a \cdot x + b \quad (7.15)$$

We need to determine the unknown coefficients a and b to be able to solve this equation. One approach to determine these coefficients would be to write S as a system of n simultaneous linear equations in two unknowns. The system of equations is called overdetermined, if n is greater than the number of unknown coefficients.

$$S = \sum_{i=1}^n (y_i - a \cdot x_i - b)^2 \quad (7.16)$$

As the least squares approximation method minimizes the summed square of the residuals, the coefficients can be determined by differentiating S with respect to each parameter and setting the result equal to zero. Solving equation 7.16 for a results in

$$a = \frac{n \sum x_i y_i - \sum x_i \sum y_i}{n \sum x_i^2 - (\sum x_i)^2} \quad (7.17)$$

where the summations run from $i = 1 \dots n$. Solving for equation 7.16 b using the value of a :

$$b = \frac{1}{n} \left(\sum_i^n y_i - a \sum_i^n x_i \right) \quad (18)$$

Thus only some calculations are necessary to determine the coefficients a and b . It is now also evident how to determine the solution for a higher degree polynomial, as only an additional normal equation, for each linear term added to the model, is necessary.

Cross-correlation

The cross-correlation coefficient for two discrete functions f and g is given by

$$(f \star g)[n] \stackrel{\text{def}}{=} \sum_{m=-\infty}^{\infty} f^*[m] g[n+m]. \quad (7.19)$$

where m, n are the number of samples of each function. Pearson's correlation coefficient is given by

$$r_{xy} = \frac{\sum x_i y_i - n \bar{x} \bar{y}}{(n-1) s_x s_y} = \frac{n \sum x_i y_i - \sum x_i \sum y_i}{\sqrt{n \sum x_i^2 - (\sum x_i)^2} \sqrt{n \sum y_i^2 - (\sum y_i)^2}}. \quad (7.20)$$

where x_i and y_i are a series of measurements (samples) with $i = 1 \dots n$ and s_x, s_y are the standard deviations of and \bar{x}, \bar{y} are the means of those series.

The correlation coefficient is a measure of similarity between two functions. Hence, this coefficient is often used in pattern recognition to measure the similarity between two patterns and weigh the classification decision process.

Conclusions

The most popular pattern classification techniques in supervised machine learning have been presented. These techniques usually try to emulate human behavior in pattern classification, which also implies that these techniques are liable to human subjectivity and interscorer differences. Supervised machine learning techniques require a training and a test stage where the algorithm learns to classify. The results can be visually represented with the ROC curves and their performance measured with the area under the curve.

Chapter VIII: Non-invasive, automatic identification of inspiratory flow limitation during sleep

Introduction

Several groups have tried in the last decade to find a reliable non-invasive indicator for UA resistance and respiratory effort, as a valid non-invasive alternative to esophageal pressure measurement. Techniques like Pulse-Transit-Time (PTT) [11, 22], forced-oscillation-technique (FOT) to determine respiratory resistive impedance [23, 24], intercostal EMG signal filtering [25 - 27], critical pressure measurement with therapy devices [28 - 31], the phase angle modification of thoracic and abdominal muscle movement measured by Resistive Inductance Plethysmography (RIP) belts [32, 33], Cyclical Alternating Patterns (CAPs) [34, 35] or analysis of the audio (snoring) signal [36 – 46, 131] are promising and interesting approaches but they still have to show its validity in clinical routine. One of the most promising signals for non-invasive assessment of SDB related events seems to be airflow signal, as flattening patterns present during inspirations seem to contain direct information on changes in UA resistance and respiratory effort [14 - 16]. In the following, some of the most important non-invasive techniques to assess SDB events are presented, to finally introduce a new proposal for a non-invasive method to detect IFL and subtle variations in UA resistance in the airflow signal.

Analysis of snoring

At first placed at the beginning of the severity scale of sleep disorders (followed by UARS, OSAHS and SHVS), it is now understood that snoring is a separate entity that

usually co-exists with other forms of sleep-disordered breathing [74] and may be an indicative of sleep disorders. With better understanding of breathing during sleep and better monitoring technology, it has become clear that the existence of benign snoring should be questioned. Snoring has been proposed to be evaluated especially for adults, because many are supposed to suffer from UARS [72] or a related SDB pathology.

Several studies have recorded audio signals during sleep with tracheal microphones to analyze snoring [40 – 46, 131]. Findings have suggested that the spectral envelope of the snoring signal may be a valid parameter for differentiation between obstructive and non-obstructive snoring [43]. Hoffstein et al [77] found a correlation between a snoring index (snores/h) and sleep efficiency and wakefulness time after sleep onset, but no significant effect of snoring was found on sleep architecture. Woodson [84] also reported a pattern of crescendo snoring followed by transient EEG arousals in the absence of oxyhemoglobin desaturation as highly suggestive of UARS. However, this non-invasive approach of identifying increasing snoring intensity followed by EEG arousals produced a significant number of false-negatives. In summary, it appears that the scoring criteria that mainly rely on EEG arousals without taking into consideration other criteria may lack reproducibility [74].

According to Wilson et al. [38], Snoring Sound Intensity (SSI) levels are related to a number of demographic, clinical, and polysomnographic test results and shows some relation to apnea/hypopnea during sleep. The noise generated by snoring can disturb or disrupt a snorer's sleep, as well as the sleep of a bed partner. However, SSI has been rejected as a predictor for flow limitation during snoring, as high between- and within-subject variance did not allow to find a significant interdependence between tidal volume and SSI [37].

Thus, the true utility of snoring as a predictive parameter for sleep pathologies is still to be determined but could be of relevance as an additional non-invasive parameter to differentiate sleep disorders [131].

Cyclical Alternating Patterns (CAPs)

The cyclic alternating pattern (CAP) is a periodic EEG activity of non-REM sleep and is characterized by sequences of transient electrocortical events that differ from background EEG activity and can recur at up to 1 min intervals [34], see fig. 8.1. CAPs are an EEG activity that may indicate sleep instability and/or sleep disturbance, while they can appear spontaneously in non-REM sleep or occur in association with sleep disturbances like SDB and periodic leg movement [34]. Its subtype classification extends the current scorers manual's definitions [6], as a periodicity dimension and a possible marker of pre-arousal activation should also be included [34].

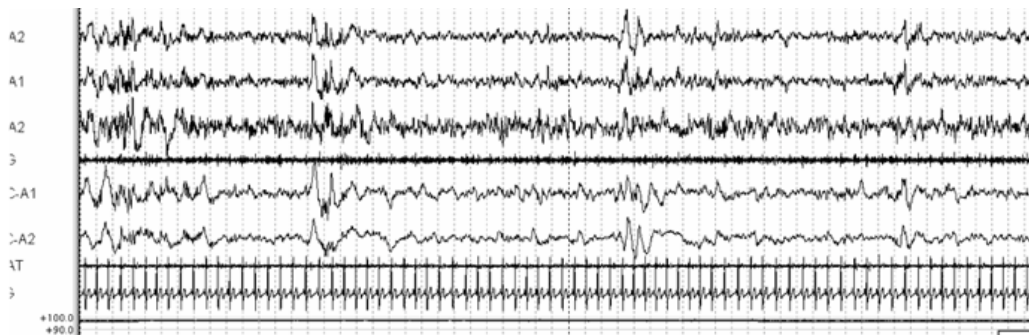


Figure 8.1: An example of CAPs. Note the repetitive pattern cycle in the EEG signal. [72]

In a study of 25 OSA patients, Guilleminault et al. [77] showed that all subjects presented at least one standard deviation higher amount of CAPs, with higher CAP rate and higher amount of phase in A2 and A3. It appears that CAPs could be a valid indicator for the persistence of some degree of sleep disturbance and instability of NREM sleep.

Other studies [35] also indicated a more disturbed NREM sleep both in sleepwalkers and UARS compared to normal controls. The findings suggested that the instability of NREM sleep may be more related to subtle SDB than to anything else, as UARS patients without sleepwalking had similar abnormal CAP findings [35].

Thus, the presence of CAPs in EEG signals is a strong indicator for sleep disturbances and can be used as a valid parameter to demonstrate abnormal NREM sleep and underlying pathologies.

A non-invasive IFL classifier with the airflow signal

Subjects

Eleven male, lung-healthy subjects without asthma nor COPD, had full nocturnal polysomnography (NPSG) with an 18-channel recorder (Somnolab PSG system V2.01, Weinmann GmbH, Hamburg, Germany) at the sleep laboratories of *Klinikum Bethanien* hospital in Solingen, Germany, according to a protocol completely new designed for this purpose and approved by the hospital's Ethics Committee. Mean values \pm *SD* of the studied population for Apnea-Hypoapnea Index (AHI) were 14.752 ± 12.53 events/h (range 1.8 – 46.9 events/h), body-mass-index (BMI) 27.67 ± 2.72 kg/m² (range 24 – 39.19 kg/m²) and age 55.36 ± 14.03 years (range 39 – 78 years). In regards to arterial oxygen saturation (SpO₂), mean SpO₂ values were $94.43\% \pm 1.45\%$, (range 92-0% - 96.5%), minimal SpO₂ values were $85.55\% \pm 3.5\%$, (range 80% - 92%) and mean SpO₂ time under 90% was 8.38 ± 15.82 minutes, (range 00.07 – 54.54 min.).

Methods

As commented in chapter III, the airflow signal seems to be a very promising signal for non-invasive monitoring of respiratory events, as it contains information on changes in UA obstruction [14 - 16] and is a simple technique that is routinely used in clinical

routine. Motivated by approaches employed in automatic object recognition [118, 119], where huge datasets have to be efficiently and accurately processed, we propose a new type of non-invasive IFL classifier [Morgenstern 2008b, 2008d, 2009a, 2009b] based upon supervised machine learning techniques like Discriminant Analysis (DA), Support Vector Machines (SVMs) and Adaboost, also see chapter VII. After extracting features that characterize a breath's airflow pattern, the classifiers should be able to automatically identify IFL episodes reliably on a significant number of breaths, see fig. 8.2. As the classifiers will be trained and tested with the previously obtained gold-standard invasive IFL annotations, the validity of the non-invasive classification should be ensured.

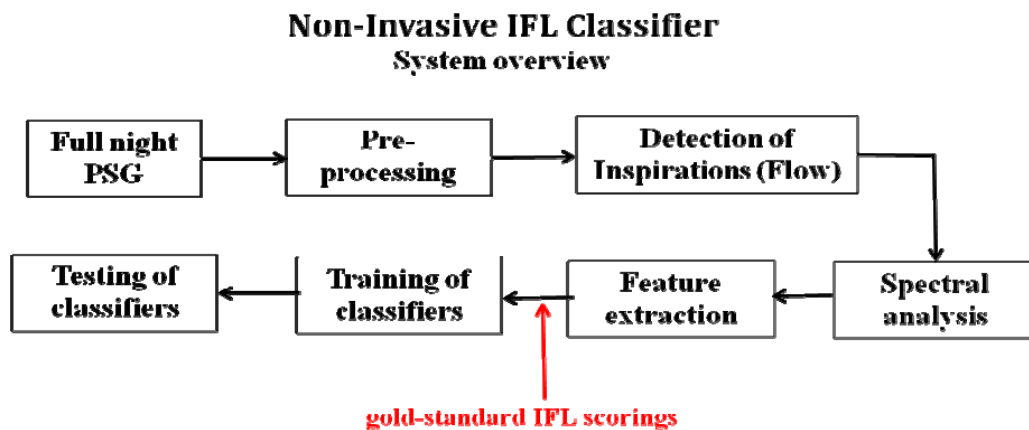


Figure 8.2: System overview of the automatic IFL classifier by means of the airflow signal (non-invasive classifier)

Non-invasive identification of IFL

The distinctive contour of an IFL inspiration (flattening), see fig. 8.3, is a key element for a successful non-invasive IFL classification, as it contains information on the relative variations in UA obstruction that causes IFL [56, 16, 15, 81, 71].

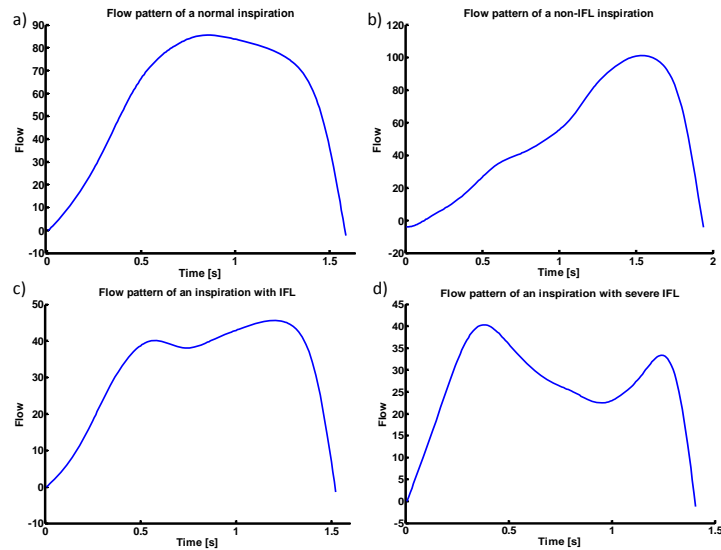


Figure 8.3: Examples of flow inspirations: (a) a normal inspiration (level 1), (b) a non-IFL inspiration (level 2), (c) an inspiration with IFL (level 3), (d) an inspiration with severe IFL (level 4). Significant changes in the breaths' flow contour can be observed between each example.

Aittokallio et al. [18] presented an interesting approach to automatically classify inspiratory flow shapes in dependence of their flattening pattern. After normalizing different shapes in duration and amplitude, they created different classes of inspiratory shapes and its subsequent hierarchy, see fig. 8.4.

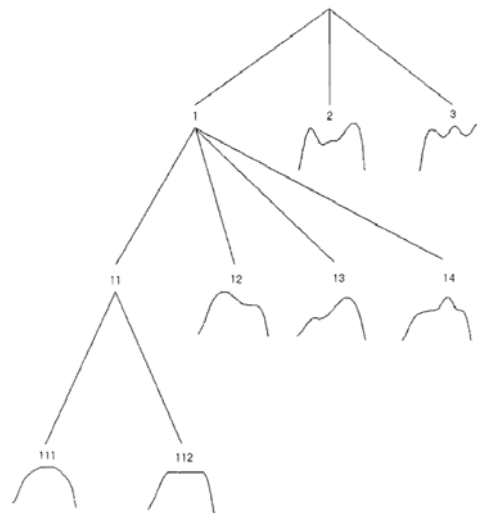


Figure 8.4: Hierarchy of the inspiratory flow shape classes. The first row represents the classes with one, two, and three or more peaks. The second row represents a further analysis of single peak shapes regarding the existence and orientation of the flat part. The last row distinguishes the sinusoidal class and the flat top flow limitation class. [18]

For the supervised machine learning methods used here (DA, SVMs and Adaboost, also see chapter VII), the training set consisted of a $(n\text{-times-}k)$ matrix with a number k of n -dimensional elements and of a label vector of length k containing the class label $\{+1;-1\}$ for each element. In our case, each inspiration had been previously labeled as an IFL $\{+1\}$ or non-IFL $\{-1\}$ episode by the automatic invasive annotation system that has been detailed before, see chapter V.

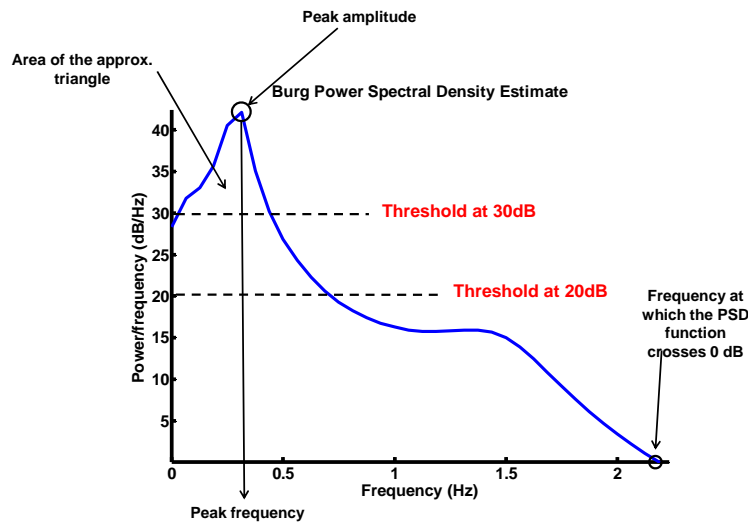


Figure 8.5: Example of a PSD function of a non-IFL breath calculated with Burg’s AR model. The indicated features were extracted from this signal to create the feature vector that was fed to the non-invasive IFL classifiers.

In order to reduce the dimensionality, hence, the complexity of the non-invasive classification problem, n features were extracted out of each inspiration’s time and frequency domains and combined into a feature vector for a total of k inspirations. We used power spectral density (PSD) analysis to obtain information from the frequency domain of an inspiration. The PSD was calculated with autoregressive (AR) modeling, as it allows increasing the observed frequency resolution and it does not suffer of the distortion effect caused by classical windowing.

Burg’s method [120] was used to fit an AR model with an order p to the input signal. The optimal order p (mean \pm SD values: 9.48 ± 3.78 , range 2 - 33) of the AR-model was

chosen by means of Rissanen's Minimum Description Length (MDL) criterion [121]. Extracted features from the time domain can be found in Table 8.1. Features extracted from the frequency domain can be seen in fig. 8.5 and Table 8.1. Sequential forward selection was used for each classifier in order to select the most relevant subset of features, respectively. Cross-validation indexing was used in order to randomly assign the breaths to the training, validation and test sets, as indicated in Table 8.2.

Index	Description	Index	Description
1	Total energy (area) of the PSD	12	(area of the first derivative of the inspiration's flow) \div (mean of dV)
2	Nr. of peaks of dPSD in [0 Hz – PSD0]	13	(area of the flow inspiration* from [0s - time of peak amplitude]) \div (total area of the inspiration*)
3	Peak amplitude of the PSD [dB]	14	Area of the inspiration* in the interval from [0s – 1/2 of the inspiration's duration]
4	Energy of the PSD in [0Hz–PSD0]	15	(PSD total energy) \times (PSD peak amplitude)
5	PSD0 [Hz]	16	(total energy of the PSD) – (energy of the PSD triangle at 20 dB)
6	Nr. of Peaks of the PSD	17	Energy of the PSD triangle at 30 dB
7	Nr. of peaks in the inspiration's flow shape	18	Energy of the PSD in [PSD freq. at 30 dB - end of PSD]
8	Duration of the inspiration [s]	19	Area of the inspiration* from [0s - the first 1/3 of the inspiration]
9	Amplitude of the inspiration normalized with the patient's peak-flow	20	(area of the first 1/3)+(area of the last 1/3) of the inspiration*
10	Energy of the PSD in [0.25 - 0.375 Hz]	21	(area of the inspiration*) \times (inspiration's duration [s])
11	Energy of the PSD in [0.375 – 0.5625 Hz]	22	Product between the peak frequency of the PSD and the total energy of the PSD

Table 8.1: Features of the non-invasive classifiers

dV: 1st derivative of the inspiration; *dPSD*: 1st derivative of the PSD; *PSD0*: freq. at which the PSD function crosses 0 dB; *with amplitude normalization (an inspiration's flow values were divided by the inspiration's maximum flow value)

	Training set	Test set	Validation set	Total
IFL breaths	2,120 (33%)	3,211 (50%)	1,091 (17%)	6,422 (100%)
non-IFL breaths	2,120	5,269	3,149	10,538
Total breaths	4,240	8,480	4,240	16,960

Table 8.2: Breath distribution

Discriminant analysis (DA) was performed with 3 different functions: Linear DA (LDA), Quadratic DA (QDA) and Mahalanobis DA (MDA). We used the validation set to find the SVM's (SVM-light v. 6.01, University of Dortmund, Dortmund, Germany) optimal parameters, testing it with a polynomial kernel with degrees (4, 8, 17, 24) and a radial-basis-function (RBF) kernel with sigma values (0.1, 0.2, ... 1.0). Our Adaboost implementation (GML Adaboost Matlab Toolbox, MSU Graphics & Media Lab, Computer Vision Group, Moscow, Russia) uses classification and regression trees (CARTs) as weak classifiers. Three different variations of the Adaboost algorithm, standard Adaboost [114, 115], "gentle" Adaboost [116] and "modest" Adaboost [117], each with different generalization capabilities, were tested with several parameters: number of CART splits (1, 3, 6, 12, 24, 36, 64, 128) and maximum iterations (100, 300, 500 cycles).

Results

The linear DA classifier achieved the best sensitivity and specificity of all DA classifiers, see Table 8.3. The SVM with the best performance was configured with a RBF kernel, a sigma of 0.7 and a vector of 7 selected features. Of all tested Adaboost classifiers, the best results were achieved with a "gentle" Adaboost algorithm with 128

CART splits, after 300 cycles of maximum iteration and a feature vector with 11 features, see Table 8.3.

As can be seen in the ROC curves, the best Adaboost classifier seems to deliver a better overall performance than the best SVM and the LDA classifiers, see fig 8.6.

	LDA	QDA	MDA	SVM	Adaboost
Se	0.81	0.81	0.89	0.86	0.87
Sp	0.85	0.81	0.74	0.79	0.85
PPV	0.77	0.72	0.68	0.72	0.78
NPV	0.88	0.87	0.91	0.90	0.91
Selected features (see Table 8.1)	1, 2, 7, 9, 11, 12, 13, 14, 15, 17, 18, 19, 20, 21	7, 9, 10, 13	3, 7, 9, 10, 13, 15, 16, 19, 21, 22	1, 7, 8, 9, 13, 14, 19	2, 3, 4, 5, 6, 7, 8, 9, 13, 14, 19
Vector length	14	4	10	7	11

Table 8.3: Classification results of the non-invasive classifiers for classical criteria Sensitivity (Se), specificity (Sp), Positive Predictive Value (PPV) and Negative Predictive Value (NPV).

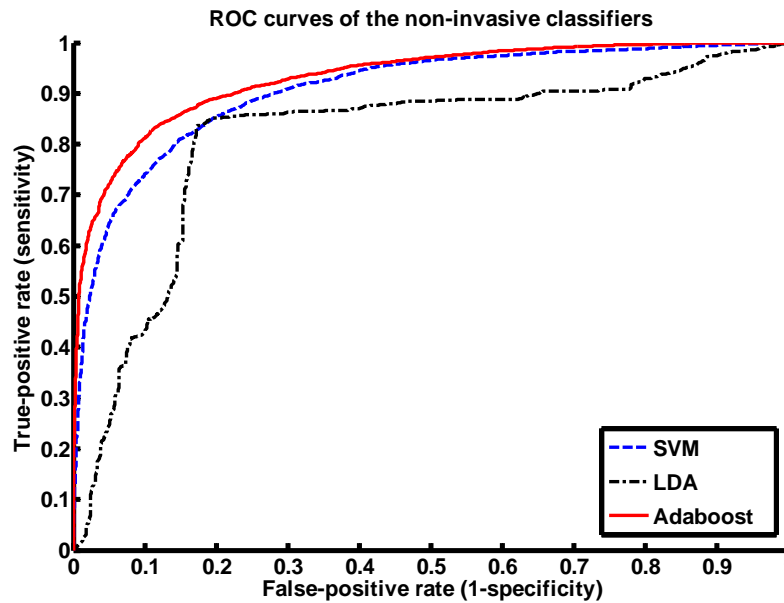


Figure 8.6: Receiver Operator Characteristic (ROC) curves for the Linear DA (LDA) classifier, the SVM classifier and the Adaboost classifier for IFL classification by classical criteria. The curves were obtained by varying the threshold value of the classifier's output in the range between -1 and $+1$.

Discussion

In respect to the non-invasive classifiers, IFL incidence had been previously annotated with the gold-standard esophageal pressure/flow relationship of each inspiration's measured values. As the non-invasive automatic classifiers were trained with these gold-standard references, the objectiveness and validity of the non-invasive classification should be ensured. Only the gold-standard annotations of the measured P/\dot{V} -relationships by classical criteria were used for the non-invasive classification, so the reported non-invasive classification scores represent the overall score. Although the flow signal quality varied from patient to patient, the non-invasive classifiers did not present any patient-specific limitations during the classification.

The Adaboost classifier shows a promising classification performance, as the classification sensitivity of 0.87 of our best classifier is very close to the sensitivity of 0.88 reported by Ayappa et al. [14] for manual classification by human experts, while

the specificity of 0.85 of our best classifier, see Table 8.3, clearly outperformed their specificity of 0.77. It should be added that Ayappa et al.'s sensitivity and specificity included also the detection of gross respiratory events, such as apneas/hypoapneas, that are usually easier to detect. Other studies of non-invasive systems [19, 20] presented a distinctively smaller amount of analyzed breaths, making it more difficult to fairly compare them with our classification results.

Conclusions

In conclusion, several techniques have been proposed to non-invasively assess changes in UA resistance. The airflow signal seems to be one of the most promising non-invasive signals with an easy and simple acquisition in clinical routine and that contains direct information on respiratory events. The automatic non-invasive classifier presented here for IFL detection achieved promising results on a considerable number of breaths with low computational costs, outperforming prior manual classification results achieved by human experts. As the classifier had been trained and validated with invasive gold-standard references, it could represent a promising tool for use in a clinical scenario.

Chapter IX: Automatic differentiation of central and obstructive hypopneas with esophageal pressure during sleep

Introduction

One of the most important aspects of the diagnosis of Sleep Disordered Breathing (SDB) in regards of the appropriate choice of treatment, is the correct identification of respiratory events. Particularly, the correct differentiation between central and obstructive apneas/hypopneas is one of the most recurrent tasks due to the prevalence of the corresponding syndromes (OSAHS/CSAHS) [5]. Currently, esophageal pressure (Pes) measurement is considered the gold-standard technique for measurement of respiratory effort and the identification of obstructive and central events [6, 7]. Still, the complexity and invasiveness of esophageal pressure manometry and its impact on sleep [10] limits its usage in clinical routine. So, researchers have been recently trying to develop non-invasive systems for the differentiation between central and obstructive apneas/hypopneas [11, 12]. However, the clinical adoption of these techniques has been slow, mostly due to their limited clinical validation. The bottleneck when creating a gold-standard validation set is usually found in the manual identification of the mentioned events by a human expert, as it is a cumbersome procedure that may suffer of interscorer differences and subjective interpretation. Hence, the development of an objective and efficient method for automatic invasive assessment of central and obstructive events is desirable, as new invasive approaches have also been recently suggested [129].

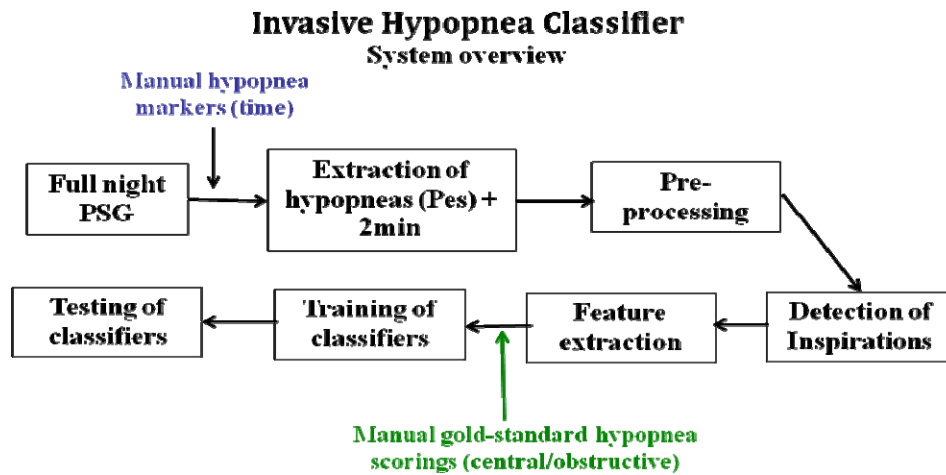


Figure 9.1: System overview of the automatic hypopnea classifier by means of the esophageal pressure signal (invasive classifier)

In this work a new automatic classifier is proposed based upon supervised machine learning techniques, see chapter VII, to automatically differentiate between central and obstructive hypopneas with the gold-standard Pes signal, see fig. 9.1. Our system focused on the differentiation of hypopneas, because pressure swings during a hypopnea are more subtle than during other events, therefore being considered one of the most challenging tasks [6, 7]. In a first step, hypopneas were manually scored by human experts to create a gold-standard validation set. Then, a specific set of features was extracted from the Pes-signal of each hypopnea in order to train and test the classifiers. Finally the performance of the different classifiers is evaluated and compared.

Methodology

Subjects

Twenty-eight subjects had full nocturnal polysomnography (NPSG) with an 18-channel recorder (Somnolab V2.01 Weinmann GmbH, Hamburg, Germany) at the sleep laboratories of Klinikum Bethanien hospital in Solingen, Germany. The clinical protocol was specifically designed for these purposes and approved by the hospital's Ethics Committee. Twenty-three subjects were male and five were female. Mean values

\pm SD of the studied population for Apnea-Hypopnea Index (AHI) were 18.9 ± 18.5 events/h (range 2.3 – 91.2 events/h) with a Hypopnea Index (HI) of 10.4 ± 6.6 events/h (range 1.1 – 27.3 events/h), body-mass-index (BMI) 28.5 ± 4.5 kg/m² (range 21.0 – 41.9 kg/m²) and age 52.6 ± 15.6 years (range 23 – 78 years).

Sleep stages, apneas, hypopneas and other respiratory events were scored applying standard criteria [6]. According to these criteria, a hypopnea lasts for at least 10 seconds and is identified by a clear decrease ($>50\%$) from baseline in the amplitude of a valid measure of breathing during sleep or is associated with either an oxygen desaturation of $> 3\%$ or an arousal [6]. The baseline is defined as the mean amplitude of stable breathing and oxygenation in the two minutes preceding the onset of the event [6]. With these criteria, hypopneas were independently identified in the the full-night PSG recordings of our twenty-eight patients by two human experts and the final hypopnea scorings were reconciled.

For the scoring of a central apnea or a central hypopnea, a clear reduction in esophageal pressure swings from the baseline, as defined before, is required [6]. According to the guideline [3], there is no relative or absolute reduction in esophageal pressure during the event that can be used to differentiate between a central and an obstructive event, increasing the difficulty for the automatic differentiation. A human expert reviewed the priorly manually identified hypopneas and differentiated them into obstructive and central by using the airflow and Pes signals. Undifferentiated hypopneas, mixed hypopneas and apneas were excluded from this study. A total of 477 obstructive and 292 central hypopneas were manually scored, resulting in an overall of 769 manual hypopnea scorings. Pre-processing and detection of inspirations

The time markers of the manually scored hypopneas were imported for our automatic processing, as the automatic detection of apneas/hypopneas in the flow signal has already been proficiently solved by others [12]. The specific purpose of this study is to propose a new method for the differentiation of obstructive/central hypopneas.

The Pes signal presented noise and physiological disturbances (like swallowing or coughing artifacts) that had to be reduced. Flow and Pes pre-processing stages were performed as detailed in chapter V.

Index	Description	Index	Description
1	Number of amplitude difference values of hPes	6 and 7	Median of the amplitude difference values of hPes + and - its standard deviation, respectively
2	Median of the amplitude difference values of Pes2min	8	Relative respiratory effort index
3	Median of the superior group of difference values of Pes2min	9	Correlation index of the amplitude difference values of hPes
4	Median of the inferior group of difference values of Pes2min	10	Median of the 1 st derivative of the maxima in hPes
5	Median of the amplitude difference values of hPes	11	Median of the 1 st derivative of the minima in hPes

Table 9.1: Extracted features

In order to differentiate a hypopnea, the Pes signal of the hypopnea (hPes) and the 2 min prior to the hypopnea's start (Pes2min) were extracted and processed separately. In case hPes or Pes2min presented a significant baseline oscillation, linear trends were automatically removed from the signals (detrending).

Respiratory periods in the extracted airflow and Pes signals were detected as described in chapter V, obtaining the signal's maxima and minima for each respiratory cycle, see fig. 9.2. The corresponding flow/Pes inspiration pairs were then separately extracted in order to allow the individual analysis of each inspiration. In the case that less than two inspirations could not be detected in the Pes signal of a hypopnea due to artifacts, the

whole hypopnea was discarded. A 7% of the 769 hypopneas were discarded by the pre-processing algorithm because of artifacts, resulting in a total of 715 hypopneas that were finally available for the automatic processing and analysis.

We used the manual hypopnea time markers to separate the Pes signal of the hypopnea (**hPes**), the flow signal of the hypopnea (**hflow**) and the 2 min prior to the hypopnea's start (**Pes2min** and **flow2min**, respectively), see fig 9.2.

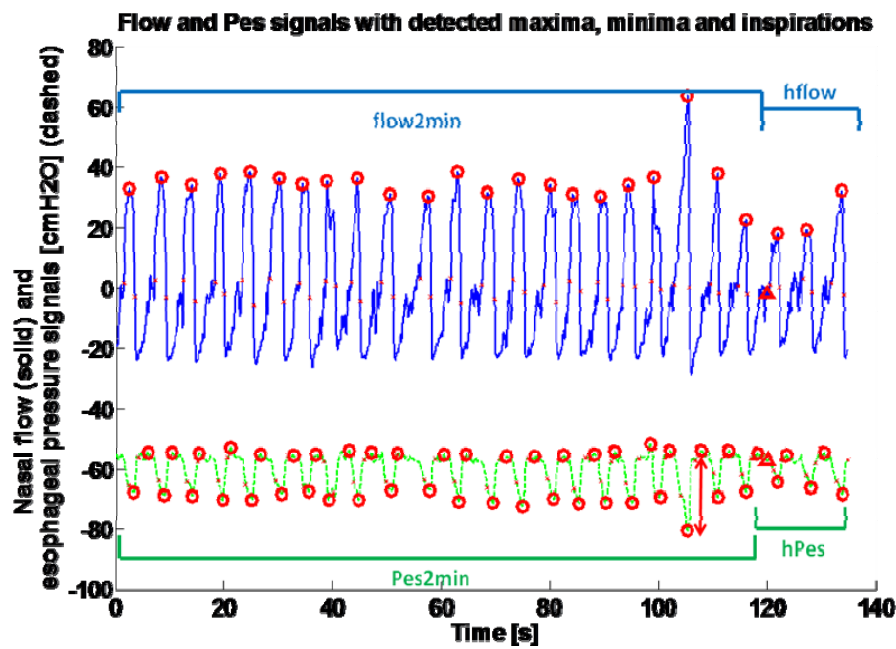


Figure 9.2: Example of a central hypopnea after pre-processing. Maxima were detected in the airflow signal and maxima and minima were detected in the Pes signal (circles). The crosses indicate the beginning and ending of the inspiratory periods, respectively. The triangle indicates the original, manual hypopapnea marker that indicates the beginning of the hypopnea. The arrow at the Pes signal indicates the amplitude difference for that respiratory cycle. The signals were separated into the signals of the hypopnea (**hPes** and **hflow**) and the signals of the 2min prior to the hypopnea's onset (**Pes2min** and **flow2min**), respectively. Note the significant decrease in flow after the hypopnea's onset in respect to **flow2min** and the significant decrease in respiratory drive for **hPes** in comparison to **Pes2min**, indicating the presence of a central hypopnea.

Feature extraction

The accurateness of the differentiation process will primarily depend on how well the extracted features characterize the pressure swings of central and obstructive

hypopneas. As no relative or absolute reduction in esophageal pressure during a hypopnea's interval can be used to distinguish between central and obstructive hypopneas, the relative changes in amplitude in hPes in respect to Pes2min had to be compared to assess the relative changes in respiratory effort of an hypopnea. In order to minimize the effects of possible baseline drifts during the observed segments of the Pes signal, we were inclined to work with the amplitude difference of the corresponding minimum (inspiration) and maximum (expiration) of each respiratory cycle, see the arrow in fig. 9.2, instead of only using the Pes minima's absolute amplitude values.

After this preliminary processing, we started looking for the features that best characterize the differences between obstructive and central hypopneas and could be used to train our classifiers (Table 9.1). So, the overall number of amplitude difference values of the hPes signal was used as the first feature, see Table 9.1. As seen in figs. 9.3 and 9.4, we computed the median of the amplitude differences of the Pes2min signal, see solid line on the left in figs. 9.3 and 9.4, dividing the Pes2min amplitude difference values in two groups, one located above this median and another located below. For each of these two groups, their respective median was computed again, see dashed lines on the left in figs. 9.3 and 9.4. The standard deviations of the Pes2min signal around the median can also be seen in figs. 9.3 and 9.4 as dash-dot lines on the left. For the hPes signal the median was computed, see solid line on the right of figs. 9.3 and 9.4, \pm the standard deviation of hPes see dashed red lines on the right in figs. 9.3 and 9.4. All these parameters were assembled in the feature pool, see features (2 - 7) in Table 9.1, for the automatic classifier.

With these visual references, we defined a relative respiratory effort index, see feature 8 in Table 1, that defined four amplitude difference intervals of where the median of hPes could be located in respect to Pes2min, and assigned to these intervals numerical

values within the range $[1, \dots, 4]$ (figs. 9.3 and 9.4). E.g. if the median of hPes was located above the median of the superior group of Pes2min, the relative respiratory effort index was assigned the value 1, see fig. 9.3, while if the median of hPes was located below the median of the inferior group of Pes2min, the relative respiratory effort index was assigned the value 4, see fig. 9.4.

Furthermore, we observed that an obstructive hypopnea usually presented a sequential, (approx.) linear increase of amplitude differences (fig 9.4) representing the subsequent increase in respiratory effort typical of obstructive events, while the amplitude differences of central hypopneas (fig. 9.4) usually are more constant, not showing a specific recurrent pattern. We assessed this characteristic by computing Pearson's correlation coefficient of the hPes amplitude differences, using its value as a characteristic feature for the differentiation, see feature 9 in Table 9.1.

Finally, we also observed a recurrent divergent behavior of the envelope of the hPes maxima and minima for obstructive hypopneas. So, we computed the median of the first derivatives of the amplitudes of the maxima and minima, respectively, see features 10 and 11 in Table 9.1.

The automatic invasive classifier was trained, tested and validated with the manual, gold-standard (Pes) annotations.

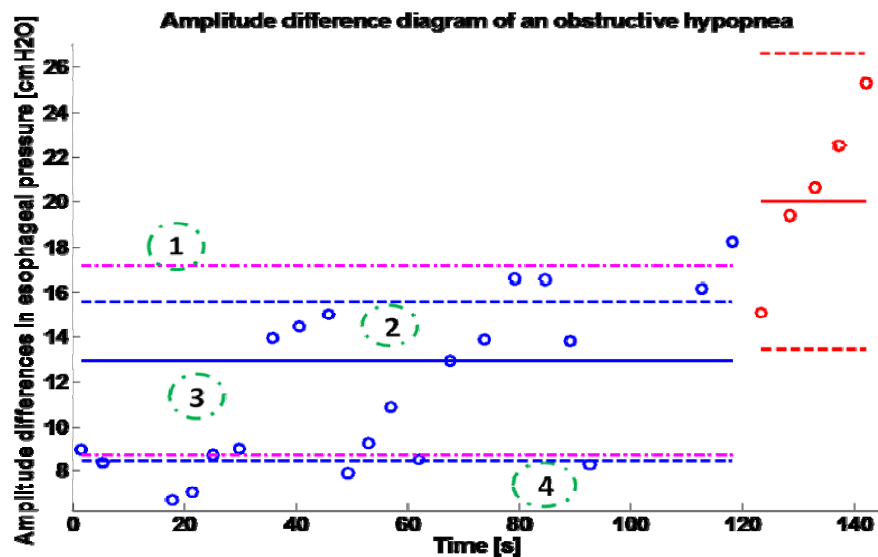


Figure 9.3: Example of the distribution of amplitude differences for an obstructive hypopnea. The amplitude difference values (circles) of the hPes segment are located on the right side of the figure and its median (solid line on the right) is located above the median (solid line on the left) of difference values of the Pes2min (circles on the left), representing an increase in absolute values of the respiratory effort. The values of the location index are indicated in the dash-dot circles. Note that the hPes difference values for the obstructive apnea show an approximate sequential increment, representing a progressive increase in respiratory effort due to the elevated UA resistance.

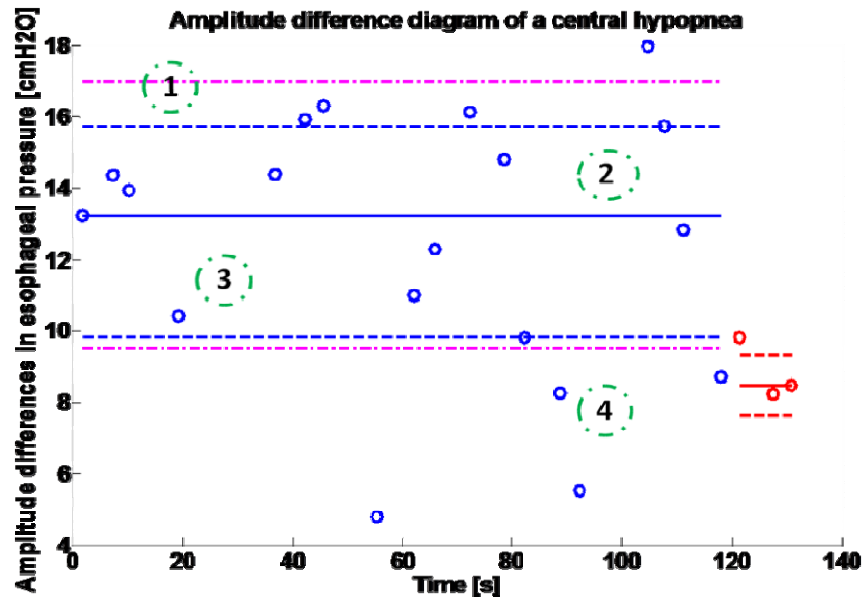


Figure 9.4: Example of the distribution of amplitude differences for a central hypopnea. The amplitude difference values (circles) of the hPes segment are located on the right side of the figure and its median (solid line on the right) is located below the median (solid line on the left) of difference values of the Pes2min (circles on the left), representing a decrease in absolute values of the respiratory effort. The values of the location index are indicated in the dash-dot circles. Note that the hPes difference values for the central apnea do not show a specific pattern.

Furthermore, we also calculated Pearson's correlation coefficient of the hPes amplitude differences, as we observed that an obstructive hypopnea usually presented a higher linear correlation of its amplitude differences fig 9.3 in comparison to a central hypopnea fig. 9.4, see feature (2), Table 9.1.

Finally, we also usually observed a divergent behavior of the envelope of the hPes maxima and minima for obstructive hypopneas fig. 9.2 (above). So, we computed the median of the first derivatives of the amplitudes of the maxima and minima, respectively, see features (4, 5), see Table 9.1.

Training and testing of the classifiers

Supervised machine learning techniques, like Discriminant Analysis (DA), Support Vector Machines (SVMs) or boosting algorithms like adaboost, try to predict the belonging of a case to a pre-defined class from training data. During the training phase,

the classifiers learn how to solve the problem with a number of input values (features) that should be selected in order to best characterize the function to be predicted by the classifier. The training set is usually composed of a number k of cases (here $k = 715$ hypopneas) characterized each by a number n of features, resulting in a $(n\text{-times-}k)$ -input matrix, and an output vector of length k containing the desired output classes $\{+1;-1\}$ for each case. Here, the desired output values correspond to the manual, gold-standard annotations for the obstructive $\{+1\}$ and central $\{-1\}$ hypopneas. A validation set is usually used in order to optimize and fine-tune each classifier's parameters. Finally, the optimized and trained classifier is applied on a test set. The classifier's predicted values are then compared to the desired output values in order to estimate the classifier's performance.

A cross-validation algorithm was used in order to randomly assign the hypopneas in a previously designated proportion to the training, test and validation sets, see (Table 9.2). In order to obtain the automatic invasive classifier that is closest to generalization, an i -fold hold-out cross-validation was performed with $i=100$ iterations. The advantage of hold-out cross-validation over i -fold cross-validation is that the proportion of the training/validation split is not dependent on the number of folds (iterations). Thus, a number i of random training, validation and test sets were iteratively created to train, validate and test our classifiers. Finally, the mean outcome for the classification results of the i iterations was computed to obtain the overall score of the global classifier.

	Obstructive	Central	Total
Training set	157	93	250 (35%)
Validation set	68	40	108 (15%)
Test set	225	132	357 (50%)
Total	450	265	715 (100%)

Table 9.2: Hypopnea distribution for the training, validation and test sets

Existing supervised machine learning techniques differ in their generalization capability and computational complexity. For this study, we selected three of the most popular classification techniques with increasing computational complexity. .

Five different functions were used during the DA analysis: linear DA (LDA), diagonal linear DA (DLDA), quadratic DA (QDA), diagonal quadratic DA (DQDA) and Mahalanobis DA (MDA). The best performing function was chosen during the optimization phase with the validation set.

SVM classification (SVM-light v. 6.01, University of Dortmund, Dortmund, Germany) also requires the optimization of several parameters. We used the validation set in order to chose between a polynomial kernel of degrees (4, 8, 16, 24) and a Gaussian kernel with sigma values (0.1, 0.2...0.9).

Adaboost combines and weighs a set of weak classifiers to boost them into a strong final classifier. The weak classifiers here were classification and regression trees (CARTs) with an arbitrary number of splits. Different variations of the adaboost algorithm with different generalization properties have also been recently proposed. Standard adaboost, “gentle” adaboost and “modest” adaboost are the most important algorithms that will be used here (GML adaboost Matlab Toolbox, Moscow, Russia). Again the validation set was used to optimize the commented parameters, like the number of CART splits (1, 3, 6, 12, 24, 36, 64, 128) and maximum cycles of the adaboost algorithm (100 and 300 iterations).

The extracted features did not always individually allow a strict characterization of obstructive and central events. Thus, the best differentiation results were obtained by using a specific combination of features for each classifier, respectively. So, sequential forward selection was used to automatically select the most relevant subset of the described features that best fit each classifier for the hypopnea's characterization.

Results

The invasive classifiers used the features extracted exclusively from the esophageal pressure signal in order to differentiate between central and obstructive events. After a 100-fold hold-out cross-validation with the validation set, the best classification results for DA were achieved with the diagonal quadratic DA (DQDA) function and a feature vector comprising the features (1, 3, 7, 8), see Table 9.1. The best classification results for the SVM classifier were achieved with a Gaussian kernel, a sigma of 0.3 and a feature vector with the features (8, 9, 11). Of all tested adaboost classifiers, the best results were achieved with the gentle adaboost algorithm, 1 CART split and after 100 cycles of maximum iteration. The feature vector for the adaboost classifier comprised the features (1, 2, 4, 5, 8).

The mean classification results of the automatic classifiers in comparison to the manual, gold-standard hypopnea scorings after a 100-fold hold-out cross-validation can be seen in Table 9.3. In order to better observe and compare the classification performance, the results of each classifier for a random test and training set (Table 9.4) were plotted in form of ROC curves (fig. 9.5). According to the ROC curves, the adaboost classifier seems to deliver a better overall performance than the SVM and the DQDA classifiers.

	DQDA	SVM	Adaboost
Sensitivity	0.85	0.82	0.90
Specificity	0.81	0.89	0.90
PPV	0.83	0.90	0.91
NPV	0.83	0.82	0.90
Accuracy	0.83	0.86	0.90
Selected features (see Table 9.1)	1, 3, 7, 8	8, 9, 11	1, 2, 4, 5, 8
Vector length	4	3	5

Table 9.3: Mean classification results after a 100-fold cross validation. Obstructive events were labeled as {+1} and central events as {-1}.

As seen in the ROC curves, see fig. 9.5, the adaboost classifier seems to deliver a better overall performance than the SVM and the QDA classifiers when a specific test set is taken, see Table 9.4.

	DQDA	SVM	Adaboost
Sensitivity	0.88	0.82	0.87
Specificity	0.80	0.92	0.92
PPV	0.83	0.92	0.92
NPV	0.86	0.82	0.87
Accuracy	0.84	0.87	0.89

Table 9.4: Classification results for a random test set. Obstructive events were labeled as {+1} and central events as {-1}.

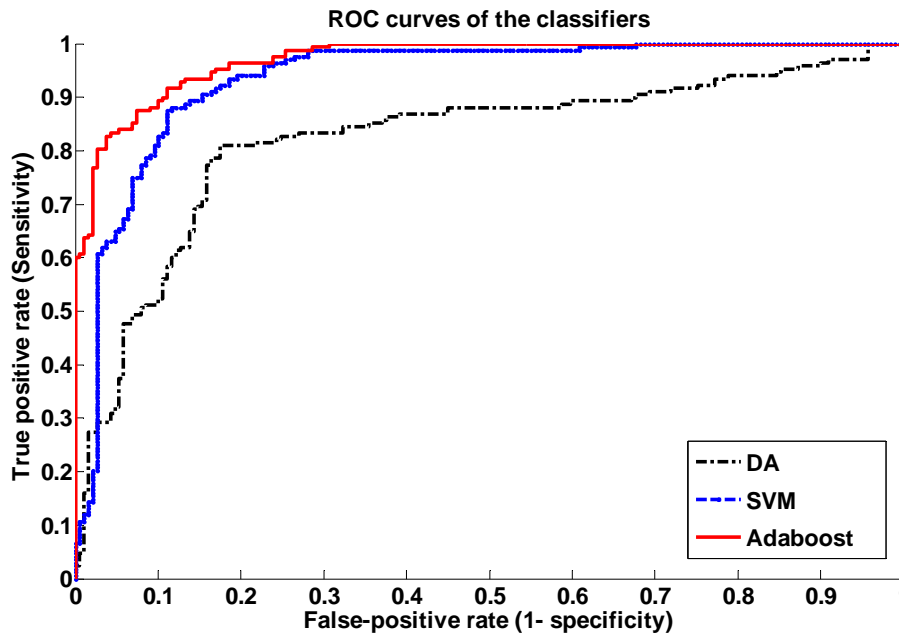


Figure 9.5: Receiver Operator Characteristic (ROC) curves for the QDA, the best SVM and best adaboost classifiers for the differentiation between central and obstructive hypopneas. The curves were obtained by varying the threshold value of the classifier's output in the range between -1 and $+1$.

Discussion

An overall of 715 manual, gold-standard hypopnea scorings of 28 patients were automatically classified, representing a significant increase in the number of patients with systematic Pes measurement and in the number of gold-standard annotations than in comparable studies [11, 12].

In regard to the invasive, automatic classifier, the information contained in the features extracted from the Pes signal seems to be adequate for the automatic differentiation of obstructive and central hypopneas. It strikes out that feature 8 (Table 9.1) was the only feature selected by all three classifiers, underlining the importance of the relative respiratory effort index for the classification process. The Pes differentiation criteria of hypopneas are identical to those of apneas [6], implying that the presented automatic differentiation system may also be applicable for the automatic differentiation of central and obstructive apneas. The elevated accuracy of our automatic hypopnea classifier

after a 100-fold hold-out cross-validation, see Table 4 , and using only 35% of the hypopneas for the training set, see Table 3, strikes out the system's robustness and generalization capability.

The adaboost classifier showed the best overall classification results (Table 4, fig. 5), although it was also the classifier with the highest computational complexity, the largest feature vector and processing time. The DQDA classifier showed a remarkable overall performance given the fact that it is the classifier with the lowest computational complexity, see Table 4 and fig. 5.

Currently, only manual annotations of the Pes signal by human experts are accepted as gold-standard annotations for hypopnea differentiation [6]. As all classifiers here were trained and validated with manual, gold-standard annotations, the validity of the automatic classifier's scorings should consequently be ensured. However, it should be remarked that because of a human scorer's subjective interpretation, human interscorer agreement usually ranges between [80- 90%]. This limitation imposes an upper limit on the classification performance that can be achieved by an automatic classifier. The scores reported in this study are within this range of human interscorer agreement, so the classifiers presented here seem to be promising for the automatic, invasive differentiation of obstructive and central hypopneas and an objective and time-efficient creation of gold-standard validation sets.

Conclusions

A new system for differentiation of central and obstructive hypopneas with the gold-standard esophageal pressure signal was presented. The outcome reported in this study represent the upper limit of human interscorer agreement [123]. Given that currently the only accepted gold-standard annotations are manual scorings by human experts, these

results should also correspond to the overall limit to be reached by an automatic classifier. Hence, the classification techniques presented in this study seem to be promising for the automatic, invasive differentiation of obstructive and central hypopneas and an objective and time-efficient creation of gold-standard validation sets. This should help to validate more efficiently and objectively non-invasive differentiation systems that have already been or are to be developed.

Chapter X: Non-invasive, automatic differentiation of central and obstructive hypopneas

Introduction

As commented in chapter IX, the non-invasive differentiation between central and obstructive events has been one of the main challenges in recent time in SDB research. Different approaches for the non-invasive differentiation of hypopneas have been recently proposed [11 - 13] but their clinical adoption has been slow due to the limited clinical validation of these techniques. As our database contains systematic esophageal pressure (Pes) measurement, we have now the unique opportunity to achieve the gold-standard validation [6, 7] of any new non-invasive technique that is developed and ease up its implementation in clinical routine.

The main objective of this thesis has been the development of non-invasive assessment techniques for UA obstruction and respiratory effort. In the following, the techniques and systems presented in chapters VI, VIII and IX will be combined to create a new system that permits the non-invasive differentiation of obstructive and central hypopneas. This new automatic, non-invasive classifier, as the automatic invasive classifier in chapter IX, will also be based upon supervised machine learning techniques, see chapter VII, but the system's input data will solely consist of information contained in the airflow signal. However, the validation of this system will be based upon the gold-standard Pes signal. Again, our system will focus on the differentiation of hypopneas, because hypopneas are one of the most subtle events during SDB and are therefore considered one of the most challenging tasks for

differentiation [6, 7]. The purpose of this work is, that after exhaustively validating the non-invasive algorithm, this new non-invasive system is finally implemented into the therapy devices of Weinmann GmbH by our partner R&D company MCC GmbH & Co. KG in Karlsruhe, Germany, to enhance the treatment of patients suffering of OSAHS, CSAHS and Cheyne-Stokes respiration.

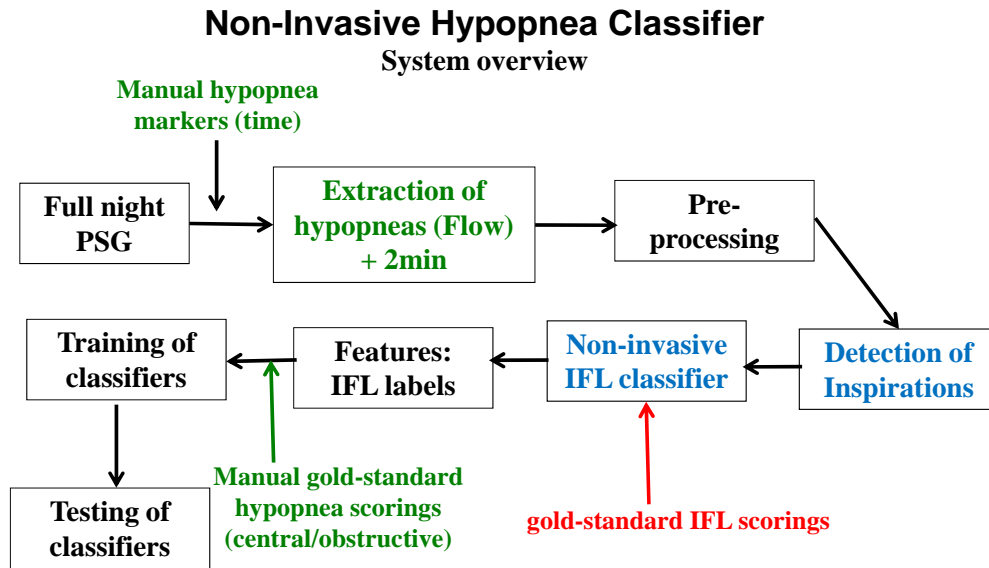


Figure 10.1: System overview of the automatic hypopnea classifier by means of the flow signal (non-invasive classifier)

In a first step, hypopneas were manually scored by human experts with classic NPSG criteria [6] and were then invasively and non-invasively differentiated by a human expert [6] to create a manual gold-standard annotation set and a non-invasive manual comparative set, respectively. Then, the non-invasive classifier described in chapter VIII was used on the airflow signal to obtain IFL related information of each hypopnea and the 2min prior to the onset of each event. With this and other information contained in the flow signal, a specific set of features was extracted from the flow signal of each hypopnea in order to train and test the classifiers. Finally the performance of the different classifiers is evaluated and compared.

Methodology

Subjects

Twenty-eight subjects had full nocturnal polysomnography (NPSG) with an 18-channel recorder (Somnolab V2.01 Weinmann GmbH, Hamburg, Germany) at the sleep laboratories of Klinikum Bethanien hospital in Solingen, Germany. The clinical protocol was specifically designed for these purposes and approved by the hospital's Ethics Committee. Given the complexity to record the Pes signal in NPSG studies, the number of patients in our study already represents an up to a three-fold increase in the overall cohort size in comparison to other studies with Pes measurement [12, 14, 16, 81].

Sleep stages, apneas, hypopneas and other respiratory events were scored applying standard criteria [6]. According to these criteria, a hypopnea lasts for at least 10 seconds and is identified by a clear decrease ($>50\%$) from baseline in the amplitude of a valid measure of breathing during sleep or is associated with either an oxygen desaturation of $> 3\%$ or an arousal [6]. The baseline is defined as the mean amplitude of stable breathing and oxygenation in the two minutes preceding the onset of the event [6]. With these criteria, hypopneas were independently identified in the the full-night PSG recordings of our twenty-eight patients by two human experts and the final hypopnea scorings were reconciled.

For the scoring of a central apnea or a central hypopnea, a clear reduction in esophageal pressure swings from the baseline, as defined before, is required [6]. According to the guideline [3], there is no relative or absolute reduction in esophageal pressure during the event that can be used to differentiate between a central and an obstructive event, increasing the difficulty for the automatic differentiation. A human expert reviewed the priorly manually identified hypopneas and differentiated them into

obstructive and central by using the airflow and Pes signals. Undifferentiated hypopneas, mixed hypopneas and apneas were excluded from this study. A total of 477 obstructive and 292 central hypopneas were manually scored, resulting in an overall of 769 manual hypopnea scorings. This represents a distinctive increase in manual hypopnea annotations in comparison to other studies that only analyzed an overall of 167 manually scored apneas and hypopneas [11], 120 apneas and hypopneas [12] or 200 hypopneas [129], respectively.

Patient	Central hypopnea	Obstructive Hypopnea	Total
1	20	1	21
2	0	0	0
4	0	0	0
5	23	9	32
6	16	21	37
7	1	1	2
8	12	7	19
13	9	4	13
14	7	19	26
15	1	4	5
16	8	2	10
17	0	0	0
18	4	8	12
19	15	4	19
20	1	13	14
21	75	25	100
22	11	10	21

23	0	1	1
24	2	0	2
25	3	33	36
26	1	42	43
27	6	66	72
28	8	1	9
29	0	18	18
30	8	28	36
31	12	73	85
32	21	43	64
33	28	44	72
Total: 28	292	477	769

Table 10.1: Gold-standard hypopneas scorings performed by a human expert with the Pes signal

The Solingen algorithm

As commented in chapter IV, the research group of our partner hospital Klinikum Bethanien in Solingen, Germany, have been developing a decision tree algorithm for human experts to differentiate non-invasively between central and obstructive hypopneas. The decision tree is mainly based upon flattening information contained in the hypopnea's respiratory pattern and some context-based information on the flow signal, this is information about events occurring around each hypopnea.

With this new algorithm, human experts reviewed the full-night recordings of all the 28 patients in our database, see chapter IV, and manually scored hypopneas with the mentioned criteria, only using the airflow signal. A total of 357 obstructive hypopneas and 412 central hypopneas were scored, resulting in an overall of 769 hypopneas. The classification results can be seen in Table 10.2 and Table 10.3

Patient	Central hypopnea	Obstructive Hypopnea	Total
1	19	2	21
2	0	0	0
4	0	0	0
5	29	3	32
6	35	2	37
7	2	0	2
8	18	1	19
13	9	4	13
14	8	18	26
15	4	1	5
16	9	1	10
17	0	0	0
18	12	0	12
19	18	1	19
20	1	13	14
21	99	1	100
22	17	4	21
23	0	1	1
24	2	0	2
25	5	31	36
26	1	42	43
27	4	68	72
28	9	0	9
29	3	15	18

30	6	30	36
31	11	74	85
32	22	42	64
33	69	3	72
Total: 28	412	357	769

Table 10.2: Non-invasive hypopneas scorings performed by a human expert only with the airflow signal

Sensitivity	0.68
Specificity	0.88
PPV	0.91
NPV	0.62
Accuracy	0.75

Table 10.3: Overall classification results for the non-invasive Solingen algorithm in comparison to the gold-standard scorings with the same test set used by the automatic classifier. Obstructive hypopneas used the label {+1}, central hypopneas the label {-1}.

A new automatic, non-invasive differentiation algorithm

The time markers of the manually scored hyopapneas that indicated the starting time and the duration in seconds of each hypopnea were imported for the automatic processing, as the automatic detection of apneas/hypopneas in the airflow signal has already been proficiently solved [12, 13]. The specific purpose of this study is to find a new method for the automatic differentiation of obstructive/central hypopneas.

Respiratory periods in the extracted airflow and Pes signals were detected as described in chapter V, obtaining the signal's maxima and minima for each respiratory cycle. The corresponding flow/Pes inspiration pairs were then separately extracted in order to allow the individual analysis of each inspiration. In the case that less than two

inspirations were automatically detected in the flow and Pes signals during a hypopnea event, the hypopnea was discarded as an artifact. A 7% of the 769 hypopneas were discarded as artifacts by the pre-processing algorithm, such that a total of 715 hypopneas were finally available for the automatic processing and analysis.

In order to differentiate a hypopnea, we used the manual hypopnea markers to separate the Pes signal of the hypopnea (**hPes**), the flow signal of the hypopnea (**hflow**) and the 2 min prior to the hypopnea's start (**Pes2min** and **flow2min**, respectively). In case the hPes or Pes2min signals did not start with a maximum, the manual markers were automatically shifted (maximal 1 second) until a maximum was found at the beginning of each signal.

IFL detection in hypopneas as a possible critical differentiation feature

Flattening patterns [14, 16, 18, 81] usually appear in inspiratory cycles during episodes of inspiratory flow limitation (IFL), which have been defined as a lack of increase in airflow despite increasing respiratory effort (decreasing intrathoracic pressure) [14, 16, 18]. Thus, the presence of flattening provides information on changes in UA resistance and respiratory effort. During an obstructive hypopnea, the partial collapse of the UA leads to an increase in UA resistance which consequently prevents an increase in airflow despite the increasing respiratory effort [6, 7]. However, during a central hypopnea the cessation of flow is not caused by the collapse of the UA, but because of lack of neural input from the central nervous system to the diaphragm, representing diminished or even absent respiratory effort [77].

Hence, we hypothesized that the incidence of flattening in the inspiratory cycles of a hypopnea should provide direct information on the hypopnea's etiology, as we would expect to find more inspirations affected by flattening in an obstructive hypopnea than

in a central hypopnea. In order to prove this hypothesis, we needed to objectively quantify and compare the presence of IFL in inspirations of obstructive and central hypopneas. Previous studies [81, Morgenstern 2009b], also see chapter VI, have already introduced an automatic system that allows objectively assessing the presence of IFL by means of an inspiration's P/\dot{V} -relationship. IFL has been formally defined as a min. decrease of 1 cmH₂O (0.7356 mmHg) of intrathoracic pressure without a corresponding increase in airway flow rate [14, 16, 18]. As the corresponding airflow and Pes-inspirations of each breath were here separately available after the pre-processing stage, we were able to reconstruct the P/\dot{V} -relationship as indicated in [81, Morgenstern 2009b], see chapter VI, to objectively automatically assess the presence of IFL in an inspiration. If an inspiration was assessed with IFL, it was assigned the value $\{+1\}$, while if it was a non-IFL inspiration it obtained the value $\{0\}$. The mean IFL value for all inspirations of an hypopnea, see feature 3 in (Table 10.4), and all inspirations of the 2min prior to the hypopnea's onset, see feature 1 in (Table 10.4), were computed. This process was repeated for each of the 715 manually scored, gold-standard hypopneas. Finally, the overall mean IFL values for all hypopneas and all the 2min segments was calculated. To prove the hypothesis that the IFL values of obstructive hypopneas were significantly ($p < 0.01$) different than those of central hypopneas, Mann-Whitney U tests were performed for these two features, respectively.

The rest of the features of this hypopnea differentiation system, see features 2 and 4 – 10 (Table 10.4), were exclusively extracted from the airflow signal.

	Feature		Feature
1	mean IFL value of the inspirations in <i>flow2min</i>	6	Mean value of the maximas of all inspirations in <i>hflow</i>
2	Number of inspirations in <i>flow2min</i>	7	Difference between feature 5 and feature 6
3	mean IFL value of the inspirations in <i>hflow</i>	8	Maximal area of an inspiration in <i>hflow</i> divided by the maximal area of an inspiration in <i>flow2min</i>
4	Number of inspirations in <i>hflow</i>	9	Number of IFL inspirations in <i>flow2min</i>
5	Mean value of the maximas of all inspirations in <i>flow2min</i>	10	Number of IFL inspirations in <i>hflow</i>

Table 10.4: Feature table

Training and testing of the classifiers

As commented in chapter VII, Supervised machine learning techniques were used for the classification. Here, the desired output values correspond to the manual, gold-standard scorings for the obstructive $\{+1\}$ and central $\{-1\}$ hypopneas.

A cross-validation algorithm (MATLAB v.7.6, The Mathworks Inc., Natick, MA, USA) was used in order to randomly assign a proportion of the hypopneas to the training, test and validation sets, see (Table 10.5). In order to obtain the automatic invasive classifier that is closest to generalization, also k -fold hold-out cross-validation was performed with $k=100$ iterations. The advantage of hold-out cross-validation over k -fold cross-validation is that the proportion of the training/validation split is not dependent on the number of folds (iterations). Thus, a number k of random test and training sets were iteratively created to train, validate and test our classifiers. Finally,

the mean outcome for all the classification results of the k iterations was computed to obtain the overall score of the global classifier.

Not all extracted features contained in the training set allowed a strict characterization of obstructive and central events. Thus, the combination of all features to train a classifier was not always of interest to obtain the best differentiation results. So, sequential forward selection was used to select the most relevant subset of the described features that best fit each classifier for the hypopnea's characterization.

	Obstructive	Central	Total
Training set	157	93	250 (35%)
Validation set	68	40	108 (15%)
Test set	225	132	357 (50%)
Total	450	265	715 (100%)

Table 10.5: Hypopnea distribution for the training, validation and test sets

Results

For the automatic, non-invasive feasibility study, only the two features containing the IFL-related information, were obtained using the Pes-signal, see features 1 and 3 (Table 10.4). All other features were extracted exclusively from the airflow signal. The mean IFL values \pm standard deviation for features 1 and 3 (Table 10.4) for the 715 hypopneas separated into obstructive and central hypopneas can be seen in (Table 10.6). The mean IFL values were significantly different ($p < 0.01$) between obstructive and central hypopneas for the inspirations during a hypopnea (feature 3) and for the inspirations in the 2min. prior to a hypopnea's onset (feature 1). However, the difference between the IFL mean values between central and obstructive hypopneas was significantly higher for feature 3, see (Table 10.6).

The best results for the automatic classification were achieved with a diagonal quadratic DA (DQDA) classifier, see (Table 10.7). The manual, non-invasive classification by human experts was only based upon features contained in the airflow signal, see (Table 10.7), the Pes signal was not employed at any time.

	Mean IFL values for the 2 min preceding a hypopnea (feature 1)	Mean IFL values for the hypopnea (feature 3)
Obstructive hypopneas	0.3938 ± 0.2409	0.4721 ± 0.3391
Central hypopneas	0.3092 ± 0.2127	0.3380 ± 0.3277
Mean differences	0.0846	0.1341

Table 10.6: Mean IFL values \pm standard deviation for the inspirations in the 2min preceding a hypopnea and for the inspirations of a hypopneas

	DQDA	Solingen
Sensitivity	0.72	0.68
Specificity	0.71	0.88
PPV	0.81	0.91
NPV	0.60	0.62
Accuracy	0.72	0.75
Features	3, 7, 8, 10	Flattening and context-based information

Table 10.7: Mean classification results after a 100-fold cross validation. Obstructive events were labeled as {+1} and central events as {-1}

Discussion

This chapter presented a new a new concept for the non-invasive differentiation of obstructive and central hypopneas with the esophageal pressure and the nasal airflow

signals. An overall of 715 manual, gold-standard hypopnea scorings of 28 patients were automatically processed, representing a significant increase in the number of patients with systematical Pes measurement and in the number of gold-standard annotations than in comparable studies [11, 12].

The system presented here uses the information indirectly contained in the flattening patterns of airflow inspirations to differentiate hypopneas. Unlike the invasive classifier which, as commented, should be applicable to both apneas and hypopneas, the non-invasive classifier should solely work with hypopneas, as it would be difficult to assess flow patterns during apneas as the flow signal is very close to the baseline.

We have, to our knowledge for the first time, objectively demonstrated that obstructive hypopneas have a significantly higher ($p < 0.01$) incidence of IFL than central hypopneas. For the objective assessment of IFL we used the P/\dot{V} -relationship that has been routinely used by others [16, 81, Morgenstern 2009b], also see chapter VI, to reliably identify flattening patterns. Furthermore we have also shown that the difference between the overall mean IFL scores of central and obstructive hypopneas when observing just the hypopnea episode (0.13) are higher than during the corresponding 2min segment prior to the hypopnea's onset (0.08), see (Table 10.6). This may be the reason why the forward selection method prioritized feature 3 over feature 1 for the classification process, see (Table 10.7). The importance of the IFL related information contained in features 1 and 3 for the accurate differentiation of central and obstructive hypopneas is underlined by the fact that when we trained classifiers with combinations of the features extracted only from the airflow signal, see features 5-10 (Table 10.4), they scored a distinctively lower specificity and/or accuracy on the same training and test sets as the original classifier.

Even though features 8 and 10 (Table 10.4) of the automatic hypopnea classifier (Table 7) were obtained non-invasively just by analyzing the airflow signal, features 3 and 10 (Table 10.4), which have been shown to be critical for the automatic classification process, were obtained by means of the invasive P/\dot{V} -relationship [Morgenstern 2009b]. However, recent developments, see Chapter VII and [Morgenstern 2009b], have suggested new approaches that allow assessing IFLe episodes non-invasively with the airflow signal. Hence, these methods should then permit acquiring also features 1 and 3 non-invasively and, consequently, the development of an entirely non-invasive automatic hypopnea differentiation system.

The results for our automatic classifier are promising and demonstrate the feasibility of a non-invasive classification, as the classifier's accuracy is approximately on par with the results obtained with the manual, non-invasive scoring, see Table 10.7. We were inclined to use the results of this algorithm to compare the performance of our automatic system, as other non-invasive systems in the literature [12] presented a significantly smaller amount of analyzed hypopneas than our system. Furthermore, the only non-invasive study [12] the airflow signal for the hypopnea differentiation did not use gold-standard Pes signal annotations to validate their classifier. This increases the difficulty to fairly compare these studies' respective classification results with our system. Consequently, we decided to use the manual non-invasive classification algorithm to evaluate our automatic classifiers' performance. The manual non-invasive classification by human experts was only based upon features contained in the airflow signal (Table 10.7), the Pes signal was not employed for the classification. As with most systems only using NPSG signals [129], the manual classification algorithm showed a strong tendency to over-classify central events (0.88) in detriment of the correct

identification of obstructive events (0.68), see Table 10.7. The automatic classifier showed a better balanced identification performance of the two hypopnea classes, see Table 10.7. This underline the importance of using objectively extracted respiratory effort related information during the hypopnea's differentiation process. As with the invasive classifier, the manual, gold-standard hypopnea annotations were also here used for the training and testing of the automatic classifier, so the validity of the automatic differentiation scores should be ensured. However, further development is needed to obtain the robustness and classification and generalization results comparable to those of the invasive classifier, see chapter IX. Still, we are confident that the promising insights obtained in this study allow coming closer to the implementation of a robust, automatic, entirely non-invasive hypopnea differentiation system that is validated with an extensive set of manually or automatically created gold-standard, hypopnea annotations.

Outlook: A continuous measurement of IFL by analyzing flattening patterns

The described non-invasive IFL classifier, see chapter VIII, has a discrete, binary outcome of $\{0\}$ or $\{1\}$ (IFL present/ not present) for each inspiratory cycle. Obtaining a continuous indicator for IFL/flattening would be the next logical step for the non-invasive estimation of UA obstruction and changes in respiratory effort. The goal is to rebuild the “ideal airflow curve” of a breath with IFL, this is, the corresponding non-IFL airflow pattern of that IFL breath with the proportional correspondence in airflow amplitude and area in order to permit a continuous numerical assessment of the changes that have affected that breath. The information on the changes in UA obstruction and respiratory effort are implicitly contained in the flattening pattern of the IFL affected

breath. So, the characteristics of the flattening pattern should give hints on how to reconstruct that ideal curve, see fig 10.2. Thus, the final differences between the IFL affected inspiration and the reconstructed ideal airflow curve of that breath should permit closely quantifying the UA obstruction and/or changes in respiratory effort that have occurred

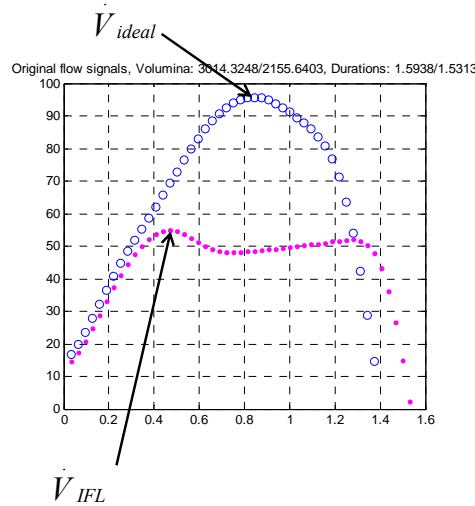


Figure 10.2: Hypothesis on the geometric reconstruction of the ideal flow curve

In order to find a valid base for the reconstruction of the ideal airflow curve, we started looking for Pes-curves with the most similar amplitude value and correlation coefficient value (similarity in shape) but presenting different UA obstructions. Thus, we looked for inspirations with very similar characteristics of their Pes values and patterns but significant differences in their respective airflow inspirational patterns (IFL or non-IFL), see fig. 10.3. We had to limit the time intervals in which to search for similar Pes-curves, as the proportionality between the Pes and flow values was only valid for a certain time interval, see fig. 10.4 The optimal interval length was estimated at 30 min after analyzing different interval lengths in a range from [1 min. 2 hours] for all patients and computing the correlation coefficient between Pes and flow values for non-IFL

breaths. The interval with the highest correlation coefficient value, this is the interval with highest flow-Pes proportionality, was selected as the optimal interval length.

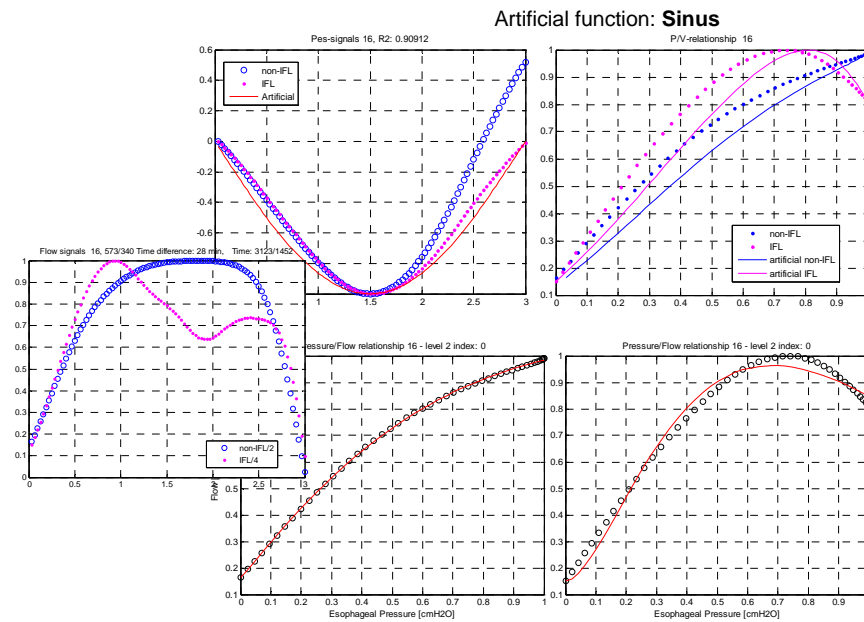


Figure 10.3: Example of two different Pes inspirations obtained in a 30 min interval (above left). The flow inspirations (left) show a clear difference in UA obstruction (IFL and non-IFL), such that their respective P/V-relationship differ (below). The P/V-relationship with an artificial sinus-function as a substitute for the original Pes signal shows significant deviations from the original (above right).

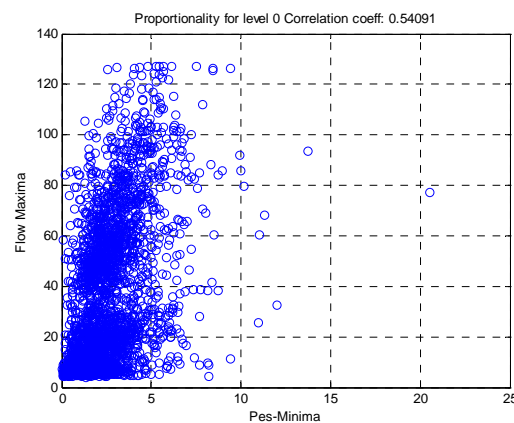


Figure 10.4: Pes (min) and flow (max) values correspondence for non-IFL breaths of patient 4. Although a linearity is present with a correlation coeff. > 0.5 , it was necessary to split up the patient into shorter intervals to achieve a higher linearity between Pes and flow.

We guessed that amplitude and time normalization of the Pes and airflow signals of an inspiration could help to simplify the ideal curve reconstruction problem. However, this procedure distorts the original flattening patterns. In order to avoid the error caused by amplitude normalization, we also explored the possibility to approximate an inspiration's resistance values by differentiating between IFL and non-IFL cases with the P/\dot{V} -relationship.

We hypothesized that the exponential model (see chapter VI) could be used to approximate the original IFL P/\dot{V} -relationship and that the exponential model's coefficients could be used to regress to the non-IFL P/\dot{V} -relationship. However, in order to make a non-invasive estimation, we would need to avoid using the Pes signal or substitute the Pes curve used to calculate the P/\dot{V} -relationship with an artificial function. After manually analyzing an important number of IFL/non-IFL cases with the same respiratory effort, see fig. 10.5, we came to the conclusion that an artificial function such as a sinus curve, an exponential curve or a parabola could be used to reconstruct the original Pes curve. When comparing the cross-correlation coefficient of a sinus curve with the Pes inspiration curve of all breaths, an overall correlation value of 82% was achieved. This implies that the Pes-inspiration curve could be replaced with an artificial curve suffering a limited estimation error. Other functions, such as a trapezium, see fig. 10.6, are of limited value because of their tendency to under- or overestimate the area for the flattening curves, see fig. 10.7. The inspiration would have to be normalized in time (width) but should not be normalized in amplitude for the reconstruction to be proportional and valid.

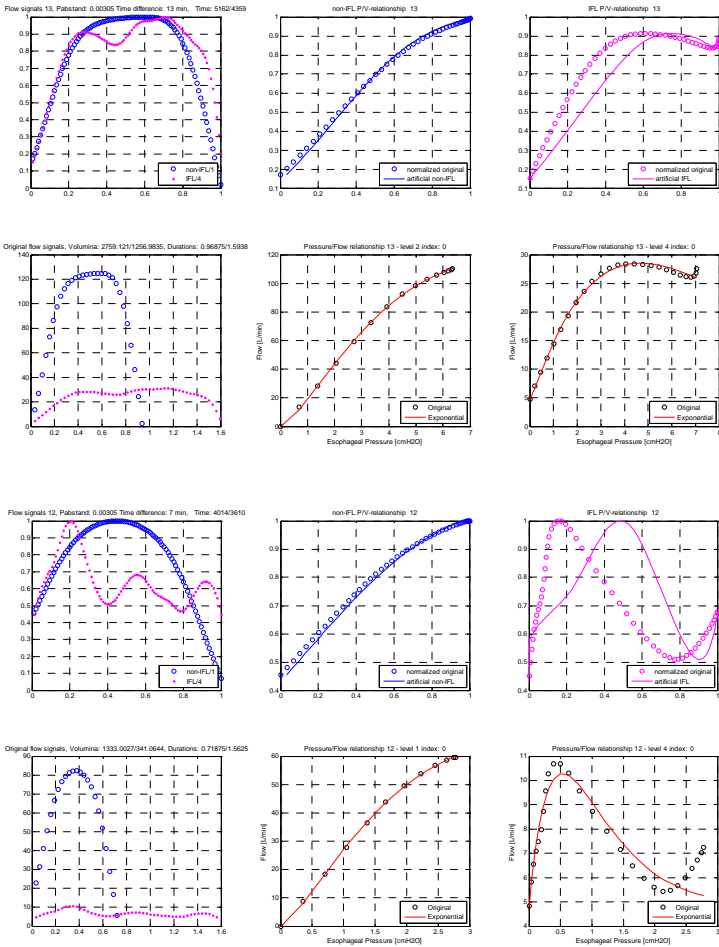


Figure 10.5: Two different examples for two correlated flow curves

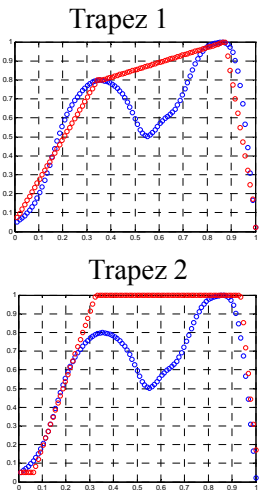


Figure 10.6: Examples for reconstruction functions to estimate a numerical value of the resistance factor

These results were later confirmed by comparing the estimation of the real resistance values with the estimated respiratory resistance. Real resistance was calculated by dividing the area of the Pes curve with the area of the flow curve according to the general formula $R = P / \dot{V}$.

Conclusions

A new system for non-invasive differentiation of central and obstructive hypopneas has been presented. This system uses only the airflow signal to extract information on flattening and other parameters to feed a classifier that bases its decision process upon this information. We were able to confirm that obstructive hypopneas consist of significantly more inspirations with flattening pattern than central hypopneas, representing an important feature for their correct differentiation. Primary results are promising and match up with the results obtained by human experts in non-invasive classification, underlining the feasibility of this study. Further work will be required to optimize the classification process and permit the non-invasive system's implementation into a current therapy device for treatment of OSAHS, CSAHS and Cheyne-Stokes respiration. For this purpose, a continuous flattening measurement based upon the geometrical reconstruction of the ideal flow curve for an IFL-affected flow curve seems a promising approach.

Chapter XI: Conclusions

Contributions of this thesis

The contributions of this thesis have been focused in the design and assessment of novel processing and analysis methods of the airflow and esophageal pressure (Pes) signals during sleep in order to invasively and non-invasively assess UA obstruction and respiratory effort. In total, four different systems, see chapters VI and VIII - X, have been proposed to detect inspiratory flow limitation (IFL) and differentiate obstructive and central hypopneas invasively and non-invasively. The results have been submitted and published in international journals and national and international scientific congresses [Morgenstern 2008a-d, 2009a-e].

Database

Given that Pes measurement is not common in clinical routine and that NPSG studies that include Pes measurement are rare, the development from scratch of the new protocol for a NPSG database with systematic pressure measurement and the acquisition of the NPSG of 28 patients has been an important task of this thesis. The NPSG database was acquired in cooperation with the group of Prof. Randerath at Klinikum Bethanien, Solingen, Germany. The majority of the quoted studies in the literature that worked with esophageal pressure measurement, presented a significantly inferior number of patients than our study, like e.g. Hosselet et al. [16] with 10 patients, Ayappa et al. [14] with 15 patients, Clark et al. [81] with 7 patients, Tamisier et al. [71] with 12 patients or Hudgel et al. [57] with 5 patients. Thus, the cohort size of 28 patients of our study is quite superior to that of comparable studies with esophageal pressure measurement. Our NPSG database represents an important asset that will be used for

further medical, clinical and technical investigation purposes by the group in Solingen, our research group and other research groups that may be granted the access to this database in a recent future.

IFL detection

Invasive IFL detection

A new exponential model was proposed [Morgenstern 2008a, 2008c, 2009a, 2009b] to enhance the automatic classification of IFL with esophageal pressure measurement. The model proved to be superior to the other models in the literature in two out of the three evaluation criteria that were chosen for its assessment. An automatic, gold-standard IFL classification system like described in [81] was implemented in order to obtain the gold-standard IFL labels for each inspiration and validate our model, see chapter VI.

Non-invasive IFL detection

A new non-invasive system of IFL classification was presented [Morgenstern 2008b, 2008d, 2009a, 2009b] to allow the classification of IFL only by means of the airflow signal, see chapter VIII. Using spectral analysis to analyze the characteristic flattening pattern of IFL breaths, we were able to obtain excellent detection results with our new system using supervised machine learning techniques. As the gold-standard IFL labels of the system presented in chapter VI were used, the validity of the non-invasive classification should be ensured.

Differentiation of hypopneas

Invasive hypopnea differentiation

A new invasive system for differentiation of obstructive and central hypopneas was proposed [Morgenstern 2009c, 2009d, 2009e] , see chapter IX. Hypopneas were manually classified and differentiated by a human expert using the airflow and the Pes

signal, delivering gold-standard hypopnea markers for our processing. By analyzing the evolution of pressure swings during these hypopneas and the 2min prior to the onset of the events, we were able to characterize and differentiate automatically between central and obstructive events. This system opens the way to create a valid and extensive validation set for the non-invasive system.

Non-invasive hypopnea classifier

Finally, the feasibility of a non-invasive hypopnea differentiation system was demonstrated [Morgenstern 2009e], see chapter X. We were able to use the IFL-related information of the inspirations during a hypopnea to differentiate between obstructive and central events. We objectively demonstrated, to our knowledge for the first time, that obstructive hypopneas showed significantly ($p < 0.01$) more IFL inspirations than central hypopneas. The results of our system were compared to the outcome of a new non-invasive and context-based algorithm developed for manual classification by human experts, matching their results. A new system for the continuous and numerical assessment of flattening was proposed by means of geometrically reconstructing the ideal airflow curve of IFL breaths.

Outlook

The feasibility non-invasive system presented here represents an important step towards the non-invasive differentiation of obstructive and central events. The insights obtained here and the classification results that have been achieved allow an objective invasive and non-invasive estimation of UA obstruction and respiratory effort, representing an important step towards the correct diagnosis of SDB events. Should the ideal flow-curve algorithm be further developed and then implemented into this system, we expect a significant enhancement of the non-invasive differentiation results. Once this non-

invasive algorithm has been optimized to achieve an overall accuracy of over 80% and a robust generalization capability, a possible application in a clinical scenario could be considered. Our partner company MCC GmbH & Co. KG has suggested that the implementation of this non-invasive system in commercially available therapy devices (Weinmann GmbH, Hamburg, Germany) could be feasible and would provide another clinical tool for the therapy of patients suffering of SDB.

In conclusion, the physiological and technical insights obtained in this thesis represent an important advancement in the invasive and non-invasive estimation of UA resistance and respiratory effort during sleep, paving the way to allow a better and more objective diagnosis of SDB events in clinical scenarios.

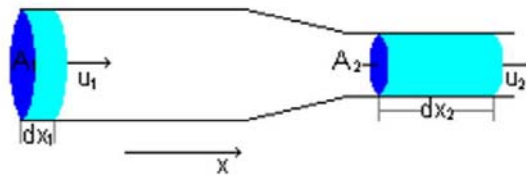
Appendix A

An approach to the derivation

of Aittokallio et al.'s mathematical model

In the following, an approach is intended to explain and derive Aittokallio et al.'s [56] model and the origin of its partial differential equations. The following slides and figures were extracted from a presentation created by the author of this thesis [29].

Law of Conservation of Mass:



$$(1) \quad \text{Flow} \quad \frac{dM}{dt} = \rho \cdot A_1 \cdot \frac{dx_1}{dt} = \rho \cdot A_1 \cdot u_1 = \rho \cdot A_2 \cdot u_2 = \rho \cdot A_2 \cdot \frac{dx_2}{dt} \quad \longleftrightarrow \quad A_1 u_1 = A_2 u_2$$

$$\longrightarrow \frac{\partial M}{\partial t} = \int_A \rho \cdot \vec{u} \cdot d\vec{A} \stackrel{\substack{\text{Gaußscher} \\ \text{Integralsatz}_V}}{=} \int_V \text{div}(\rho \cdot \vec{u}) dV$$

$$(2) \quad \text{Mass} \quad M = \int \rho dV$$

$$\longrightarrow \frac{\partial M}{\partial t} = \frac{\partial}{\partial t} \int_V \rho dV = \int_V \frac{\partial \rho}{\partial t} dV$$

u,v: velocity
ρ : density
M: Mass

Law of Conservation of Mass:

$$(1) = (2) \quad \int_V \frac{\partial \rho}{\partial t} dV = \int_V \text{div}(\rho \cdot \vec{u}) dV$$

$$\longrightarrow \frac{\partial \rho}{\partial t} = \text{div}(\rho \cdot \vec{u})$$

The differential form of the continuity equation is given by (volume changes are equal for both sides)

$$\frac{D(\rho u)}{Dt} = \frac{\partial \rho}{\partial t} + \nabla \cdot (\rho \mathbf{u}) = \frac{\partial \rho}{\partial t} + \mathbf{u} \cdot \nabla \rho + \rho \nabla \cdot \mathbf{u}$$

But for incompressible flow, $\rho = [\text{constant}]$, so the steady-state equation is then

$$\text{Euler equation} \quad \frac{\partial \rho}{\partial t} + \nabla \cdot (\rho \mathbf{v}) = 0$$

$$\text{Aittokallio et al. [1]} \quad \frac{\partial A}{\partial t} + \frac{\partial uA}{\partial x} = 0$$

[1] T. Aittokallio, M. Gyllenberg and O. Polo: A model of a snorer's upper airway, Mathematical Biosciences 170 (2001) 79-90.

u,v: velocity
 ρ : density
M: Mass

The equation for the force per unit volume of a Newtonian fluid. It is given by

$$\frac{\mathbf{F}}{V} = \frac{1}{V} \frac{d\mathbf{p}}{dt} = \rho \frac{D\mathbf{u}}{Dt} \quad \text{Momentum} \quad \mathbf{p} \equiv m\mathbf{v} = m \frac{d\mathbf{x}}{dt}.$$

$$= \rho \frac{\partial \mathbf{u}}{\partial t} + \rho \mathbf{u} \cdot \nabla \mathbf{u}, \quad \text{Mass} \quad m = \int \rho dV,$$

where \mathbf{p} is the momentum of a fluid parcel, ρ is the fluid density (assumed to be constant, i.e., the fluid is incompressible), D/Dt is the substantive derivative, and \mathbf{u} is the fluid velocity field.

There are **THREE PROCESSES** acting on fluid parcels:

$$1.- \text{The pressure force} \quad \frac{\mathbf{F}_{\text{pressure}}}{V} = -\nabla P, \quad (1) \text{ where } P \text{ is the pressure}$$

$$2.- \text{The so-called body force} \quad \mathcal{F} = \frac{\mathbf{F}_{\text{body}}}{V}. \quad (2)$$

$$3.- \text{The viscous force} \quad \frac{\mathbf{F}_{\text{viscous}}}{V} = \eta \nabla^2 \mathbf{u}, \quad (3)$$

The Navier-Stokes equations are the fundamental partial differential equations that describe the flow of incompressible fluids. Using the rate of stress and rate of strain tensors, it can be shown that the components F_j of a viscous force **F in a nonrotating frame are given by**

$$\frac{F_i}{V} = \frac{\partial}{\partial x_j} \left[\eta \left(\frac{\partial u_i}{\partial x_j} + \frac{\partial u_j}{\partial x_i} \right) + \lambda \delta_{ij} \nabla \cdot \mathbf{u} \right] \quad (4)$$

(Tritton 1988, Faber 1995), where η is the dynamic viscosity, λ is the second viscosity coefficient, δ_{ij} is the Kronecker delta, $\nabla \cdot \mathbf{u}$ is the divergence and Einstein summation ^② has been used to sum over $j = 1, 2$, and 3 .

Now, for an incompressible fluid, the divergence $\nabla \cdot \mathbf{u} = 0$ and $\rho = [\text{constant}]$
 \Rightarrow So the λ term drops out of (1).

Taking η to be constant in space and writing the remainder of (4) in vector form then gives

$$\frac{\mathbf{F}_{\text{viscous}}}{V} = \eta \nabla^2 \mathbf{u}, \quad (3)$$

Laplace Operator: $\Delta = \nabla^2 = \nabla \cdot \nabla$.

$$\begin{array}{c} \text{Conservation of momentum} \\ \uparrow \\ \rho \frac{\partial \mathbf{u}}{\partial t} + \rho \mathbf{u} \cdot \nabla \mathbf{u} = -\nabla P + \eta \nabla^2 \mathbf{u} + \mathcal{F}, \end{array} \quad (5)$$

There are **THREE PROCESSES** acting on fluid parcels:

1.- The pressure force $\frac{\mathbf{F}_{\text{pressure}}}{V} = -\nabla P$, (1) where P is the pressure

2.- The so-called body force $\mathcal{F} = \frac{\mathbf{F}_{\text{body}}}{V}$. (2)

3.- The viscous force $\frac{\mathbf{F}_{\text{viscous}}}{V} = \eta \nabla^2 \mathbf{u}$, (3)

dividing (5) through by the density ρ gives

Navier-Stokes eq. (n-dimensional model) $\frac{\partial \mathbf{u}}{\partial t} + \mathbf{u} \cdot \nabla \mathbf{u} = -\frac{\nabla P}{\rho} + \nu \nabla^2 \mathbf{u} + \frac{\mathcal{F}}{\rho}$, kinematic viscosity: $\nu \equiv \frac{\eta}{\rho}$.

Aittokallio et al. [1] (1-dimensional model) $\frac{\partial u}{\partial t} + u \frac{\partial u}{\partial x} = -\frac{1}{\rho} \frac{\partial p}{\partial x} - f(A, u)u$. $f(A) = \begin{cases} 8\pi\nu/(\rho A) & \text{for } A \geq A_u, \\ 8\pi\nu A_u/(\rho A^2) & \text{for } A < A_u. \end{cases}$

Here: ν is viscosity of air

Poiseuille's Law

To get the total volume that flows through the tube, we need to add up the contributions from each lamina. To calculate the flow through each lamina, we multiply the velocity (from above) and the area of the lamina.

$$\text{Flow } \Phi(r) = \frac{1}{4\eta} \frac{|\Delta P|}{\Delta x} (R^2 - r^2) 2\pi r dr = \frac{\pi}{2\eta} \frac{|\Delta P|}{\Delta x} (rR^2 - r^3) dr$$

where P is the pressure, R is the radius and x the length of the lamina cylinder

Finally, we integrate over all lamina via the radius variable.

$$\text{Viscous Resistance} \longrightarrow R = \frac{\Delta P}{\dot{V}} = \frac{8\eta\Delta x}{\pi R^4} = \frac{8\pi\eta\Delta x}{\pi^2 R^4} = \frac{8\pi\eta\Delta x}{A^2}$$


$$\text{Aittokallio et al. } f(A) = \begin{cases} 8\pi\nu/(\rho A) & \text{for } A \geq A_u, \\ 8\pi\nu A_u/(\rho A^2) & \text{for } A < A_u. \end{cases}$$

Aittokallo et al. [1]

1-D model for a collapsible tube (Starling Resistor)

Conservation of mass $\frac{\partial A}{\partial t} + \frac{\partial uA}{\partial x} = 0,$

modified Navier-Stokes $\frac{\partial u}{\partial t} + u \frac{\partial u}{\partial x} = - \frac{1}{\rho} \frac{\partial p}{\partial x} + f(A, u)u.$



$f(A) = \begin{cases} 8\pi\nu/(\rho A) & \text{for } A \geq A_u, \\ 8\pi\nu A_u/(\rho A^2) & \text{for } A < A_u. \end{cases}$
 here: ν is viscosity of air

Mathematical Reminders

Nabla-Operator $\vec{\nabla} = \left(\frac{\partial}{\partial x_1}, \dots, \frac{\partial}{\partial x_n} \right)$

- Used on a scalar field $\Phi(x, y, z)$ we obtain the gradient of that scalar field

$$\text{grad } \Phi = \vec{\nabla} \Phi = \left(\frac{\partial \Phi}{\partial x}, \frac{\partial \Phi}{\partial y}, \frac{\partial \Phi}{\partial z} \right) = \frac{\partial \Phi}{\partial x} \vec{e}_x + \frac{\partial \Phi}{\partial y} \vec{e}_y + \frac{\partial \Phi}{\partial z} \vec{e}_z.$$

The result is a vector field. $\vec{e}_x, \vec{e}_y, \vec{e}_z$ the cartesian unity vectors of \mathbb{R}^3 .

- Applied on a vector field $\vec{V}(x, y, z)$ we obtain the divergence of the vector field in form of a formal scalar product with the vector field to

$$\text{div } \vec{V} = \vec{\nabla} \cdot \vec{V} = \frac{\partial V_x}{\partial x} + \frac{\partial V_y}{\partial y} + \frac{\partial V_z}{\partial z},$$

this is, a scalar field.

- The rotation results after the (right.-sided) connection of the formal cross-product

$$\text{rot } \vec{V} = \vec{\nabla} \times \vec{V} = \begin{pmatrix} \frac{\partial V_z}{\partial y} - \frac{\partial V_y}{\partial z} \\ \frac{\partial V_x}{\partial z} - \frac{\partial V_z}{\partial x} \\ \frac{\partial V_y}{\partial x} - \frac{\partial V_x}{\partial y} \end{pmatrix}$$

again to a vector field.

Laplace Operator & Substantive Derivative

The Laplace operator is a second order differential operator in the n -dimensional Euclidean space, defined as the divergence of the gradient:

• Laplace Operator: $\Delta = \nabla^2 = \nabla \cdot \nabla$.

$$\Delta = \sum_{i=1}^n \frac{\partial^2}{\partial x_i^2}.$$

in Cartesian coordinates: $\Delta = \frac{\partial^2}{\partial x^2} + \frac{\partial^2}{\partial y^2} + \frac{\partial^2}{\partial z^2}.$

A form of derivative which takes into account the fact that a quantity changes both as it moves to a different region and as the overall field is changing. It is most commonly used in fluid mechanics, is also called the advective derivative, and is defined by

• Substantive derivative: $\frac{D}{Dt} = \frac{\partial}{\partial t} + \mathbf{u} \cdot \nabla$

Partial differential equations (PDEs)

General definition of PDEs

$$A u_{xx} + 2B u_{xy} + C u_{yy} + D u_x + E u_y + F = 0,$$

Elliptic PDE

>

Parabolic PDE

Hyperbolic PDE $\det \begin{pmatrix} A & B \\ B & C \end{pmatrix} = AC - B^2 < 0$

Part of the equations exposed in this annex were obtained in part from The Free Encyclopedia Wikipedia (www.wikipedia.org).

Bibliography

- [1] National Sleep Disorders Research Plan, National Center on Sleep Disorders Research, U.S. Department of Health and Human Services, NIH Publication No. 03-5209, 2003
- [2] Pack AI, Advances in Sleep Disordered Breathing, *Am J Respir. Crit Care Med* 172, 7-15, 2006
- [3] Guilleminault C, Stoohs R, Clerk A, Cetel M, Maistros P. "A cause of excessive daytime sleepiness. The upper airway resistance syndrome." *Chest* 104:781–787 1993
- [4] Bixler EO, Vgontzas AN, Ten Have T, Tyson K, Kales A. Effects of age on sleep apnea in men: I. Prevalence and severity. *Am J Respir Crit Care Med* 1998;157:144–148.
- [5] Young T, Palta M, Dempsey J, Skatrud J, Weber S, Badr S. The occurrence of sleep-disordered breathing among middle-aged adults. *N Engl J Med* 1993;328:1230–1235.
- [6] The Report of an American Academy of Sleep Medicine Task Force, Sleep-Related Breathing Disorders in Adults: Recommendations for Syndrome Definition and Measurement Techniques in Clinical Research, *SLEEP*, Vol. 22, No. 5, 1999
- [7] Iber, C., Anoni-Israel S., Chesson A. L., Qua S.F., The AASM Manual for the Scoring of Sleep and Associated Events, American Academy of Sleep Medicine, Westchester, IL, 2007
- [8] Gould GA, Whyte KF, Rhind GB, Airlie MA, Catterall JR, Shapiro CM, Douglas NJ. The sleep hypopnea syndrome. *Am Rev Respir Dis* 1988;137:895–898
- [9] Guilleminault C, Stoohs R, Shoimi T, Kushida C, Schnittiger I, Upper airway resistance syndrome, nocturnal blood pressure monitoring and borderline hypertension. *Chest* 109: 901-908-1996
- [10] Chervin R., Aldrich M., Effects of Esophageal Pressure Monitoring on Sleep Architecture, *Am J Respir Crit Care Med*;156:881–885, 1997

- [11] Argod J, Pépin JL, Lévy P., Differentiating Obstructive and Central Sleep Respiratory Events through Pulse Transit Time, *Am J Respirat Crit Care Med* 158:1778–1783. 1998
- [12] O. Fontenla-Romero, B. Guijarro-Berdiñas, A. Alonso-Betanzos, V. Moret-Bonillo, A new method for sleep apnea classification using wavelets and feedforward neural networks, *Artificial Intelligence in Medicine*, 34:1, pp. 65-76, 2005
- [13] Yen FC, Behbehani K, Lucas EA, Burk JR, Axe JR, A Nonnvasive Technique for Detecting Obstructive and Central Sleep Apnea, *IEEE Transactions on Biomedical Engineering*, Vol. 44, No. 12, December 1997
- [14] Ayappa I., Norman RG, Krieger AC, Rosen A, O'Malley RL. Rapoport DM, Non-Invasive Detection of Respiratory Effort-Related Arousals (RERAs) by a Nasal Cannula/Pressure Transducer System, *Sleep*, Vol. 23, No. 6, 2000
- [15] Aittokallio T, Gyllenberg M, Saaresranta T, Polo O, Prediction of Inspiratory Flow Shapes During Sleep with a Mathematic Model of Upper Airway Forces, *SLEEP* Vol. 26, No. 7, 2003
- [16] Hosselet J., Norman R., Ayappa A., Rapoport D., Detection of Flow Limitation with a Nasal Cannula/ Pressure Transducer System, *Am J Respir Crit Care Med* Vol 157. pp 1461–1467, 1998
- [17] Aittokallio T., Malminen J., Pahikkala T., Polo O., Nevalainen O., Inspiratory flow shape clustering: An automated method to monitor upper airway performance during sleep, *Computer Methods and Programs in Biomedicine* 85, 8-18, 2007
- [18] T. Aittokallio, O. Nevalainen, U. Pursiheimo, T. Saaresranta, O. Polo, Classification of Nasal Inspiratory Flow Shapes by Attributed Finite Automata, *Computers and Biomedical Research* 32, 34–55 1999
- [19] Norman RG, Rapoport DM, Ayappa I., Detection of flow limitation in obstructive sleep apnea with an artificial neural network., *Physiological measurement* 28(9):1089-100, 2007
- [20] K. F. Mansour, J. A. Rowley and M. S. Badr, Noninvasive determination of upper airway resistance and flow limitation, *J Appl Physiol*, November 1, 97 (5): 1840-1848, 2004

- [21] Matthew D. Epstein, Sheryl A. Chicoine, R. Choudary Hanumara, "Detection of Upper Airway Resistance Syndrome Using a Nasal Cannula/Pressure Transducer", *Chest* 117/4 April 2000
- [22] Nanba, Shinji, Ohsaki, Rie, Shiomi, Toshiaki, "Apparatus and method for electronically predicting pleural pressure from pulse wave signals", United States Patent Application, 2002014326, October 3, 2002
- [23] Lorino AM, Lofaso F, Duizabo D, Zerah F, Goldenberg F, d'Ortho MP, Harf A, Lorino H, "Respiratory Resistive Impedance as an Index of Airway Obstruction during Nasal Continuous Positive Airway Pressure Titration", *Am J Respir Crit Care Med* Vol 158. pp 1465–1470, 1998
- [24] Navajas D, Farré R, Rotger M, Badia R, Puig-de-Morales M, Montserrat JM, "Assessment of Airflow Obstruction during CPAP by Means of Forced Oscillation in Patients with Sleep Apnea", *Am J Respir Crit Care Med* Vol 157. pp 1526–1530, 1998
- [25] R. A. Stoohs, H. C. Blum, L. Knaack, C. Guilleminault, "Non-invasive Estimation of Esophageal Pressure Based on Intercostal EMG Monitoring", *Proceedings of the 26th Annual International Conference of the IEEE EMBS San Francisco, CA, USA, September 1-5, 2004*
- [26] Riccardo A. Stoohs, Hans-Christian Blum, Lennart Knaack, Berthold Butsch-von-der-Heydt, Christian Guilleminault, "Comparison of Pleural Pressure and Transcutaneous Diaphragmatic Electromyogram in Obstructive Sleep Apnea Syndrome", *SLEEP*, Vol. 28, No. 3, 2005
- [27] Lennart Knaack, Hans-Christian Blum, Winfried Hohenhorst, Jan Ryba, Christian Guilleminault and Riccardo A. Stoohs, "Comparison of Diaphragmatic EMG and Oesophageal Pressure in Obstructed and Unobstructed Breathing during Sleep", *Somnologie* 9: 159–165, 2005

- [28] Avram R. Gold, Carole L. Marcus, Francis Dipalo and Morris S. Gold, “Upper Airway Collapsibility During Sleep in Upper Airway Resistance Syndrome”, *Chest* 121;1531-1540, 2002
- [29] C. Morgenstern, “A simple model to reduce time delays in the UA”, Universitat Politècnica de Catalunya, Technical Report, 2007
- [30] Susheel P Patil; Naresh M Punjabi; Hartmut Schneider; Christopher P O'Donnell et al., “A Simplified Method for Measuring Critical Pressures during Sleep in the Clinical Setting”, *American Journal of Respiratory and Critical Care Medicine*; 170, 1; Health & Medical Complete pg. 86, Jul 1, 2004
- [31] Condos R., R. G. Norman, I. Krishnasamy, N. Peduzzi, R. M. Goldring, D. M. Rapoport, “Flow limitation as noninvasive assessment of residual upper-airway resistance during continuous positive airway pressure therapy of obstructive sleep apnea.”, *Am. J. Respir. Crit. Care Med* , 150, pp. 475-480, 1994
- [32] Daniel I. Loube, Teotimo Andrada, Robin S. Howard, “Accuracy of Respiratory Inductive Plethysmography for the Diagnosis of Upper Airway Resistance Syndrome”, *Chest* 115;1333-1337, 1999
- [33] Peter Varady, Szabolcs Bongar, Zoltan Benyo, “Detection of Airway Obstruction and Sleep Apnea by Analyzing the Phase Relation of Respiration Movement Signals”, *IEEE Transactions on Instrumentation and Measurement*, Vol. 52, No. 1, February 2003
- [34] Mario Giovanni Terzano, Liborio Parrino, Adriano Sherieri, Ronald Chervin, Sudhansu Chokroverty, Christian Guilleminault, et al., “Atlas, rules, and recording techniques for the scoring of cyclic alternating pattern (CAP) in human sleep”, *Sleep Medicine* 2 537–553, 2001

- [35] Guilleminault C., Kirisoglu C., da Rosa A., L C.opes, Chan A., “Sleepwalking, a disorder of NREM sleep instability”, *Sleep Medicine* 7 163–170, 2006
- [36] Stoohs R., Guilleminault C., “Snoring during NREM sleep: Respiratory timing, esophageal pressure and EEG arousal”, *Respiration Physiology*, 85 151-167, 1991
- [37] R. Stoohs, A. Skrobal and C. Guilleminault, “Does snoring intensity predict flow limitation or respiratory effort during sleep?”, *Respiration Physiology*, 92 27-38, 1993
- [38] Wilson K, Stoohs RA, Mulrooney TF, Johnson LJ, Guilleminault C, Huang Z, “The Snoring Spectrum; Acoustic Assessment of Snoring Sound Intensity in 1,139 Individuals Undergoing Polysomnography”, *Chest* 115;762-770, 1999
- [39] C.D. Hanning, M. Welsh, “Sleepiness, snoring and driving habits”, *Journal of Sleep Res.* 5, 51-54, 1996
- [40] Antoni Homs-Corbera, José Antonio Fiz, José Morera, and Raimon Jané, “Time-Frequency Detection and Analysis of Wheezes During Forced Exhalation”, *IEEE Trans. on Biomed. Eng.*, VOL. 51, NO. 1, JANUARY 2004
- [41] J.A. Fiz, J. Abad, R. Jané, M. Riera, M.A. Mañanas, P. Caminal, D. Rodenstein, J. Morera, “Acoustic analysis of snoring sound in patients with simple snoring and obstructive sleep apnoea”, *Eur Respir J*, 9, 2365–2370, 1996
- [42] José A. Fiz, Raimon Jané, Antonio Homs, José Izquierd, Maria A. García, José Morera, “Detection of Wheezing During Maximal Forced Exhalation in Patients UIT Obstructed Airways”, *CHEST / 122 / 1 / JULY*, 2002
- [43] R. Jané, J. A. Fiz, J. Solà-Soler, S. Blanch, P. Artís, J. Morera, “Automatic Snoring Signal Analysis in Sleep Studies”, *IEEE EMBS International Conference*, 2003

- [44] Antoni Homs-Corbera, Raimon Jané, José Antonio Fiz, José Morera, "Algorithm for Time-Frequency Detection of Analysis of Wheezes", Proceedings of the 22nd annual EMBS International Conference, Chicago, IL, July 23-28, 2000
- [45] R. Jané, D. Salvatella, J.A. Fiz, J. Morera, "Spectral Analysis of Respiratory Sounds to Assess Bronchodilator Effect in Asthmatic Patients", Proceedings of the 20th Annual International Conference of the IEEE Engineering in Medicine and Biology Society, Vol. 20, No 6, 1998
- [46] José Antonio Fiz, Raimon Jané, David Salvatella, José Izquierdo, Luis Lores, Pere Caminal, José Morera, "Analysis of Tracheal Sounds During Forced Exhalation in Asthma Patients and Normal Subjects", CHEST / 116 / 3 / SEPTEMBER, 1999
- [47] T.M. Maksimova, A.I. Romanov, E.P. Kakorina, N.P. Lushkina, M.V. Tokurov, "Social-Hygienic evaluation of the prevalence of sleep-disorders", Probl. Sotsianolnig. Istor. Med. Vol 6, p 14, 1997
- [48] Jennum P, Sjol A. "Epidemiology of snoring and obstructive sleep apnoea in a Danish population age 30–60.", J Sleep Res; 1: 240–244, 1992
- [49] Fleetham JA, "A wake up call for sleep disordered breathing", Br Med J, 328, pp. 839-840, 1997
- [50] Philipson EA, "Sleep apnea – a major public health problem.", N Engl J Med, 328, pp 1271-1273, 1997
- [51] Silverberg DS, Oksenberg A, "Essential hypertension and abnormal upper airway resistance during sleep.", Sleep, 20, pp. 794-806, 1997
- [52] American Thoracic Society, "Sleep Apnea, sleepiness and driving risk.", Am J Respir Crit Care Med, 150, 1463-1473, 1994

- [53] Dement WC, "The perils of drowsy driving." N Engl J Med, 337, pp. 783-784, 1997
- [54] Mitler MM, Miller JC, Lipsitz JJ, Walsh JK, Wyle C.D., "The sleep of long-haul truck drivers.", N Engl J Med, 337, pp. 755-761, 1997
- [55] Thomas Penzel, "Pathophysiologie schlafbezogener Atmungsstörungen", 1995
- [56] Aittokallio T., Gyllenberg M., Polo O., A model of a snorer's upper airway, Mathematical Biosciences 170, 79-90, 2001
- [57] Hudgel, D., M. Mulholland, and C. Hendricks. 1987. Neuromuscular and mechanical responses to inspiratory resistive loading during sleep. *J.Appl. Physiol.* 63:603–608.
- [58] Iber, C., A. Berssenbrugge, J. B. Skatrud, and J. A. Dempsey. 1982. Ventilatory adaptations to resistive loading during wakefulness and non-REM sleep. *J. Appl. Physiol.* 52:607–614.
- [59] Drake R., Vogl W., Mitchell A., Gray's Anatomy for Students, 1st edition, copyright Elsevier, 2004
- [60] S. Isono, D.L. Morrison, S.H. Launois, T.R. Feroah, W.A. Whitelaw, J.E. Remmers, Static mechanics of the velopharynx of patients with obstructive sleep apnea, Journal of Applied Physiology, 75(1):148-154, 1993
- [61] Brouillete R.T., Thach T., A neuromuscular mechanism maintaining extrathoracic airway patency, J Appl Physiol., 46: 772-779, 1979
- [62] Remmers J.E., Degroot W.J., SAuerland E.K., Anch A.M., Pathogenesis of upper airway occlusion during sleep, J Appl. Physiol. 44: 931-938, 1978
- [63] Shepard JW, Thawley SE, Localization of upper airway collapse during sleep in patients with obstructive sleep apnea, Am. Rev. Respir. Dis. 132:221-215, 1985
- [64] Clete A. Kushida, Obstructive Sleep Apnea: Pathophysiology, Comorbidities, and Consequences, Vol. 3, 2007, informa healthcare USA, Inc.

- [65] Schwartz A.R., Smith P.L., Wie A., Bankman I., Permutt S., Effect of positive nasal pressure on upper airway pressure-flow relationships. *J Appl. Physiol.* 66: 1626-1634, 1989
- [66] AR Gold and AR Schwartz, "The pharyngeal critical pressure. The whys and hows of using nasal continuous positive airway pressure diagnostically", *Chest*, 110;1077-1088, 1996
- [67] Haponik EF, Smith PL, Bohlman ME, et al., Computerized tomography in obstructive sleep apnea: correlation of airway size with physiology during sleep and wakefulness. *Am Rev Resp Dis*, 127:221-226, 1983
- [68] Avram R. Gold, Carole L. Marcus, Francis Dipalo and Morris S. Gold, "Upper Airway Collapsibility During Sleep in Upper Airway Resistance Syndrome", *Chest* 121;1531-1540, 2002
- [69] Huang L, Quinn SJ, Ellis PDM, JE Ffowcs Williams, Biomechanics of snoring, *Endeavour* 19, 96, 1995
- [70] Ferris BG, Mead J, Opie LH, Partitioning of respiratory flow resistance in man. *J Appl Physiol* 19:653-658, 1964
- [71] R. Tamisier, J. L. Pepin, B. Wuyam, R. Smith, J. Argod and P. Levy "Characterization of pharyngeal resistance during sleep in a spectrum of sleep-disordered breathing", *Journal of Applied Physiology* 89:120-130, 2000
- [72] Gang Bao, Christian Guilleminault, "Upper Airway Resistance Syndrome-One Decade Later", *Curr Opin Pulm Med* 10(6):461-467, 2004
- [73] Guilleminault C., Douglas N., Pro/Con Editorials "Upper Airway Resistance Syndrome Is/Is Not a Distinct Síndrome", *Am J Resp Crit. Care Med*, Vol. 161, 2000

- [74] Elliott N. Exar, Nancy A. Collop, "The Upper Airway Resistance Syndrome", *Chest* 115;1127-1139, 1999
- [75] Daniel I. Loube, Teotimo F. Andrada, "Comparison of Respiratory Polysomnographic Parameters in Matched Cohorts of Upper Airway Resistance and Obstructive Sleep Apnea Syndrome Patients", *Chest* 115;1519-1524 1999
- [76] Christian Guilleminault, Ceyda Kirisoglu, Dalva Poyares, Luciana Palombini, Damien Leger, Mehran Farid-Moayer, Maurice M. Ohayon, "Upper airway resistance syndrome: A long-term outcome study", *Journal of Psychiatric Research* 40 273–279, 2006
- [77] Guilleminault C., Robinson A., "Central sleep apnea, upper airway resistance and sleep", *Sleep Medicine* 7, 189-191, 2006
- [78] R. L. Wilkin, *Clinical Assessment in Respiratory Care*. St. Louis, MO: Mosby, pp. 268–272, 1985
- [79] R. A. Pascualy and S. W. Soest, *Snoring and Sleep Apnea*. New York: Raven, 1994, ch. 7, p. 87.
- [80] A. Rechtschaffen and A. Kales "A Manual of Standardized Terminology, Techniques and Scoring System for Sleep Stages of Human Subjects", *Brain Information Service/Brain Research Institute*, Los Angeles, 1968
- [81] S. A. Clark, C. R. Wilson et al., "Assessment of Inspiratory Flow Limitation Invasively and Noninvasively during Sleep", *Am J Respir Crit Care Med*, 158, pages 713-722, 1998
- [82] Joshua O Benditt, "Esophageal and Gastric Pressure Measurements", *Respiratory Care*, Vol. 50 (1), Jan. 2005
- [83] Hoffstein V., Mateika JH, Mateika S., „Snoring and sleep architecture“, *Am Rev. Respir. Dis.* 143, pp. 92-96, 1991

- [84] Woodson BT, „Upper Airway resistance Syndrome after uvulopharyngoplasty for obstructive sleep apnea syndrome.“, *Otolaryngol Head Neck Surg* 114, pp. 457-461, 1996
- [85] Atsushi Horiuchi, “Measurement Techniques Predicting the Effectiveness of an Oral Appliance for Obstructive Sleep Apnea Hypopnea Syndrome”, *Angle Orthod* 75:1003–1011, 2005
- [86] Baydur A, Behrakis PK, Zin WA, Jaeger M, Milic-Emili J. “A simple method for assessing the validity of the esophageal balloon technique.”, *Am Rev Respir Dis*;126(5):788–791, 1982
- [87] Gappa M, Jackson E, Pilgrim L, Costeloe K, Stocks J., “A new microtransducer catheter for measuring esophageal pressure in infants.”, *Pediatr Pulmonol*. Aug;22(2):117-124. 1996
- [88] R. Tutuian, A. Agrawal, I. Mainie, J. Freeman, D. O. Castell, “Disposable balloon-based oesophageal motility catheters: comparison with solid-state transducers”, *Neurogastroenterol Motil* 17, 453–457, 2005
- [89] John Fang, Kristen Hilden, Ashok Tuteja, Kathryn Peterson, “Comparison of air coupled balloon esophageal manometry catheters with solid-state esophageal manometry catheters”
- [90] Rapoport D., Norman R., Nielson M., “Nasal Pressure Measurement, an introduction”, Pro-Tech Services,
- [91] Norman RG, Ahmed MM, Walsleben JA, Rapoport DM. Detection of Respiratory Events During NPSG : Nasal Cannula/Pressure Sensor Versus Thermistor. *Sleep* 20: 1175-1184, 1997.
- [92] Montserrat JM, Farre R, Ballester E, Felez MA, Pasto M, Navajas D., Evaluation of Nasal Prongs for Estimating Nasal Flow., *Am J Respir Crit Care Med* 155:211-215, 1997
-

- [93] Hernandez L., Ballester E., Farre R., Badia J.R., Lobelo R., Navajas D., Montserrat J.M., Performance of nasal prongs in sleep studies: spectrum of flow related events, *Chest* 119, 37-44, 2001
- [94] Mansour K., Rowley J., Meshenish A., Shkoukani M., Badr M., A mathematical model to detect inspiratory flow limitation during sleep, *J App Physiology*, 93:1084-1092, 2002
- [95] Randerath WJ; Galetke W; Stieglitz S; Laumanns C; Schäfer T, Adaptive servo-ventilation in patients with coexisting obstructive sleep apnoea/hypopnoea and Cheyne-Stokes respiration. *Sleep medicine* ;9(8):823-30. 2008
- [96] Galetke W.; Anduleit N.; Richter K.; Stieglitz S.; Randerath WJ Comparison of automatic and continuous positive airway pressure in a night-by-night analysis: a randomized, crossover study., *Respiration*;75(2):163-9. 2008
- [97] Randerath WJ, APAP or CPAP: who benefits?, *Sleep medicine* ;8(7-8):691-2. 2007
- [98] Galetke W; Feier C; Muth T; Ruehle K-H; Borsch-Galetke E; Randerath W, Reference values for dynamic and static pulmonary compliance in men. *Respiratory medicine*;101(8):1783-9. 2007
- [99] Skobel E. C; Sinha A.; Norra C.; Randerath W.; Breithardt O.; Breuer C.; Hanrath P.; Stellbrink C., Effect of cardiac resynchronization therapy on sleep quality, quality of life, and symptomatic depression in patients with chronic heart failure and Cheyne-Stokes respiration. *Sleep & breathing*;9(4):159-66. 2005
- [100] Randerath WJ; Galetke W; Domanski U; Weitkunat R; Ruhle KH, Tongue-muscle training by intraoral electrical neurostimulation in patients with obstructive sleep apnea. *Sleep* ;27(2):254-9. 2004
- [101] Randerath WJ; Heise M; Hinz R; Ruehle KH, An individually adjustable oral appliance vs continuous positive airway pressure in mild-to-moderate obstructive sleep apnea syndrome. *Chest* ;122(2):569-75. 2002

- [102] Randerath WJ; Meier J; Genger H; Domanski U; Rühle K, Efficiency of cold passover and heated humidification under continuous positive airway pressure. *The European Respiratory Journal*;20(1):183-6. 2002
- [103] Bob Kemp, Alpo Värri, Agostinho C. Rosa, Kim D. Nielsen and John Gade, "A simple format for exchange of digitized polygraphic recordings“, *Electroencephalography and Clinical Neurophysiology*, 82, 391-393, 1992
- [104] SIESTA - A New Standard for Integrating Polygraphic Sleep Recordings into a Comprehensive Model of Human Sleep and its Validation in Sleep Disorders, Project # Biomed-2 BMH4-CT97-2040 funded by the European Commission, DG XII, Sep 1997 - Aug 2000
- [105] Schwaibold M, Schöller B, Penzel T, Bolz A, Artificial intelligence in sleep analysis (ARTISANA) - modelling visual processes in sleep classification, *Biomedizinische Technik/Biomedical engineering* 46(5):129-32, 2001
- [106] P Ask, PA Oberq, L Tibbling, Frequency content of esophageal peristaltic pressure, *Am J Phys Endocr Metab*, 236: E296-E300, 1979
- [107] M. van der Torn, C. D. L. van Gogh, I. M. Verdonck-de Leeuw, J. M. Festen, G. J. Verkerke, H. F. Mahieu, Assessment of alaryngeal speech using a sound-producing voice prosthesis in relation to sex and pharyngoesophageal segment tonicity, *Head & Neck*, Volume 28 Issue 5, Pages 400 – 412, 2006
- [108] M van der Torn, C D L van Gogh, I M Verdonck-de Leeuw , J M Festen, H F Mahieu, Analysis of failure of voice production by a sound-producing voice prosthesis *The Journal of Laryngology & Otology*, 120:6:455-462, 2006
- [109] Mehnert U., Knapp P. A., Mueller N., Reitz A., Schurch B., Heart rate variability: An objective measure of autonomic activity and bladder sensations during urodynamics, *Neurourology and Urodynamics*, [Epub ahead of print], Dec 4. 2008

- [110] Jaeger MJ, Matthys H., The pattern of flow in the upper human airways. *Respir Physiol.* Dec;6(1):113-27, 1968
- [111] N. Nagelkerke, A Note on a General Definition of the Coefficient of Determination, *Biometrika*, vol. 78, no. 3, pp. 691-692, 1991
- [112] Christopher J.C. Burges. "A tutorial on Support Vector Machines for pattern recognition", Bell Labs., Lucent Technologies, 1998.
- [113] Vapnik, V. *The Nature of Statistical Learning Theory*. Springer-Verlag, New York, 1995
- [114] Yoav Freund and Robert E. Shapire, "A short introduction to boosting.", In *Journal of Japanese Society for Artificial Intelligence*, volume 14, pages 771-780, September 1999.
- [115] Freund Y, Schapire R. Game theory, on-line prediction and boosting. In *Proc. 9th ann. Conf. on Comp. Learning Theory*, pp. 325-332, 1996
- [116] Friedman J, Hastie T, Tibshirani R. Additive logistic regression: A statistical view of boosting. *Annals of Statistics*, 38(2):337-374, 2000.
- [117] Vezhnevets A. Vezhnevets V., Modest AdaBoost- teaching AdaBoost to generalize better. *Graphicon 2005*
- [118] Heisele B., Riskov I., Morgenstern C., Components for Object Detection and Identification, in *Towards Category-Level Object Recognition*, Ponce J., Hebert M., Schmid C., Zisserman A., *Lecture Notes in Computer Science*, Springer-Verlag, Vol. 4170, XI, 2006
- [119] Morgenstern C, Heisele B, Component based recognition of objects in an office environment, *CSAIL Technical Report*, Massachusetts Institute of Technology, CSAIL Memo-2003-024, CBCL Paper-232, 2003
- [120] Burg JP, Maximum likelihood spectral analysis, *Proc 37th Meet Soc. Exploration Geophysicist*, Oklahoma City, OK, 1-6, 1967
- [121] Rissanen J, Modeling by Shortest Data Description, *Automatica*, 14, 445-471, 1978
- [122] Krzanowski, W. J., *Principles of Multivariate Analysis*, Oxford University Press, 1988

- [123] Steltner H, Staats R, Timmer J, Vogel M, Guttman J, Matthys H, Virchow JC, Diagnosis of Sleep Apnea by Automatic Analysis of Nasal Pressure and Forced Oscillation Impedance, *Am J Respir Crit Care Med* Vol 165. pp 940–944, 2002
- [124] Hart Peter E. Stork David G. Duda, Richard O. Pattern Classification. John Wiley & Sons Inc., 2001.
- [125] Ralf Eger Uwe Kiencke, Heinz Kronmüller. Meßtechnik. Systemtheorie für Elektrotechniker. Springer Verlag, 2001.
- [126] Curve Fitting Toolbox Function Reference, The MathWorks Inc. MATLAB Version 7.6, R2008a, 2008
- [127] Johnstone I. Efron B., Hastie T. and Tibshirani R. *Least Angle Regression*. Statistics Department, Stanford University, June 16 2003.
- [128] Statistical Tool Box Reference, The MathWorks Inc. MATLAB Version 7.6, R2008a, 2008
- [129] Luo YM, Tang J, Steier J, Zhong NS, Moxham J, Polkey MI., Distinguishing Obstructive From Central Sleep Apnea Events: Diaphragm Electromyogram and Esophageal Pressure Compared, *Chest*. 135 (5), 1133-1141, 2009
- [130] José Antonio Fiz, Raimon Jané, Jordi Solà-Soler, Jorge Abad, M. Ángeles García, José Morera, Continuous analysis and monitoring of snores and their relationship to the apnoea-hypopnea index, *The Laryngoscope*, 2009 (in press, lscope-09-1180.R1)
- [131] Lopez-Gimenez F, Sert-Kuniyoshi F, Gami A., Somers VK, Obstructive sleep apnea implications for cardiac and vascular disease, *Chest* 133:793-804, 2008
- [132] M. Schwaibold. Automatische Schlafstadienerkennung unter Verwendung wissensbasierter Systeme. Master's thesis, Universität Karlsruhe, Institut für Biomedizinische Technik, 2000
- [133] Bijaoui EL, Champagne V, Baconnier PF, Kimoff RJ, Bates JH. Mechanical properties of the lung and upper airways in patients with sleep-disordered breathing. *Am J Respir Crit Care Med*. 2002 Apr 15;165(8):1055-61.

- [134] Bijaoui E, Tuck SA, Remmers JE, Bates JH. Estimating respiratory mechanics in the presence of flow limitation. *J Appl Physiol.* 1999 Jan;86(1):418-26.
- [135] C. Morgenstern, Component based recognition of objects in an office environment, Diplomarbeit, Institut für Biomedizinische Technik, Universität Karlsruhe (TH), 2003
- [136] Kushida C., Giacomini A., Lee MK., Guilleminault C., Dement WC, Technical protocol for the use of esophageal manometry in the diagnosis of sleep-related breathing disorders, *Sleep Medicine* (3), 163-173, 2002

Publications derived from this thesis

[Morgenstern 2008a] Morgenstern C., Jané R., Schwaibold M., Randerath W., Characterization of inspiratory flow limitation during sleep with an exponential model, Proc. of IEEE Eng Med Biol Soc. 30th Annual Int. Conf., Vancouver, BC, Canada, pp. 2439-2443, 2008

[Morgenstern 2008b] Morgenstern C., Jané R., Schwaibold M., Randerath W., Automatic classification of inspiratory flow limitation assessed noninvasively during sleep, Proc. of IEEE Eng Med Biol Soc. 30th Annual Int. Conf., Vancouver, BC, Canada, pp. 1132-1135, 2008

[Morgenstern 2008c] Morgenstern C., Jané R., Schwaibold M., Randerath W., Caracterización de limitaciones de flujo inspiratorio durante el sueño mediante un modelo exponencial, Proc. of XXVI Congreso de la Sociedad Española de Ingeniería Biomédica (CASEIB), Valladolid, Spain, ISBN: 978-84-691-3641-6, October 2008

[Morgenstern 2008d] Morgenstern C., Jané R., Schwaibold M., Randerath W., Clasificación automática de limitación de flujo inspiratorio adquirido de forma no-invasiva durante el sueño, Proc. of XXVI Congreso de la Sociedad Española de Ingeniería Biomédica (CASEIB), Valladolid, Spain, ISBN: 978-84-691-3641-6, October 2008

[Morgenstern 2009a] Morgenstern C., Schwaibold M., Randerath W., Bolz A., Jané R., Assessment of changes in upper airway obstruction by automatic identification of inspiratory flow limitation during sleep, Proc. of 2nd IBEC Symposium on Bioengineering and Nanomedicine, Barcelona, Spain, April 14-15, 2009

[Morgenstern 2009b] Morgenstern C., Schwaibold M., Randerath W., Bolz A., Jané R., Assessment of changes in upper airway obstruction by automatic identification of inspiratory flow limitation during sleep, **IEEE Trans. on Biomedical Engineering**, Vol. 56 (8), pp. 2006-2015, August 2009

[Morgenstern 2009c] Morgenstern C., Schwaibold M., Randerath W., Bolz A., Jané R., Automatic differentiation of obstructive and central hypopneas with esophageal pressure measurement during sleep, Proc. of IEEE Eng Med Biol Soc. 31st Annual Int. Conf., Minneapolis, MN, USA, pp. 7102 - 7105, 2009

[Morgenstern 2009d] Morgenstern C., Schwaibold M., Randerath W., Bolz A., Jané R., Diferenciación automática de hipopneas mediante la señal de presión esofágica durante el sueño, Proc. of XXVII Congreso de la Sociedad Española de Ingeniería Biomédica (CASEIB), Cádiz, Spain, ISBN: 978-84-608-0990-6, 2009

[Morgenstern 2009e] Morgenstern C., Schwaibold M., Randerath W., Bolz A., Jané R., An invasive and a non-invasive approach for the automatic differentiation of obstructive and central hypopneas, **IEEE Trans. on Biomedical Engineering**, submitted 12/2009, major revision 01/2010, TBME-01059-2009

Das Problem

*Der Zwölf-Elf kam auf sein Problem
und sprach: Ich heiße unbequem.
Als hieß' ich etwa Drei-Vier
statt Sieben -- Gott verzeih mir!*

*Und siehe da, der Zwölf-Elf nannt' sich
von jenem Tag ab Dreiundzwanzig.*

Christian Morgenstern, 1905